

FlowDike-D

**Freibordbemessung von Ästuar-  
und Seedeichen unter  
Berücksichtigung von Wind und  
Strömung**

Stand der Arbeiten - März 2010

Dipl.-Ing. Stefanie Lorke<sup>1</sup>  
Dipl.-Ing. Anja Brüning<sup>1</sup>  
Dr.-Ing. Antje Bornschein<sup>2</sup>  
Dipl.-Ing. Stefano Gilli<sup>2</sup>  
cand.-Ing. Nadine Krüger<sup>2</sup>  
Univ.-Prof. Dr.-Ing. Holger Schüttrumpf<sup>1</sup>  
Prof. Dr.-Ing. habil. Reinhard Pohl<sup>2</sup>

Aachen und Dresden, März 2010

---

<sup>1</sup> Institut für Wasserbau und Wasserwirtschaft (IWW), RWTH Aachen

<sup>2</sup> Institut für Wasserbau und Technische Hydromechanik (IWD), TU Dresden



|   |  |                    |
|---|--|--------------------|
| Zuwendungsempfänger:  |  | Förderkennzeichen: |
|                    | Lehrstuhl und Institut für Wasserbau und Wasserwirtschaft (IWW)<br>Rheinisch-Westfälische Technische Hochschule (RWTH) Aachen<br>Univ.-Prof. Dr.-Ing. Holger Schüttrumpf         | 03KIS075           |
|                    | Institut für Wasserbau und Technische Hydromechanik (IWD)<br>Technische Universität (TU) Dresden<br>Lehrgebiet Hydromechanik im Wasserbau<br>Prof. Dr.-Ing. habil. Reinhard Pohl | 03KIS076           |
|                    | Unterstützt durch<br>EU - Hydralb III  |                    |
| Vorhabenbezeichnung:  |  |                    |
| Verbundprojekt: FlowDike-D  |  |                    |
| Vorhaben: Freibordbemessung von Ästuar- und Seedeichen unter Berücksichtigung von Wind und Strömung |  |                    |
| Laufzeit des Vorhabens: 01/2009 bis 10/2011   |  |                    |
| Berichtszeitraum: 01/2009 bis 03/2010   |  |                    |

#### Anschriften der Projektpartner:

Institut für Wasserbau und Wasserwirtschaft (IWW), RWTH Aachen

Univ.-Prof. Dr.-Ing. Holger Schüttrumpf

Mies-van-der-Rohe-Straße 1, 52056 Aachen

Institut für Wasserbau und Technische Hydromechanik (IWD), TU Dresden

Prof. Dr.-Ing. habil. Reinhard Pohl

George-Bähr-Str. 1, Beyer-Bau Zimmer 82/84, 01069 Dresden

---

## Inhaltsverzeichnis

|  |          |
|--|----------|
| <b>Vorwort</b>   | <b>1</b> |
| <b>1 Kurzgefasste Angaben zum Projekt</b>  | <b>2</b> |
| 1.1 wichtige wissenschaftlich-technische Ergebnisse und wesentliche Ereignisse.....          | 2        |
| 1.2 Arbeits-, Zeit- und Aufgabenplanung.....   | 3        |
| 1.3 Aussichten für die Erreichung der Ziele des Vorhabens .....                              | 6        |
| 1.4 Ergebnisse von dritter Seite, die für die Durchführung des Vorhabens relevant sind ..... | 6        |
| 1.5 Änderungen in der Zielsetzung .....  | 6        |
| 1.6 Fortschreibung des Verwertungsplans .....  | 6        |
| <b>Anhang</b>  | <b>7</b> |

## Vorwort

Eine Analyse von Deichschäden z.B. nach dem Hurrikan Katrina in den USA oder der großen Sturmflut in Hamburg im Jahr 1962 hat gezeigt, dass viele Deichschäden und Deichbrüche auf Wellenüberlauf zurückzuführen sind. Daher ist der Wellenüberlauf aber auch die Wellenaufbauhöhe für die Ermittlung der Kronenhöhe von Fluss-, Ästuar- und Seedeichen eine maßgebende Bemessungsgröße. Heutige Bemessungsformeln für Wellenaufbau und Wellenüberlauf (z.B. EUROTOP-Manual, 2008) berücksichtigen neben der Deichgeometrie insbesondere die Wellenhöhe, die Wellenperiode sowie die Wellenangriffsrichtung. Die deichparallele Strömung sowie der lokale Wind werden bislang in diesen Formeln nicht berücksichtigt. Im Rahmen eines Hydralab III - Projektes wurden daher zu diesem Aspekt experimentelle Untersuchungen im Wellenbecken von DHI in Kopenhagen im Jahr 2009 an einem 1:3 geböschten Deich durchgeführt. Die experimentellen Daten stehen für das vorliegende Projekt vollständig zur Verfügung und wurden durch eine zweite Versuchsreihe mit einem 1:6 geböschten Deich im Rahmen dieses BMBF Projektes erweitert.

Ziel des Projektes ist es, den Einfluss von Strömung und Wind auf die mittlere Wellenaufbauhöhe und Wellenüberlaufhöhe auf der Grundlage verfügbarer experimenteller Untersuchungen aus dem Projekt zu ermitteln und bestehende Wellenaufbau- und -überlaufformeln (siehe Eurotop-Manual) entsprechend zu adaptieren bzw. zu erweitern.

Dieser Zwischenbericht 2009 stellt in Stichworten die bisher vorliegenden wesentlichen Erkenntnisse und Ergebnisse aus dem Projekt FlowDike-D vor und gibt einen Überblick über die bereits durchgeführten und noch zu bearbeitenden Teilaufgaben des Projektes. Als Anhang liegt die aktuelle Version des Berichtes „FlowDike-D: Freibordbemessung von Ästuar- und Seedeichen unter Berücksichtigung von Wind und Strömung“ in englischer Sprache bei.

# 1 Kurzgefasste Angaben zum Projekt

## 1.1 wichtige wissenschaftlich-technische Ergebnisse und wesentliche Ereignisse

Die experimentellen Untersuchungen wurden am DHI in Kopenhagen erfolgreich durchgeführt. Erste Ergebnisse der Referenztests zeigen bereits eine gute Übereinstimmung mit vorherigen Untersuchungen. Im Folgenden werden die ersten vorläufigen Ergebnisse stichpunktartig zusammengestellt.

### Wellenauflauf

- Wellenauflaufergebnisse im brandenden und Übergangsbereich zeigen gute Übereinstimmung mit früheren Versuchen
- Die untersuchten Querströmungen führen zu einer geringen Abminderung der Wellenhöhen am Böschungsfuß
- Schräge Anlaufrichtung der Wellen ergibt leichte Abminderung der Auflaufhöhe

### Wellenüberlauf

- Schräger Wellenangriff hat einen reduzierenden Einfluss auf den Wellenüberlauf; gute Übereinstimmung mit bestehenden Untersuchungen (BMBF-Projekt Schräger Wellenauflauf)
- Eine küstenparallele Strömung hat einen reduzierenden Einfluss auf den Wellenüberlauf
- Wind hat einen Einfluss auf kleine Wellenüberlaufsraten, bei hohen Wellenüberlaufsraten ist der Windeinfluss jedoch vernachlässigbar
- Eine Kombination der verschiedenen Einflussfaktoren ist noch nicht ausreichend untersucht worden.





zu 8.) Erste Ideen für neue Berechnungsansätze liegen vor, werden aber noch verifiziert

zu 9. bis 11.) geplant für 2011

### 1.3 Aussichten für die Erreichung der Ziele des Vorhabens

- Arbeiten sind gut im Zeitplan (vgl. Tabelle 1 und Tabelle 2)
- Erste Ergebnisse der Referenztests stimmen gut mit bestehenden Untersuchungen überein (siehe Bericht)
- Erste Analysen der Untersuchungen zeigen plausible Ergebnisse
- Es sind keine Änderungen in dem weiteren Vorgehen des Projektes geplant
- Die Diskussion von Modell- und Maßstabeffekten wurde auf Ende 2010 verschoben. Sie beeinflusst nicht die Messergebnisse und kann im Anschluss an die Auswertung durchgeführt werden. So kann sich die Diskussion auch auf neue Ergebnisse beziehen.

### 1.4 Ergebnisse von dritter Seite, die für die Durchführung des Vorhabens relevant sind

Es sind keine Ergebnisse von dritter Seite bekannt geworden, die für die Durchführung der vorliegenden Arbeit relevant sind.

### 1.5 Änderungen in der Zielsetzung

Zurzeit sind keine Änderungen der Zielsetzungen vorgesehen.

### 1.6 Fortschreibung des Verwertungsplans

Weitreichende Ziele des Projektes:

- Ermittlung neuer Bemessungsansätze für die Bestimmung der Freibordhöhe von Ästuar- und Seedeichen unter Berücksichtigung von Wind und Strömung
- Höhere Sicherheit von Deichen, ggf. Einsparungen von Sanierungs- und / oder Baukosten
- Es ist geplant, die Ergebnisse in die Erarbeitung des International Levee Manual einfließen zu lassen

## Anhang

Preliminary report of FlowDike-D

“Influence of wind and current on wave run-up and wave overtopping”

### Veröffentlichungen

Brüning, A.; Gilli, S.; Lorke, S.; Pohl, R.; Schlüter, F.; Spano, M.; van der Meer, J.; Werk, S.; Schüttrumpf, H. (2009); FlowDike - Investigating the effect of wind and current on wave run-up and wave overtopping; 4th SCACR - International Short conference on APPLIED COASTAL RESEARCH, Barcelona

Brüning, A.; Gilli, S.; Lorke, S.; Pohl, R.; Schlüter, F.; Spano, M.; van der Meer, J.; Werk, S.; Schüttrumpf, H. (2010); FlowDike - Investigating the effect of wind and current on wave run-up and wave overtopping; Hydralab III Joint User Meeting, Hannover

Lorke, S., Brüning, A.; Bornschein, A.; Gilli, S.; Pohl, R.; Spano, M.; van der Meer, J.; Werk, S.; Schüttrumpf, H. (2010); On the effect of wind and current on wave run-up and wave overtopping; 32nd International Conference on Coastal Engineering. Schanghai (accepted for publication)

Pohl, R. (2010); Neue Aspekte der Freibordbemessung an Fluss- und Ästuardeichen; Wasserbauliche Mitteilungen des Institutes für Wasserbau und Technische Hydromechanik der Technischen Universität Dresden, Heft 40, S. 467 - 478 (nicht im Anhang)

Rahlf, H.; Schüttrumpf, H. (2010); Critical overtopping rates for Brunsbüttel lock; 32nd International Conference on Coastal Engineering. Schanghai (accepted for publication)

Schüttrumpf, H. (2009) Wellenüberlauf an Deichen - Stand der Wissenschaft und aktuelle Untersuchungen. 3. Siegener Symposium "Sicherung von Dämmen, Deichen und Stauanlagen". Tagungsband

Van der Meer, J.; Hardeman, B.; Steendam, G.J.; Schüttrumpf, H.; Verheij, H. (2010) Flow depths and velocities at crest and inner slope of a dike, in theory and with the wave overtopping simulator. 32nd International Conference on Coastal Engineering. Schanghai (accepted for publication)



FlowDike-D

**Influence of wind and current  
on wave run-up and  
wave overtopping**

Preliminary report 2009

Dipl.-Ing. Stefanie Lorke<sup>1</sup>  
Dipl.-Ing. Anja Brüning<sup>1</sup>  
Dr.-Ing. Antje Bornschein<sup>2</sup>  
Dipl.-Ing. Stefano Gilli<sup>2</sup>  
cand.-Ing. Nadine Krüger<sup>2</sup>  
Univ.-Prof. Dr.-Ing. Holger Schüttrumpf<sup>1</sup>  
Prof. Dr.-Ing. habil. Reinhard Pohl<sup>2</sup>

Aachen and Dresden, March 2010

---

<sup>1</sup> Institute of Hydraulic Engineering and Water Resources Management, RWTH Aachen University, Germany

<sup>2</sup> Institute of Hydraulic Engineering and Technical Hydromechanics, TU Dresden, Germany

---

**Following partners and authors are responsible for the chapters:**

|            |   |  |
|------------|---|--|
| Chapter 1  | IWD (TU Dresden):<br>IWW (RWTH Aachen): | Bornschein, Gilli, Pohl<br>Brüning, Lorke, Schüttrumpf |
| Chapter 2  | IWW (RWTH Aachen):                      | Brüning, Lorke, Schüttrumpf                            |
| Chapter 3  | IWD (TU Dresden):<br>IWW (RWTH Aachen): | Bornschein, Gilli, Pohl<br>Brüning, Lorke, Schüttrumpf |
| Chapter 4  | IWD (TU Dresden):<br>IWW (RWTH Aachen): | Bornschein, Gilli, Pohl<br>Brüning, Lorke, Schüttrumpf |
| Chapter 5  | IWD (TU Dresden):<br>IWW (RWTH Aachen): | Bornschein, Gilli, Pohl<br>Brüning, Lorke, Schüttrumpf |
| Chapter 6  | IWD (TU Dresden):                       | Bornschein, Gilli, Pohl                                |
| Chapter 7  | IWD (TU Dresden):                       | Bornschein, Gilli, Pohl                                |
| Chapter 8  | IWW (RWTH Aachen):                      | Brüning, Lorke, Schüttrumpf                            |
| Chapter 9  | IWD (TU Dresden):<br>IWW (RWTH Aachen): | Bornschein, Gilli, Pohl<br>Brüning, Lorke, Schüttrumpf |
| Chapter 10 | IWD (TU Dresden):<br>IWW (RWTH Aachen): | Bornschein, Gilli, Pohl<br>Brüning, Lorke, Schüttrumpf |

## Table of contents

|  |           |
|--|-----------|
| List of figures  | III       |
| List of tables   | VIII      |
| <b>1 Introduction</b>  | <b>1</b>  |
| <b>2 Experimental procedure</b>  | <b>3</b>  |
| 2.1 Test program for FlowDike 1 .....  | 3         |
| 2.2 Test program for FlowDike 2 .....  | 4         |
| 2.3 Short overview of the data storage management.....   | 6         |
| <b>3 Model construction and instrumentation</b>  | <b>8</b>  |
| 3.1 Configuration .....  | 8         |
| 3.1.1 General remarks .....  | 8         |
| 3.1.2 Details of facility - Basin, Wave generator, Weir, Wind generator, Data acquisition.....   | 8         |
| 3.1.3 Construction of 1:3 dike – FlowDike 1 .....  | 10        |
| 3.1.4 Construction of 1:6 dike – FlowDike 2 .....  | 12        |
| 3.2 Instrumentation .....  | 14        |
| 3.2.1 Remarks .....  | 14        |
| 3.2.2 Measurement devices .....  | 14        |
| 3.2.3 Wave Field (Wave gauges, ADV) .....  | 17        |
| 3.2.4 Wind Field (Wind machine, Anemometer) .....  | 19        |
| 3.2.5 Current (Weir, ADV, Micro propeller) .....   | 22        |
| 3.2.6 Run-up (Capacitive gauge, Camera, Step gauge) .....  | 23        |
| 3.2.6.1 Wave run-up plate .....  | 23        |
| 3.2.6.2 Wave run-up gauge .....  | 24        |
| 3.2.6.3 Digital video cameras .....  | 26        |
| 3.2.6.4 Step gauge .....   | 27        |
| 3.2.7 Overflow velocity and layer thickness (Micro propeller, Wave gauge, Pressure sensor) ..... | 27        |
| 3.2.8 Overtopping (Load cell, Pump).....   | 28        |
| 3.3 Calibration.....   | 31        |
| 3.3.1 Gauge scale adaptation.....  | 31        |
| 3.3.2 Capacitive run-up gauge calibration.....   | 31        |
| <b>4 Literature review</b>   | <b>33</b> |
| 4.1 State of the Art.....  | 33        |
| 4.2 Influencing variables.....   | 34        |
| <b>5 Data processing</b>   | <b>37</b> |
| 5.1 Remarks .....  | 37        |
| 5.2 Evaluation methods.....  | 37        |
| 5.3 Data processing of the reference test, wave 1.....   | 38        |

---

|          |   |           |
|----------|---|-----------|
| 5.3.1    | Wave field .....  | 38        |
| 5.3.2    | Run-up .....  | 40        |
| 5.3.2.1  | Video analysis .....  | 40        |
| 5.3.2.2  | Measurement results of the run-up-gauge .....                             | 42        |
| 5.3.2.3  | Determination of $R_{2\%}$ .....  | 42        |
| 5.3.3    | Overtopping .....   | 43        |
| 5.3.4    | Flow velocity on the crest .....  | 43        |
| 5.3.5    | Flow depth on the crest .....   | 44        |
| <b>6</b> | <b>Analysis of wave field</b> .....                                       | <b>46</b> |
| <b>7</b> | <b>Analysis on run-up</b> .....   | <b>52</b> |
| 7.1      | Remarks .....   | 52        |
| 7.2      | Comparison between capacitive gauge and video .....                       | 52        |
| 7.3      | Run-up height $R_{2\%}$ and relative run-up height $R_{2\%}/H_{m0}$ ..... | 53        |
| 7.3.1    | Influence of the wave direction $\theta$ .....                            | 58        |
| 7.3.2    | Influence of current .....  | 60        |
| <b>8</b> | <b>Analysis on overtopping</b> .....                                      | <b>62</b> |
| 8.1      | Introduction .....  | 62        |
| 8.2      | Methods .....   | 62        |
| 8.3      | Influence of wave direction .....   | 64        |
| 8.4      | Analysis of the reference test serie .....                                | 66        |
| 8.5      | Influence of wind .....   | 69        |
| 8.6      | Influence of current .....  | 71        |
| 8.7      | Influence of with wind and current .....                                  | 73        |
| 8.8      | Reduction factors .....   | 75        |
| <b>9</b> | <b>Conclusion</b> .....   | <b>78</b> |
|          | <b>Glossary</b> .....   | <b>80</b> |
|          | <b>Notation</b> .....   | <b>82</b> |
|          | <b>Annex</b> .....  | <b>84</b> |

## List of figures

|             |   |    |
|-------------|---|----|
| Figure 3.1  | Completed dike slope (view from downstream), wave generator (paddles) and wind generator (fans) on the left side. ....    | 8  |
| Figure 3.2  | Upstream edge of the dike with wave absorption and beverage racks; Metallic wave absorber in front of the weir .....      | 9  |
| Figure 3.3  | Platform with data acquisition; Stand with amplifier and A/D converter .....  | 10 |
| Figure 3.4  | Overtopping boxes in front of the variable crest (left); Run-up board and variable crest during construction (right)..... | 10 |
| Figure 3.5  | Cross section of overtopping unit for the 70 cm crest .....   | 11 |
| Figure 3.6  | Wave run-up plate and rack with both digital cameras (left); Capacitive gauge, clock and scale (right) .....              | 11 |
| Figure 3.7  | Digital step gauge within the 70 cm slope (left); Capacitive wave run-up gauge on the dike slope (right) .....            | 12 |
| Figure 3.8  | View from the upstream inlet of the 1:6 dike setup, wind machines and wave gauges in front of the dike .....              | 13 |
| Figure 3.9  | Plywood boxes and drilled holes for pressure cells .....  | 13 |
| Figure 3.10 | Model setup 1 (FlowDike 1) with instruments and flow direction (1:3 sloped dike) .....                                    | 14 |
| Figure 3.11 | Model setup 4 (FlowDike 2) with instruments and flow direction (1:6 sloped dike) .....                                    | 15 |
| Figure 3.12 | Overview of the basin: Wind machines; Wave array, Anemometer; Dike and overtopping unities . .....                        | 18 |
| Figure 3.13 | Wave gauge array with minilab SD-12 (encircled).....  | 18 |
| Figure 3.14 | Anemometer (left) and fan wheel for air velocity measurement (right) .....  | 19 |
| Figure 3.15 | Wind velocity distribution for a frequency of 49 Hz (FlowDike 1) .....  | 20 |
| Figure 3.16 | Wind velocity distribution for a frequency of 25 Hz (FlowDike 1) .....  | 20 |
| Figure 3.17 | Wind velocity distribution for a frequency of 49 Hz (FlowDike 2) .....  | 21 |
| Figure 3.18 | Wind velocity distribution for a frequency of 25 Hz (FlowDike 2) .....  | 21 |
| Figure 3.19 | Beam upstream the wave machine; ADV; Micro propeller (FlowDike 1) .....   | 22 |

|              |  |    |
|--------------|--|----|
| Figure 3.20  | Beam upstream the wave machine with current devices (FlowDike 2).....  | 23 |
| Figure 3.21  | Wave run-up plate and rack with both digital cameras .....   | 24 |
| Figure 3.22: | Schema of data collecting using the capacitive wave run-up gauge .....   | 25 |
| Figure 3.23: | Capacitive wave run-up gauge on the dike slope– detailed view with the two electrodes and distance pieces. ....  | 25 |
| Figure 3.24: | Left: USB-camera, Right: Both cameras mounted on a rack in the model setup .....   | 26 |
| Figure 3.25  | Measurement of velocity and depth of flow on the crest.....  | 27 |
| Figure 3.26  | Micropropeller (left) and wave gauge (right) measurement for a sequence (s1_03_30_w5_00_00) .....  | 28 |
| Figure 3.27  | Measurement of pressure, velocity and depth of flow on the crest .....   | 28 |
| Figure 3.28  | Overtopping boxes with channel and measurement devices for flow depth and flow velocity measurements .....   | 29 |
| Figure 3.29  | Overtopping measurement a whole test (s1_03_30_w5_00_+00).....   | 30 |
| Figure 3.30  | Overtopping measurement for a sequence of 20 s (s1_03_30_w5_00_+00).....   | 30 |
| Figure 3.31  | Run-up gauge calibration (set-up 1) .....  | 31 |
| Figure 3.32  | Kalibrierung des kapazitiven Auflaufpegels beim Setup 2 .....  | 32 |
| Figure 3.33  | Kalibrierung des kapazitiven Auflaufpegels beim Setup 3 .....  | 32 |
| Figure 4.1   | Reduction Factor ( $\gamma_{\theta} = \gamma_B$ ), Reference: SCHÜTTRUMPF (2003).....  | 33 |
| Figure 5.1   | Raw data for the wave gauge array of gauges 9-5 .....  | 39 |
| Figure 5.2   | Results for spectral energy density (frequency domain); FlowDike 1.....  | 39 |
| Figure 5.3   | Linear distribution of wave height $H_{m0}$ over a Raleigh scale for a Jonswap spectrum for wave gauge array 9-5 (left) and wave gauge array 14-10 (right); FlowDike 1 ..... | 40 |
| Figure 5.4   | MATLAB interface which was used to analyse video films .....   | 40 |
| Figure 5.5   | Detected position of the highest wave tip on the run-up plate (red line with green triangle) .....   | 41 |
| Figure 5.6   | Overtopping raw data (left) and calculated overtopping discharge (right).....  | 43 |
| Figure 5.7   | Raw data with crossing level - micro propellers on 70 cm crest (left); micro propeller on 60 cm crest (right) .....  | 44 |
| Figure 5.8   | Exceedance curves for micro propellers.....  | 44 |

|             |   |    |
|-------------|---|----|
| Figure 5.9  | Raw data with crossing level – wave gauges on 70 cm crest (left); wave gauges on 60 cm crest (right)  | 45 |
| Figure 5.10 | Exceedance curves for wave gauges   | 45 |
| Figure 6.1  | Significant wave height $H_{m0}$ for the reference model test calculated at each wave gauge of the two sets of wave gauges (no. of wave spectrum see Table 2.1)   | 46 |
| Figure 6.2  | Significant wave height $H_{m0}$ of the attacking spectrums, results from the reference model tests (left: $H_{m0}$ [cm], right: $H_{m0}$ relative to the wave height created by the wave maker $H_{WM}$ )                  | 47 |
| Figure 6.3  | Energy density versus frequency: values of the incident, reflected and superposed spectrum calculated for the two sets of wave gauges (reference model test, avi-file no. 145 (see Table A 1) and wave spectrum no. 2)      | 47 |
| Figure 6.4  | Energy density versus frequency: values of the incident, reflected and superposed spectrum calculated for the two sets of wave gauges (reference model test, avi-file no. 144 (see Table A 1) and wave spectrum no. 1)      | 48 |
| Figure 6.5  | Significant wave height measured by wave gauges no. 1: comparison between reference tests and model tests with only one different influencing parameter (wind, wave direction, current)                                     | 49 |
| Figure 6.6  | Significant wave height measured by wave gauges no. 2: comparison between reference tests and model tests with only one different influencing parameter (wind, wave direction, current)                                     | 50 |
| Figure 6.7  | Wave period measured by wave gauge set 1: comparison between reference tests and model tests with only one different influencing parameter (wind, wave direction, current)  | 50 |
| Figure 6.8  | Wave period measured by wave gauge set 2: comparison between reference tests and model tests with only one different influencing parameter (wind, wave direction, current)  | 51 |
| Figure 7.1  | Wave run-up depending on time measured by capacitive gauge and video, model test 155  | 52 |
| Figure 7.2  | Wave run-up height $R_{2\%}$ (percentile 2%) for all model tests: comparison between values on basis of video analysis and capacitive gauge measurement   | 53 |
| Figure 7.3  | Relative run-up height $R_{2\%}/H_{m0}$ versus Iribarren number $\xi_{m-1,0}$ (results from video analysis; $H_{m0}$ measured at wave gauge set 1; see Table 2.2 for annotation numbers)                                    | 54 |
| Figure 7.4  | Relative run-up height $R_{2\%}/H_{m0}$ versus Iribarren number $\xi_{m-1,0}$ (results from capacitive gauge; $H_{m0}$ at wave gauge set 1; see Table 2.2 for annotation numbers)   | 54 |
| Figure 7.5  | Relative run-up height $R_{2\%}/H_{m0}$ versus Iribarren number $\xi_{m-1,0}$ (results from capacitive gauge; $H_{m0}$ at wave gauge set 1; each setup is marked by different colour; see Table 2.2 for annotation numbers) | 55 |
| Figure 7.6  | Relative run-up measured by capacitive gauge: comparison between reference tests and model tests with only one different influencing parameter (wind, wave direction, current)  | 56 |

|             |   |    |
|-------------|---|----|
| Figure 7.7  | Relative run-up height from video analysis: comparison between reference tests and model tests with only one different influencing parameter (wind, wave direction, current) .....  | 56 |
| Figure 7.8  | Run-up height measured by capacitive gauge: comparison between reference tests and model tests with only one different influencing parameter (wind, wave direction, current) .....  | 57 |
| Figure 7.9  | Run-up height from video analysis: comparison between reference tests and model tests with only one different influencing parameter (wind, wave direction, current) .....   | 58 |
| Figure 7.10 | Ratio $\gamma_\theta$ between relative run-up height of oblique waves and waves with a propagation direction orthogonal to the dike crest (results from model test without current) .....   | 58 |
| Figure 7.11 | Ratio $\gamma_\theta$ between relative run-up height with oblique waves ( $\theta = -30; -15; 15; 30; 45^\circ$ ) and waves with a propagation direction orthogonal to the dike crest (current velocity $v = 0.15$ m/s, (—) GILLI & POHL 2010, see Figure 7.10) ..... | 59 |
| Figure 7.12 | Ratio $\gamma_v$ between relative wave run-up height from model tests with current ( $v = 0.15$ and $0.30$ m/s) and without current .....   | 60 |
| Figure 8.1  | Oblique wave attack; FlowDike 1 (breaking conditions) .....   | 64 |
| Figure 8.2  | Oblique wave attack; FlowDike 1 (non-breaking conditions) .....   | 65 |
| Figure 8.3  | Oblique wave attack; FlowDike 2 (breaking conditions) .....   | 65 |
| Figure 8.4  | Reference test; FlowDike 1 (breaking condition) .....   | 67 |
| Figure 8.5  | Reference test; FlowDike 1 (non-breaking condition) .....   | 68 |
| Figure 8.6  | Reference test; FlowDike 2 (breaking condition) .....   | 69 |
| Figure 8.7  | Wind influence; FlowDike 1 (non-breaking conditions) .....  | 70 |
| Figure 8.8  | Wind influence; FlowDike 2 (breaking conditions) .....  | 71 |
| Figure 8.9  | Current influence; FlowDike 1 (breaking conditions) .....   | 72 |
| Figure 8.10 | Current influence; FlowDike 1 (non-breaking conditions) .....   | 72 |
| Figure 8.11 | Current influence; FlowDike 2 (breaking conditions) .....   | 73 |
| Figure 8.12 | Wind and current influence; FlowDike 1 (non-breaking conditions) .....  | 74 |
| Figure 8.13 | Wind and current influence; FlowDike 2 (breaking condition) .....   | 74 |
| Figure 8.14 | Comparison of reduction factors for obliqueness - FlowDike 1 and FlowDike 2 with investigations by OUMERACI ET AL. (2001) .....   | 77 |

---

**Annex**

|            |  |    |
|------------|--|----|
| Figure A 1 | Definition sketch for wave run-up and wave overtopping (Reference: OUMERACI ET AL. (2001)) | 81 |
| Figure A 2 | Setup 1 - angles of wave attack $0^\circ$ , $+15^\circ$ und $-15^\circ$ (FlowDike 1) ..... | 84 |
| Figure A 3 | Setup 2 - angles of wave attack $-30^\circ$ (FlowDike 1) .....                             | 84 |
| Figure A 4 | Setup 3 - angles of wave attack $+30^\circ$ und $+45^\circ$ (FlowDike 1) .....             | 85 |
| Figure A 5 | Setup 4 - angles of wave attack $0^\circ$ , $+15^\circ$ und $-15^\circ$ (FlowDike 2) ..... | 85 |
| Figure A 6 | Setup 5 - angles of wave attack $-30^\circ$ (FlowDike 2) .....                             | 86 |
| Figure A 7 | Setup 6 - angles of wave attack $+30^\circ$ und $+45^\circ$ (FlowDike 2) .....             | 86 |
| Figure A 8 | Calibration curves for micropropeller from TU Braunschweig .....                           | 87 |
| Figure A 9 | Calibration curves for micropropeller of RWTH Aachen .....                                 | 87 |

---

## List of tables

|                  |   |    |
|------------------|---|----|
| Table 2.1        | JONSWAP wave spectra – parameters for 1:3 slope, water level: 0.50 m .....                                      | 3  |
| Table 2.2        | Final test program (FlowDike 1) .....   | 4  |
| Table 2.3        | JONSWAP wave spectra – parameters for 1:6 slope, water level: 0.55 m .....                                      | 5  |
| Table 2.4        | Final test program (FlowDike 2) .....   | 6  |
| Table 8.1        | Slope inclination $b$ and reduction factors ( $\gamma$ ) for influencing variables (wind and current influence) | 76 |
| Table 8.2        | Slope inclination $b$ and reduction factors ( $\gamma_b$ ) for oblique wave attack.....                         | 76 |
| <br><b>Annex</b> |   |    |
| Table A 1        | Model tests and associated films (AVI-file 101 to 152).....   | 88 |
| Table A 2        | Model tests and associated films (AVI-file 153 to 201).....   | 89 |
| Table A 3        | Model tests and associated films (AVI-file 202 to 247).....   | 90 |

# 1 Introduction

A variety of structures has been built in the past to protect the adjacent areas during high water levels and storm surges from coastal or river flooding. Common use in practice is the application of smooth sloped dikes as well as steep or vertical walls. The knowledge of the design water level, wind surge, wave run-up and/or wave overtopping is used to determine the crest height of these structures. Due to the return interval considered of the design water level, the uncertainties in applied formula for wave run-up respectively wave overtopping and the incoming wave parameters, wave overtopping can not be avoided at all times.

Relevant for the freeboard design in wide rivers, estuaries and at the coast, are the incoming wave parameters at the toe of the structure. At rivers these are probably influenced by local wind fields and sometimes by strong currents - occurring at high water levels mostly parallel to the structure (cross flow). In the past no investigations were made on the combined effects of wind and current on wave run-up and wave overtopping. Only few papers, dealing either with wind effects or current influence, are publicised. To achieve an improved design of structures these effects should not be neglected, otherwise the lack of knowledge may result in too high and expensive structures or in an under design of the flood protection structure which increases the risk of flooding.

Today systematically investigations about the influence of dike-parallel flow on the wave run-up and overtopping are not yet known. Furthermore detailed studies about the interaction of wind and current in their impact on wave run-up and overtopping are not available in national or international publications. Nevertheless data from previous KFKI projects "Oblique wave attack at sea dikes" and "Loading of the inner slope of sea dikes by wave overtopping" and from the CLASH-database are at hand for comparison purposes. They represent a setup without wind and dike parallel flow. The aim of the research project presented is to close the knowledge by experimental investigations in an offshore wave basin together with currents and wind.

The subject of investigation is a dike with an outer slope of 1:3 and 1:6 which is typical for rivers, estuaries and coastal lagoons. The research deals with the wave run-up and overtopping rate originated by short-crested waves considering different current and wind velocities, dike crest levels and wave directions. The obtained data form the basis to determine the dependencies between the wave run-up respectively the overtopping rate and the swell, coastal parallel flow and wind under consideration of former approaches and theoretically analysis. Furthermore the results ought to be incorporated into freeboard design of estuary and sea dikes.

## **Model tests at the DHI in Hørsholm (Denmark)**

The experimental investigations on run-up and overtopping for smooth sloped dikes were performed twice at the DHI in Hørsholm. The first part of the model tests for a 1:3 slope took place in January 2009 (titled FlowDike 1 in the following). In November 2009 the second phase of investigations (FlowDike 2) were performed for a 1:6 sloped dike.

During both model tests, the dike was divided into two separate parts to perform wave run-up and wave overtopping experiments simultaneously. This was done due to the fact that the measuring area within the basin and the testing time was limited. Overtopping was measured for two different crest heights (70 cm and 60 cm) in order to include the influence of the freeboard and acquire more data for

the analysis. A first overall view of the model setup and a more detailed description of the model tests are given in chapter 2.3.

The test program covered model tests on wave run-up and wave overtopping with 3 setups. Combinations with and without currents and with and without wind for different wave conditions were scheduled. Wave conditions included long crested waves and perpendicular, respectively oblique wave attack.

Acquired raw data are processed to determine the degree of dependence of wave run-up and wave overtopping on wind, current and oblique wave attack. Therefore the incoming wave parameters at the toe of the structure are measured for different variations of the influencing variables. Existent approaches and theoretical investigations will be used to verify and compare the data. Finally design formulae for freeboards of dikes are supposed to be developed or modified.

### **Status quo of the project work**

This work is a preliminary report. It includes both test programs, model construction, instrumentation and short literature view, data processing for the reference test and first results of the analysis of the wave field, wave run-up and wave overtopping.

The analysis of the wave run-up is done for the three parameters of interest wave direction, wind and current for FlowDike 1 while the analysis for FlowDike 2 is in progress. Up to now the combined effect are not considered in that preliminary report.

The wave overtopping is analysed for both FlowDike 1 and FlowDike 2 for the three parameters of interest wave direction, wind and current. The combined effects are only done for the combination of wind and current.

It has to be mentioned that a more detailed analysis concerning the wave field, run-up heights and overtopping rates is obligatory in the next steps. The presented results in this report are preliminary.

## 2 Experimental procedure

### 2.1 Test program for FlowDike 1

The original test program for the Hydralab-FlowDike-Project contained 10 test series for investigation of wind and current effects on wave run-up and wave overtopping. Three different angles of wave attack  $0^\circ$ ,  $\pm 15^\circ$ ,  $\pm 30^\circ$  and  $\pm 45^\circ$  should be determined under conditions with or without a current of 0.15 m/s and 0.3m/s and with or without wind of 5 m/s and 10 m/s. Per definition a negative wave angle is with the current and a positive angle against it.

Generation and control of the wave maker was done by using the wave synthesizer, wherein a file for a set of six wave spectra could be stored. The wave spectra differ in two different wave steepness' and three different wave heights, covering the field of small (or no) overtopping to high overtopping. Each test series was foreseen to contain a set of the six wave spectra as illustrated in Table 2.1.

Table 2.1 JONSWAP wave spectra – parameters for 1:3 slope, water level: 0.50 m

| Wave spectra | $H_s = H_{WM}$<br>[m] | $T_p$<br>[s] | Steepness $s$<br>[-] | Duration<br>[min] | No. of Waves<br>[-] |
|--------------|-----------------------|--------------|----------------------|-------------------|---------------------|
| w1           | 0.07                  | 1.474        | 0.025                | 23                | 1021                |
| w2           | 0.07                  | 1.045        | 0.05                 | 16                | 1002                |
| w3           | 0.1                   | 1.76         | 0.025                | 27                | 1004                |
| w4           | 0.1                   | 1.243        | 0.05                 | 19                | 1001                |
| w5           | 0.15                  | 2.156        | 0.025                | 33                | 1002                |
| w6           | 0.15                  | 1.529        | 0.05                 | 24                | 1027                |

To improve the testing time the dike was divided in two separate parts to perform wave run-up and wave overtopping at the same time. The domain of fully developed sea state is limited by the length of the wave machine. Now the influence of current and angle of wave attack restrict the section for a reliable measurement of run-up and overtopping on the dike. Therefore three different setup configurations have been installed to cover the effective measurement range for all angles of wave attack issued within the test programme. The first setup covered perpendicular wave attack and tests for  $\pm 15^\circ$ . Setup 2 included all tests for  $-30^\circ$  and  $-45^\circ$  and setup 3 was installed for the angle of  $+30^\circ$  and  $+45^\circ$ . A detailed overall view for every test setup is given in the Annex (Figure A 2 to Figure A 7).

Table 2.2 Final test program (FlowDike 1)

| Date           | Testseries | Duration [h] | Wave direction [°] | Current [m/s] | Wind speed [m/s] | Wave spectra |
|----------------|------------|--------------|--------------------|---------------|------------------|--------------|
| <b>Setup 1</b> |            |              |                    |               |                  |              |
| 02-02-09       | T3         | 3            | 0                  | 0.3           | 0                | w1 to w6     |
| 03-02-09       | T8         | 1.5          | 0                  | 0.3           | 10               | w1, w3, w5   |
| 03-02-09       | T19        | 3            | -15                | 0.3           | 0                | w1 to w6     |
| 04-02-09       | T16        | 3            | 15                 | 0.3           | 0                | w1 to w6     |
| 04-02-09       | T8b        | 1.5          | 0                  | 0.3           | 5                | w1, w3, w5   |
| 05-02-09       | T1         | 3            | 0                  | 0             | 0                | w1 to w6     |
| 05-02-09       | T6b        | 1.5          | 0                  | 0             | 5                | w1, w3, w5   |
| 05-02-09       | T6         | 1.5          | 0                  | 0             | 10               | w1, w3, w5   |
| 06-02-09       | T12        | 3            | -15                | 0             | 0                | w1 to w6     |
| 06-02-09       | T11 = T3b  | 3            | 0                  | 0.15          | 0                | w1 to w6     |
| 09-02-09       | T13        | 3            | -15                | 0.15          | 0                | w1 to w6     |
| 09-02-09       | T15        | 3            | 15                 | 0.15          | 0                | w1 to w6     |
| <b>Setup 2</b> |            |              |                    |               |                  |              |
| 11-02-09       | T2         | 3            | -30                | 0             | 0                | w1 to w6     |
| 11-02-09       | T7b        | 1.5          | -30                | 0             | 5                | w1, w3, w5   |
| 11-02-09       | T7         | 1.5          | -30                | 0             | 10               | w1, w3, w5   |
| 12-02-09       | T20        | 3            | -30                | 0.15          | 0                | w1 to w6     |
| 12-02-09       | T4         | 3            | -30                | 0.3           | 0                | w1 to w6     |
| 13-02-09       | T9b        | 1.5          | -30                | 0.3           | 5                | w1, w3, w5   |
| 13-02-09       | T9         | 1.5          | -30                | 0.3           | 10               | w1, w3, w5   |
| <b>Setup 3</b> |            |              |                    |               |                  |              |
| 17-02-09       | T18        | 3            | 45                 | 0             | 0                | w1 to w6     |
| 18-02-09       | T5         | 3            | 30                 | 0.3           | 0                | w1 to w6     |
| 18-02-09       | T14        | 3            | 45                 | 0.3           | 0                | w1 to w6     |
| 19-02-09       | T21        | 3            | 30                 | 0.15          | 0                | w1 to w6     |
| 19-02-09       | T17        | 3            | 45                 | 0.15          | 0                | w1 to w6     |

Due to a more inclined wave direction ( $\theta = -45^\circ$ ) the wave run-up board was situated a little bit outside the part of the dike where the fully developed sea arrived. Moreover the almost diagonal up rushing waves could not develop their full run-up height because of the limitation in run-up board width. This will have to be considered during post processing and data analysis. The recorded video films were serially numbered, see Annex Table A 1 to Table A 3. The tables contain in addition the record date, setup number and test series, the name of the file respectively the folder with the raw data as well as comments and remarks.

## 2.2 Test program for FlowDike 2

The JONSWAP spectra from FlowDike 1 would not give sufficient overtopping for the analysis with a slope of the dike of 1:6 (FlowDike 2). To increase the overtopping for FlowDike 2, the Still Water Level (SWL) had to be raised about 0.05 m to a water depth of 0.55 m. Additionally the wave height was increased in comparison to FlowDike 1 for the spectra w1 to w4 with respect to the fixed

steepness. The series T1, T3 and T4 were done with the old and new wave and water level conditions, like a water level of 0.50 m and 0.55 m and the old and new wave spectra.

Table 2.3 JONSWAP wave spectra – parameters for 1:6 slope, water level: 0.55 m

| Wave spectra | $H_s = H_{WM}$<br>[m] | $T_p$<br>[s] | Steepness $s$<br>[-] | Duration<br>[min] | No. of Waves<br>[-] |
|--------------|-----------------------|--------------|----------------------|-------------------|---------------------|
| w1           | 0.09                  | 1.670        | 0.025                | 27                | 1058                |
| w2           | 0.09                  | 1.181        | 0.05                 | 19                | 1053                |
| w3           | 0.12                  | 1.929        | 0.025                | 32                | 1086                |
| w4           | 0.12                  | 1.364        | 0.05                 | 22                | 1056                |
| w5           | 0.15                  | 2.156        | 0.025                | 35                | 1062                |
| w6           | 0.15                  | 1.525        | 0.05                 | 25                | 1073                |

On the one hand an additional current of 0.4 m/s was adapted, because they give another important item for the analysis. On the other hand, wind tests were done only for or wind velocity of 10 m/s (49 Hz).

It has to be stressed out that all not repeated tests could still be analysed. Within these analyses the former conditions of FlowDike 1 (water level at 0.5 m and wave conditions from Table 2.1) will have to be taken into account. The following Table 2.4 includes the schedule of the realised test series. The three different setups, as mentioned for FlowDike 1, were repeated in the same order. To avoid confusion in the data storage the numeration of the setups was followed so setup 1, 2, 3 for the 1:3 dike will be named setup 4, 5, 6 for the 1:6 dike.

Table 2.4 Final test program (FlowDike 2)

| Date           | Testseries | Duration [h] | Wave direction [°] | Current [m/s] | Wind speed [m/s] | Wave spectra      |
|----------------|------------|--------------|--------------------|---------------|------------------|-------------------|
| <b>Setup 4</b> |            |              |                    |               |                  |                   |
| 17-11-09       | T4         | 3            | 0                  | 0.3           | 0                | w1 to w6 (FD 1)   |
| 18-11-09       | T5         | 1.5          | 0                  | 0.3           | 10               | w1, w3, w5 (FD 1) |
| 18-11-09       | T6         | 1.5          | 0                  | 0.3           | 5                | w1, w3, w5        |
| 18-11-09       | T2         | 1.5          | 0                  | 0             | 5                | w1, w3, w5        |
| 19-11-09       | T3         | 1.5          | 0                  | 0             | 10               | w1, w3, w5        |
| 19-11-09       | T1         | 3            | 0                  | 0             | 0                | w1 to w6 (FD 1)   |
| 20-11-09       | T32        | 3            | 15m                | 0.3           | 0                | w1 to w6 (FD 1)   |
| 20-11-09       | T33        | 1.5          | 15p                | 0.3           | 0                | w1 to w6 (FD 1)   |
| 23-11-09       | T34        | 2            | 15m                | 0             | 0                | w1 to w6          |
| 24-11-09       | T1a        | 3.5          | 0                  | 0             | 0                | w1 to w6          |
| 25-11-09       | T4a        | 3.5          | 0                  | 0.3           | 0                | w1 to w6          |
| 25-11-09       | T3a        | 2            | 0                  | 0             | 10               | w1, w3, w5        |
| 26-11-09       | T7         | 3.5          | 0                  | 0.15          | 0                | w1 to w6          |
| 26-11-09       | T8         | 2            | 0                  | 0.15          | 10               | w1, w3, w5        |
| 26-11-09       | T35        | 1            | 0                  | 0.15          | 0                | w1, w2 (FD 1)     |
| 27-11-09       | T10        | 3.5          | 0                  | 0.40          | 0                | w1 to w6          |
| 27-11-09       | T11        | 2            | 0                  | 0.40          | 10               | w1, w3, w5        |
| 27-11-09       | T36        | 1            | 0                  | 0.40          | 10               | w1, w2 (FD 1)     |
| <b>Setup 5</b> |            |              |                    |               |                  |                   |
| 01-12-09       | T16        | 3.5          | 30m                | 0.40          | 0                | w1 to w6          |
| 01-12-09       | T17        | 2            | 30m                | 0.40          | 10               | w1, w3, w5        |
| 01-12-09       | T15        | 2            | 30m                | 0             | 10               | w1, w3, w5        |
| 02./03-12-     | T13        | 3.5          | 30m                | 0             | 0                | w1 to w6          |
| 02-12-09       | T20        | 2            | 30m                | 0.3           | 10               | w1, w3, w5        |
| 02-12-09       | T19        | 3.5          | 30m                | 0.3           | 0                | w1 to w6          |
| 03-12-09       | T22        | 3.5          | 30m                | 0.15          | 0                | w1 to w6          |
| <b>Setup 6</b> |            |              |                    |               |                  |                   |
| 07-12-09       | T27        | 3.5          | 45p                | 0.15          | 0                | w1 to w6          |
| 07/08-12-      | T27        | 3.5          | 45p                | 0.15          | 0                | w1 to w6          |
| 08-12-09       | T26        | 3.5          | 30p                | 0.15          | 0                | w1 to w6          |
| 09-12-09       | T25        | 3.5          | 45p                | 0             | 0                | w1 to w6          |
| 09-12-09       | T28        | 3.5          | 30p                | 0.3           | 0                | w1 to w6          |
| 10-12-09       | T29        | 3.5          | 45p                | 0.3           | 0                | w1 to w6          |
| 10-12-09       | T30        | 3.5          | 30p                | 0.40          | 0                | w1 to w6          |
| 10-12-09       | T31        | 3.5          | 45p                | 0.40          | 0                | w1 to w6          |

### 2.3 Short overview of the data storage management

For a better structure, evaluated data for the defined series of tests is unified separately for each wave spectra (w1-w6) in excel data process files. One process file includes i.e. the graphics for the spectral energy density, wave height distribution, as well as some exceedance curves for flow velocities and

layer thickness. In section 5.3 the preliminary results of the processed data will be explained by means of test s1\_01\_00\_w1\_00\_00.

As explanation for the given filenames it is stated that they include the main information, such as setup number, test series, current, wave spectra, wind speed and angle of wave attack. A template for all test series would be:

setup no\_Test series no\_current [cm/s]\_wave spectra [i=1..6]\_wind Hz]\_ angle of wave attack.

For example the first test series from FlowDike 1 is named: s1\_01\_00\_wi\_00\_00. The term for angle of wave attack was changed from “-“ to “m” and from “+” to “p” within the system due to the fact that problems occurred during the data processing.

## 3 Model construction and instrumentation

### 3.1 Configuration

#### 3.1.1 General remarks

This chapter describes the details of the facility that remained the same for both model configurations. It also includes a detailed specification of the dimensions and main constructive parts of each setup configuration. Therefore it starts with the description of the 1:3 sloped dike, which is followed by the details for the 1:6 sloped configuration. A plan view of the different setups is given in the Annex.

#### 3.1.2 Details of facility - Basin, Wave generator, Weir, Wind generator, Data acquisition

##### **Basin, Wave generator**

The facility provided by the DHI in Hørsholm (Denmark) is a shallow water wave basin. It has a length of 35 m, a width of 25 m and can be flooded to a maximum water depth of 0.9 m. Along the east side (35 m in length) the basin is equipped with a 18 m long multidirectional wave maker composed of 36-segments (paddles) (see Figure 3.1). The 0.5 m wide and 1.2 m high segments can be programmed to generate multidirectional, long or short crested waves. Dynamic wave absorption is integrated in the DHI wave generation software by an automatic control system called AWACS (Active Wave Absorption Control System). This system uses the signal of separate wave gauges per paddle, to receive the actual wave height to identify and absorb the reflected waves. For further absorption of reflection and diffraction effects gravel and metallic wave absorbers were placed on the upstream and downstream edges of the dike (see Figure 3.2).

During FlowDike 1 problems with the AWACS occurred for some test with wave spectra w5 and w6. In FlowDike 2 the absorption was turned off all along, otherwise the wave generation was impossible, since the wave generator would have stopped during testing. The reason for this is not known yet.



Figure 3.1 Completed dike slope (view from downstream), wave generator (paddles) and wind generator (fans) on the left side.

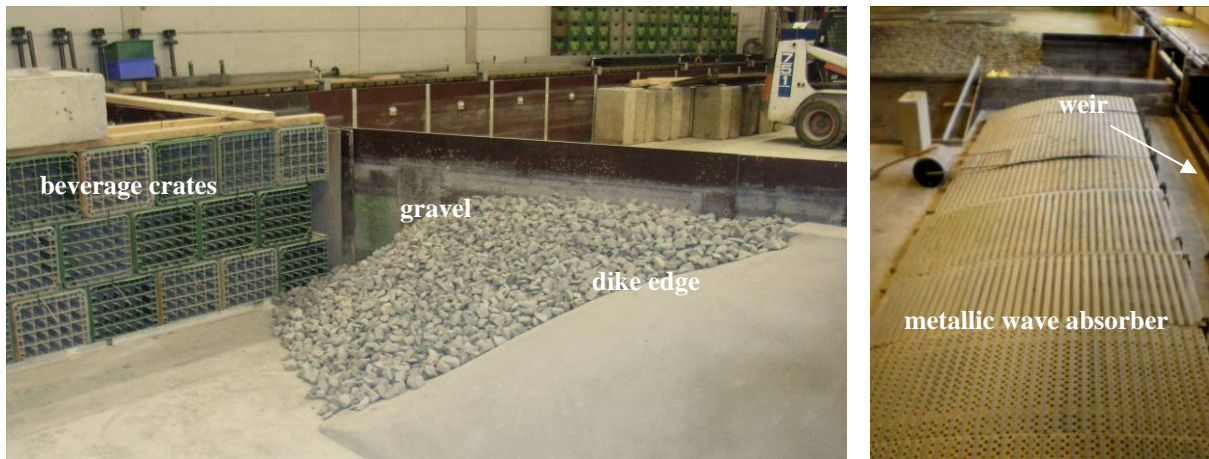


Figure 3.2 Upstream edge of the dike with wave absorption and beverage racks; Metallic wave absorber in front of the weir

### Weir and flow calming

For FlowDike 1 parallel current and constant water depth of 0.5 m were controlled by the flow capacity of the basin pump and an adjustable weir at the downstream edge of the basin. This weir had a length of 7.9 m and was adjusted by means of a long metal plate that could be adjusted in height.

Changes in weir adjustment were made, so for FlowDike 2 it was divided by metal stands into six subdivisions of 1.1 m. In the sections, between the stands, wooden parts for the exact height could be inserted. They were placed beneath the parts with a shorter, but still movable, metal plate. These changes facilitated the weir readjustment. All currents were set for a water depth of 0.55 m and controlled again with the flow capacity.

To provide aligned streamlines within the channel three rows of beverage crates were used as shown in Figure 3.2 to straighten the inflow.

### Wind generator

The wind field could be generated by six wind machines placed on metal stands (80 cm above the basin floor) in front of the wave generator. Therefore two different frequencies were set to produce a homogenous wind field with an assumed mean velocity of 10 m/s (49 Hz) and a lower one of 5 m/s (25 Hz).

### Data acquisition

Only a constant water temperature which is important for the calibration of all wave gauges and especially for the absorption system of the wave generator could be accepted for the accuracy of the tests. Therefore changes of water temperature during the beginning of a tests series with flow induced current was measured.

Data storage was simplified by using the DHI Wave Synthesizer. A sampling frequency of 25 Hz was used during the first investigation phase of FlowDike 1 to include all instrument-signals. This frequency was changed to 40 Hz for the test performed in FlowDike 2, due to the resolution of the pressure sensors which only work with 40 Hz. All acquired data were stored in .dfs0- and .daf-files. A .dfs0-file stores the frequency of the data storage and all desired signals in a readable format for the Wave Synthesizer from MikeZero, while a .daf-file (Digital Anchor File) stores the same information

in a table format. The calibration could easily be made for all instruments connected to an amplifier, such as wave gauges, load cells, micro propeller and pressure sensors. After installation of all measurement devices the whole basin was flooded. Therefore the data acquisition, amplifier, computer and spotlights, which are situated behind the dike, needed to be placed on platforms. An overall view of the data acquisition for the second investigation period illustrates Figure 3.3.



Figure 3.3 Platform with data acquisition; Stand with amplifier and A/D converter

### 3.1.3 Construction of 1:3 dike – FlowDike 1

The toe of the 1:3 dike was situated at a distance of 6.5 m and the SWL at a distance of 8.0 m from the initial position of the wave maker. The structure had a length over all of 26.5 m. This length depended on the allowable measuring sections for all wave directions of interest (see Annex Figure A 2 to Figure A 4); thus for the investigations on current and wind influence a homogeneous wave field in front of the dike was necessary. The backside and crest of the dike are brick-built with a width of 0.28 m and its core was out of compacted gravel covered with a 50 mm concreted layer.

In order to acquire wave overtopping data for freeboard heights of 0.1 m and 0.2 m the dike is divided in two sections. The first 15 m upstream from the weir have a crest height of 60 cm and 11.5 m further up the crest level is 70 cm from the basin floor. In Figure 3.4 a variable crest is visualised that extend the 70 cm crest 7 m downstream. This additional part out of plywood is used to change the setup configuration during the test programme. To prevent different roughness coefficients on the variable crest, the run-up plate and in the gap between the concrete and plywood parts a polish with sand was used.



Figure 3.4 Overtopping boxes in front of the variable crest (left); Run-up board and variable crest during construction (right)

A cross-section for the wave overtopping unit is given in Figure 3.5. For sampling the overtopping water a plywood channel was mounted at the landward edge of the crest to lead the incoming water directly into one of the four overtopping tanks. There were two tanks per section (60 cm and 70 cm crest) and the amount of water was measured by the load cells and wave gauges of each tank. Standard garden pumps were used to empty the tanks during testing, see also the description in chapter 3.2.8. Dry boxes (also named outer boxes) were constructed to contain the overtopping tanks, load cells and wave gauges and prevent these devices from uplift. The dry boxes had to be charged with concrete blocks to prevent themselves from uplift when the basin is flooded.

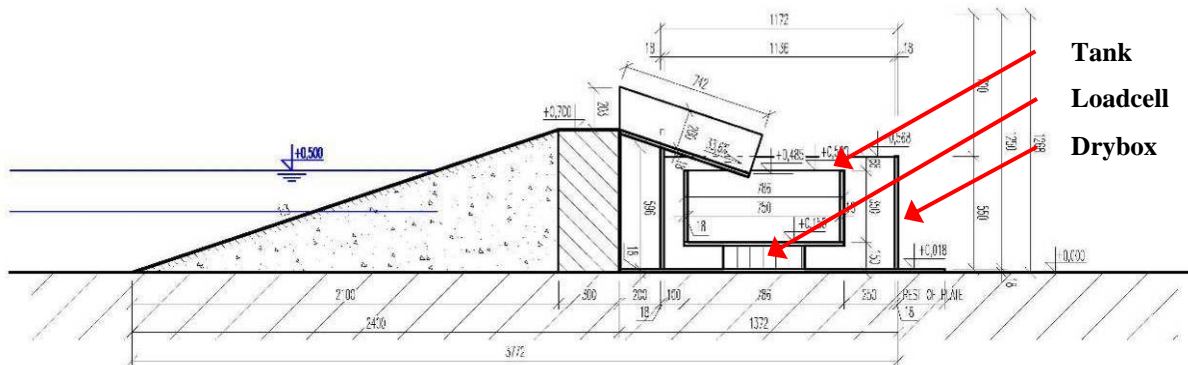


Figure 3.5 Cross section of overtopping unit for the 70 cm crest

For the wave run-up a “run-up board” out of plywood (2 m x 2.5 m) was mounted on the concrete crest to facilitate the up rush measurement by a capacity gauge and video analysis. This plate could be moved easily in its position during the changes of setups. The gap between run-up board and crest edge was filled either with a wooden piece and silicone or with a cement cover.

To get films with a better contrast the wave run-up board was enlightened by a 2000-W-spotlight which was positioned such as the light met the run-up plate within an angle of  $120^\circ$  to the optical axis of the digital cameras. On the left side of the run-up plate a digital radio controlled clock with a 0.4 m x 0.4 m display was positioned due to the purpose of synchronizing the measurements (Figure 3.6).



Figure 3.6 Wave run-up plate and rack with both digital cameras (left); Capacitive gauge, clock and scale (right)

In addition step gauges were inserted in the 70 cm crest part with a distance of 2.2 m between each other. Regarding their short length only an up rush and not the full run-up can be measured and was not analysed yet. The different devices are illustrated in Figure 3.7. The digital signals which came out of the A/D-converter of the capacitive gauge and the step gauges was transmitted to the data collection unit and stored together with the signals of the other measurement equipment.



Figure 3.7 Digital step gauge within the 70 cm slope (left); Capacitive wave run-up gauge on the dike slope (right)

#### 3.1.4 Construction of 1:6 dike – FlowDike 2

Compared to the setup of the first investigations of FlowDike 1 (1:3 sloped dike) the dimensions and some details changed for FlowDike 2. Overtopping units, run-up board and variable crest remained mostly in the same shape or could even be reused. The former inserted step gauges have not been installed during the second investigation period. As a new device, pressure sensors were added to the list of instruments and their positioning had to be taken into consideration during the model configuration.

In order to keep the Still Water Level (SWL) at the same position at 8.0 m from the wave maker, such as during the FlowDike 1 tests, the toe of the 1:6 dike should have been situated at a distance of 5.0 m from the wave maker. Due to the flatter slope of 1:6, the bottom width of the dike from the crest to the toe of the structure increased from 2.10 m to 4.20 m for the 70 cm crest section and from 1.80 m to 3.60 m for the 60 cm section.

With regard to construction failures while positioning the structures the channel width or distance between the toe of the structure and the wave maker decreased. The brick built crest was build 0.6 m closer to the wave maker, so the channel width became 4.40 m instead of 5.0 m and the SWL was situated at 7.40 m from the initial wave maker position. The length of the dike remained 26.5 m depending on the allowable measuring areas for the different wave directions.



Figure 3.8 View from the upstream inlet of the 1:6 dike setup, wind machines and wave gauges in front of the dike

The core of the dike was kept out of compacted gravel covered with 50 mm concrete and the backside and crest of the dike remained with a width of 0.28 m. Only for the newly inserted pressure sensors three gaps were left out in the wall in between the positions for both overtopping channels per crest. In these gaps small plywood boxes with a sand covered top of circa 30 cm x 20 cm have been fitted. For mounting the pressure sensors two holes were drilled within a distance of 24 cm in their lid as Figure 3.9 demonstrates.



Figure 3.9 Plywood boxes and drilled holes for pressure cells

As the essentials of the setup and test programme have not changed, i.e. two different freeboard heights (0.1 m and 0.2 m) and positions for run-up board and overtopping units, both investigations should be quite comparable. At this point it has to be mentioned, that the increase of the water level to 0.55 m after the first test, affected the setup configuration only for the position of the SWL. After the increase the SWL was at 7.70 m instead of 7.40 m from the wave maker and additionally the freeboard height decreased to 0.05 m and 0.15 m, which has to be taken into account for the analysis.

## 3.2 Instrumentation

### 3.2.1 Remarks

This chapter explains the application of the measurement devices in the previously described model configurations. It is structured in seven subsections each of them dealing with one main topic concerning the data acquisition for the following analyse divisions.

During the second phase of investigations (1:6 dike) additional devices were used or former instruments have been left out, compared to the setup of FlowDike 1. Every subdivision starts with the general instrumentation for the 1:3 sloped dike followed by the changes made for FlowDike 2.

### 3.2.2 Measurement devices

For analysis of wind and current influence on wave run-up and wave overtopping in long crested sea state, the alphabetic listed measurement devices below were installed in the basin and on the dike. Better overall views of the placement of measurement devices for both model configurations are given in Figure 3.10 for FlowDike 1 and Figure 3.11 for FlowDike 2.

The drawings give a plan view of the basin with a flow direction of the current (blue arrows) from left to right. The light yellow bars indicate the acceptable measuring area for the set parameters of perpendicular or angled wave attack with and without currents.

At the lower side of the drawing the wind and wave generator are situated. Approximately 2 m further upstream, the beam with two current meters and two micro propellers is indicated. Within the channel two or three wave arrays (FlowDike 2) are displayed in the figure. Each wave gauge array consists of five wave gauges and one velocity meter. For the run up measurements a run up board with the mounted capacitive gauge is situated within the allowable measuring range for perpendicular wave attack with and without currents. The two step gauges are showed in their position in the slope of the 70 cm crest, but only for the FlowDike 1 setup. On each crest two overtopping units are placed as depicted in the sketch. Between the inlet channels of these units, the instruments for flow velocity and flow depth measurement are marked.

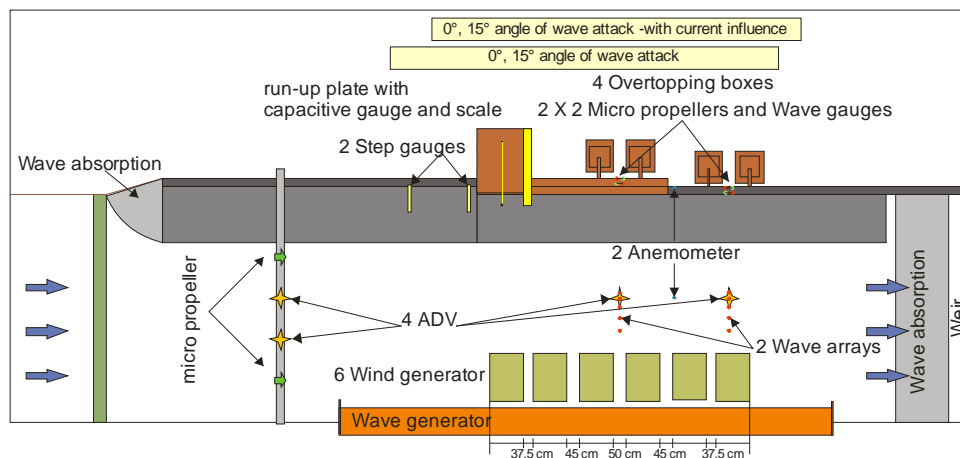


Figure 3.10 Model setup 1 (FlowDike 1) with instruments and flow direction (1:3 sloped dike)

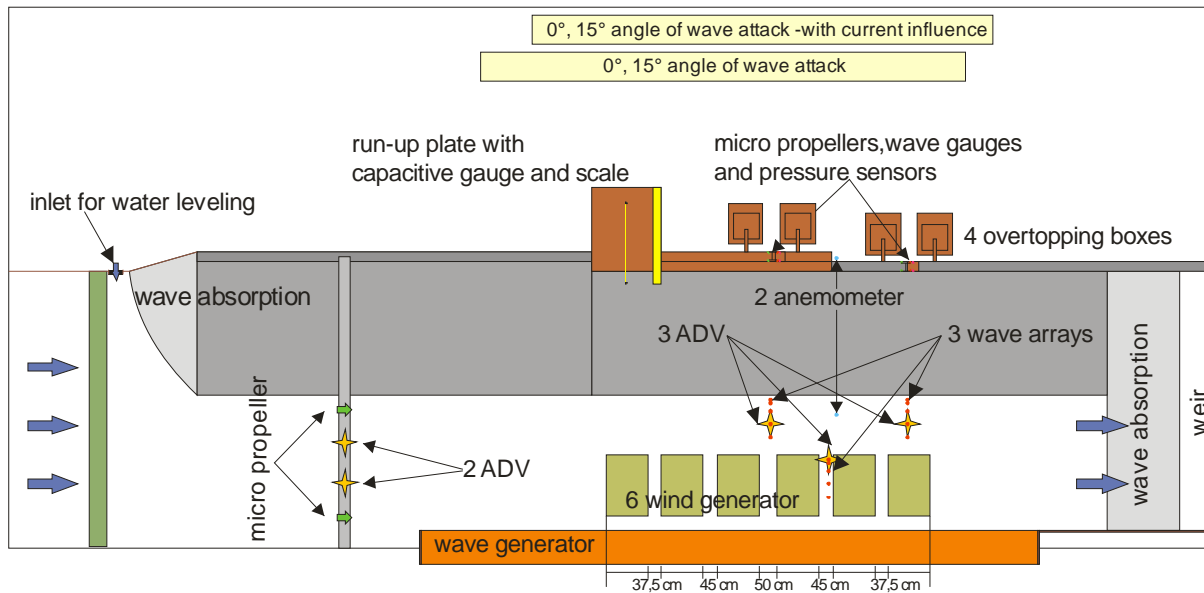


Figure 3.11 Model setup 4 (FlowDike 2) with instruments and flow direction (1:6 sloped dike)

### Instruments:

- Anemometer (TSI):

Two anemometers for wind measurement provided by DHI were installed in the set up. These thin transducers with a small window for the sensor are able to record a range of 0 V – 10 V (0 m/s – 20 m/s) with a frequency of 5 Hz.

- Capacitive gauge:

As schematically shown in Figure 3.22 the required equipment contained a submerged capacitor, a transducer and an A/D-converter. The two electrodes of the capacitor were formed by one isolated and one non isolated wire each 3.5 m long. They were mounted on the run-up plate orthogonally to the dike base. The lower end was fixed about 0.25 m above the bed which is equal to 0.25 below still-water-level (SWL). The upper end was fitted to the highest point of the run-up plate. Thus it is possible to measure both the wave run-up and the run-down. To avoid a water film between the two electrodes after a wave runs down several rubber band spacers assure a minimum distance of about 5 mm between the two wires.

Air or water between the two wires forms the dielectric fluid. Water has a permittivity which is 80 times greater than the permittivity of the air. The variation of the water level produces a measurable variation of the electrical value of the capacitor. The transducer allows loading and unloading the capacitor 25 times per second which is equal to a measurement frequency of 25 Hz. Each value of the time constant  $\tau$  of the capacitor would be transmitted to the A/D-converter as a voltage value. The scale of the voltage value ranged from 0 V to 5 V.

The capacitive gauge was non-sensitive to environmental conditions like changes in water temperature. The calibration was conducted only one time before the test start. Therefore three test with regularly waves with a mean wave height of  $\bar{H}$  of 0.1 m, 0.15 m and 0.2 m were run. The calibrated equation depends on the model setup especially on the wire length and the mounting height. That is why the calibration has to be repeated for each model setup.

- Cameras:

For FlowDike 1 one digital camera was a compact, professional USB 2.0 camera from VRmagic GmbH which is suitable for industrial purposes. The used model VRmC-3 + PRO contained a 1/3 inch-CMOS-sensor which could record up to 69 frames per second. The picture resolution of 754 x 482 pixels was adequate for measurement purposes in the model tests presented herein. The other digital camera was a SONY Camcorder (Model: DCR-TRV900E PAL), with a 3CCD (Charge Coupled Device, 1/4 inch). The objective had a focal distance between 4.3 and 51.6 mm and a 12 x optical zoom.

In FlowDike 2 both cameras were replaced with two others, which have a better resolution. Since the image-processing algorithm works with grey-level images, one color camera was replaced with a more powerful monochrome camera (1/2" Progressive-scan-CCD sensor JAI CM-140 GE of Stemmer Imaging). Its resolution of 1392 x 1040 pixels allows to produce pictures with a precision of 0.5 mm for the wave run-up. The second camera (a color area scan camera) was used for documentation purpose only. It had the same features like the monochrome one but the output-files are three times greater (about 2.6 GB/min). The same objectives as in FlowDike 1 were reused.

- Current meter (Acoustic Doppler Velocity meter (ADV), Minilab SD-12, Vectrino):

Both, ADV's and Vectrino, are a single point, Doppler current meters. Each of them has one ultrasound transmitter and three or even four receivers (ADV/ Vectrino). The current velocity is measured using the Doppler Effect, that is, the shift of the frequency received with respect to the frequency transmitted when the source is moving relative to the receiver. The transmitter generates a short pulse of sound at a known frequency. The energy of the pulse passes through the so-called sampling volume (a small volume of water in which measurements are taken). Part of this energy is reflected by suspended matter along the axis of the receiver, where it is sampled by the velocity meter, whose electronics detect the shift in frequency. According to this, to obtain measurements with a velocity meter based on the Doppler Effect, the presence of suspended matter is necessary for an accurate reflection of the pulse. The sampling volume was set to 25 Hz and a nominal velocity range of  $\pm 100$  cm/s.

The Minilab SD-12 is an ultrasonic current meter. It contains a transducer, a reflector and four receivers that measure the velocity from time difference between the send and received signal. The resolution of this current meter is 1 mm/s.

- Load cell:

The cubic shaped weighing scale has a height of 10 cm and can be mounted to beneath the overtopping tank. They were used to measure the amounts of overtopping water. It is measuring in all 3 directions, but only the z-component with a maximum capacity of 2150 N ( $\approx 220$  kg), was used. Due to its accuracy, it was used for single event detection and oscillations in x and y directions were assumed to be negligible. Therefore it had to be calibrated every day with an occurrence of 20 kg per 1 Volt.

- Micropropeller (Schiltknecht):

Schildknecht micropropellers are based on the concept of an impeller. The rotations of the fan wheel will be measured and transformed to an output signal in Volt.

#### MiniWater 20 - FlowDike 1:

The measuring range of MiniWater20 Micro lies within 0.04 m/s - 5 m/s and their accuracy is 2% of the full scale. The calibration of the micropropeller was done by the partner from Braunschweig (LWI) before using them in the Hydralab project. They evaluated for each of them its specified calibration curve containing the measured voltage for defined velocities within their flume (see Figure A 8 in the Annex).

#### MiniWater 6 - FlowDike 2:

The MiniWater 6 Micro has a measuring range of 0.04 m/s – 5 m/s with a full scale accuracy of 2%. For the 1:6 sloped dike these new type of micro propeller were bought and calibrated at the DHI. Due to its low voltage output for the signal, it had to be gained up first through an amplifier. Then the calibration was done in the setup by recording the Voltage for certain defined flow velocities in a circular flow (see calibration curves in the Annex Figure A 9).

- Pressure sensors:

The water resistant pressure sensors have a threaded “head” that was inserted flush to the top of the lid. A small air filled pipe secured that the pressure module stayed water tight within their welded body. Therefore it had to be assured, that the end of this pipe never submerged. The measuring range of the pressure sensors is 25 mV for 0.75 m water column. The voltage outputs for a constant calibration of 10 cm per 1 Volt worked within a full scale accuracy of +/- 0.1%.

- Step gauges:

The step gauges have a total length of 1 m and include 4 successive parts with 24 electrodes and a continuous wire. Wave run-up is measured by a signal when a short cut is caused between electrode and wire. A constant distance between the pins of 1 cm gives for a slope of 1:3 a vertical precision of 0.32 cm. This device was only applied during FlowDike 1 and has not been evaluated yet.

- Wave gauges:

The water surface elevation and the flow depth on the crest were determined by wave gauges as a change of conductivity between two thin, parallel stainless steel electrodes. The conductivity changes proportionally to changes in the surface elevation of the water between the electrodes. An analogue output is taken from the Wave Meter conditioning module, where the wave gauge is connected to, and compiled in the data acquisition system.

Calibration should be done for a constant water temperature and has to be repeated if it deviates more than 0.5°C. Hereby a calibration factor of 10 cm per 1 Volt was used. The calibration factor for the small wave gauges on the crest was 10 cm per 0.5 Volt during FlowDike 1 and 10 cm per 1 Volt for FlowDike 2.

### 3.2.3 Wave Field (Wave gauges, ADV)

#### FlowDike 1

The data readings for wave field analysis on incident and reflected waves and the directional spreading contained both surface elevation and velocity. These signals were determined by two wave arrays of 5 wave gauges (with a length of 60 cm each) and a current meter. An overall view given in Figure 3.12

demonstrates that each of them is orthogonal aligned between the wave machine and the overtopping unity per dike crest. Each array was assigned to one crest height and placed at the toe of the structure positioned between the overtopping channels.



Figure 3.12 Overview of the basin: Wind machines; Wave array, Anemometer; Dike and overtopping unities

For the following reflection analysis a defined alignment of 0.00 m– 0.40 m– 0.75 m– 1.00 m– 1.10 m was kept for the single wave gauges. Both, ADV and Minilab SD-12 are positioned close to one wave gauge of the array (see Figure 3.13). The simultaneously measured surface elevation and velocity in this point will be used for the directional spreading analysis. Reflection, crossing and directional analysis will be evaluated from each array and its defined velocity meter.

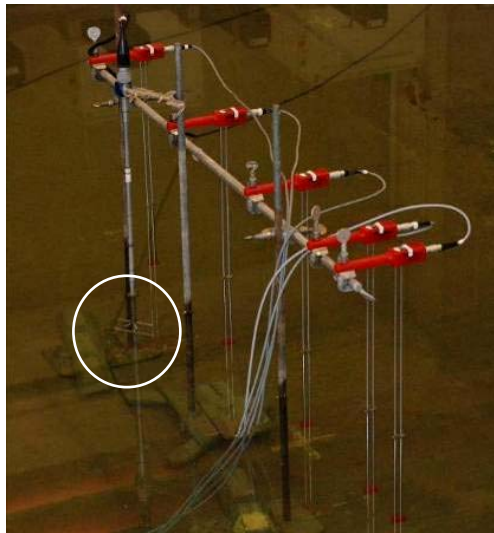


Figure 3.13 Wave gauge array with minilab SD-12 (encircled)

## FlowDike 2

An additional interest during FlowDike 2 was to determine the development of the wave field due to current affection. This was taken into account by adding a third wave array, which was placed in front of the wave maker. Both other arrays were situated as close as possible to the toe of the structure. Each of them was assigned to one of the crests and aligned between the channels of the overtopping units. In order to distinguish the effect of the current on the directional change of the wave field a distance of 1.12 m was kept between the two wave arrays at the toe of the structure and the one near the wave maker. For the directional analysis of this third wave gauge array an additional current meter was needed; this is why the Vectrino was used in FlowDike 2.

### 3.2.4 Wind Field (Wind machine, Anemometer)

#### FlowDike 1

The wind field, focused onto the dike, was generated by six wind machines using a wind turbine. Each of them was controlled by the frequency adjustment of revolutions for the rotator and performs a conus as wind field. In order to create a homogeneous wind field the distances between the six wind machines are different (37.5 cm - 45 cm - 50 cm - 45 cm - 37.5 cm) and were determined in some preliminary tests (see annex Figure A 2 to Figure A 4).

Two anemometers for velocity measurements provided by DHI were installed in the set up (see in the annex Figure A 2 to Figure A 4). One was situated 2m in front of the dike toe and the second was placed above the crest. Both measured within a height of 1m above the basin ground, just in the middle between the overtopping unities for each crest as shown in Figure 3.14.

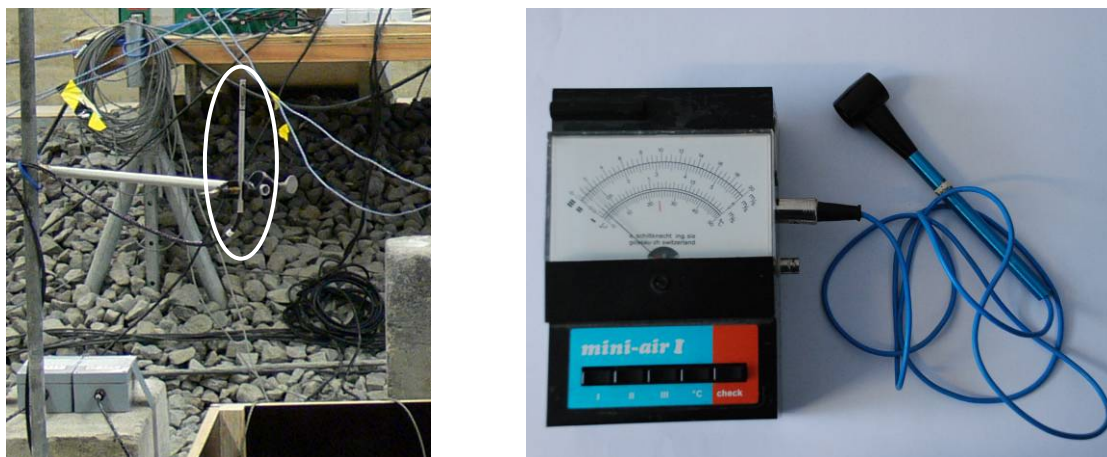


Figure 3.14 Anemometer (left) and fan wheel for air velocity measurement (right)

To prove the homogeneous distributed wind field along the dike, the wind velocity for two different frequencies was measured with a fan wheel (see Figure 3.14) in defined distances on the dike crest before testing. Reflection effects induced by the water surface and parallel flow from adjacent generators were observed by an increase of the velocity range. In Figure 3.15 and Figure 3.16 the results for a frequency of 49 Hz and 25 Hz are plotted along the crest of the 1:3 dike.

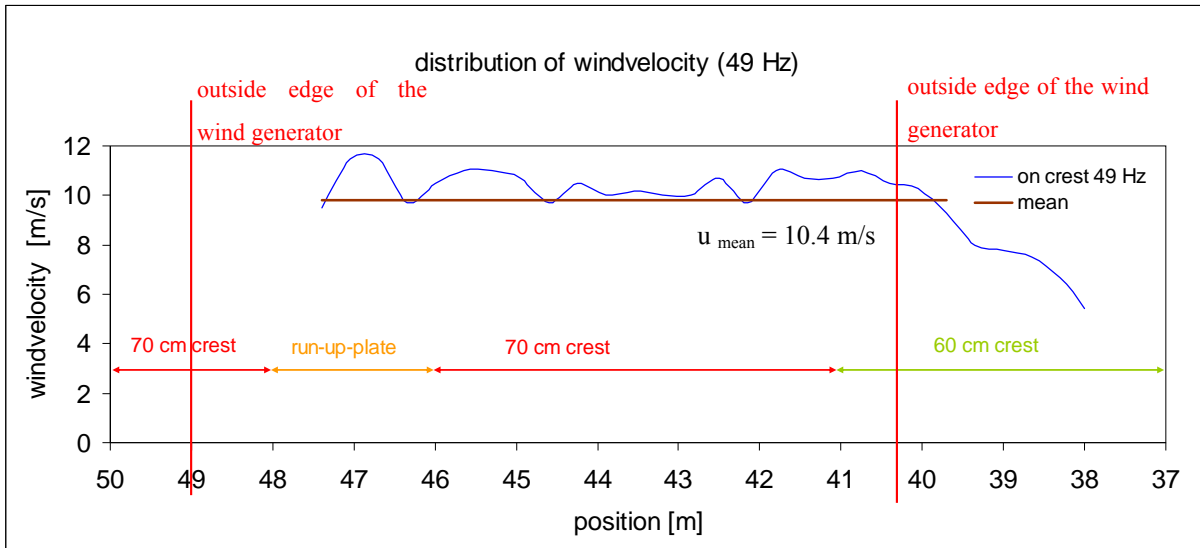


Figure 3.15 Wind velocity distribution for a frequency of 49 Hz (FlowDike 1)

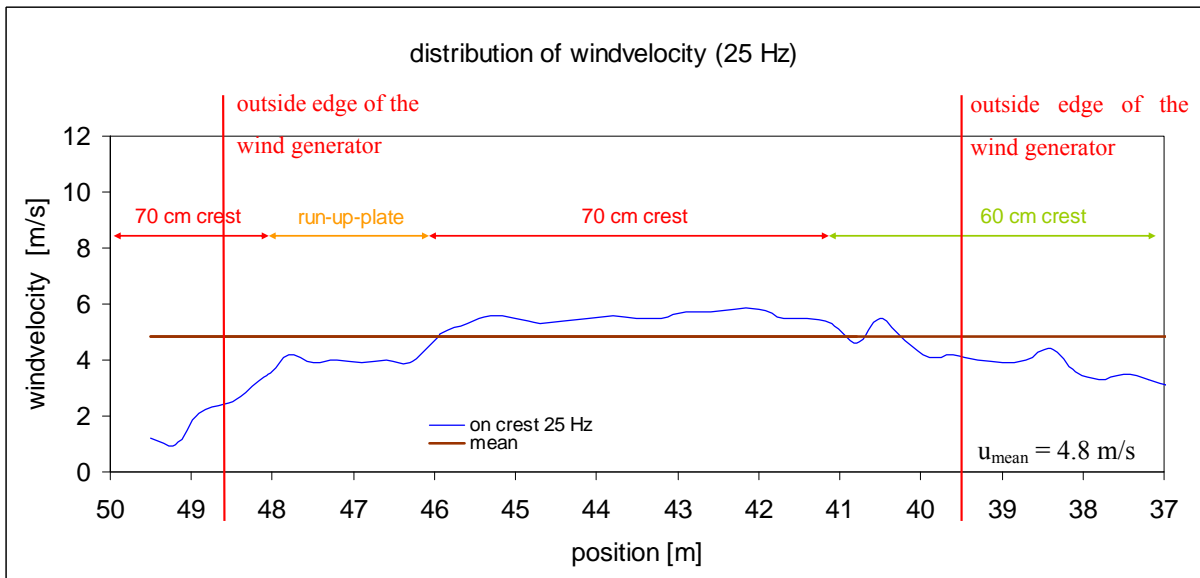


Figure 3.16 Wind velocity distribution for a frequency of 25 Hz (FlowDike 1)

**FlowDike 2**

The alignment of the wind machines did not change compared to the setup of the 1:3 dike. Here the average wind velocity was slightly lower than for the 1:3 dike, but still homogeneously distributed. Only the larger distance between the wind generator and the dike crest lead to a wind velocity of 8 m/s and 4m/s on the crest. Furthermore, the anemometer in the channel had to be moved closer to the blower, due to the narrow spacing between dike toe and wind machine. The results for the measurements on the crest of the 1:6 dike are illustrated in Figure 3.17 and Figure 3.18. For both models, wind velocity is assumed to be 10 m/s respectively 5 m/s in the following analysis.

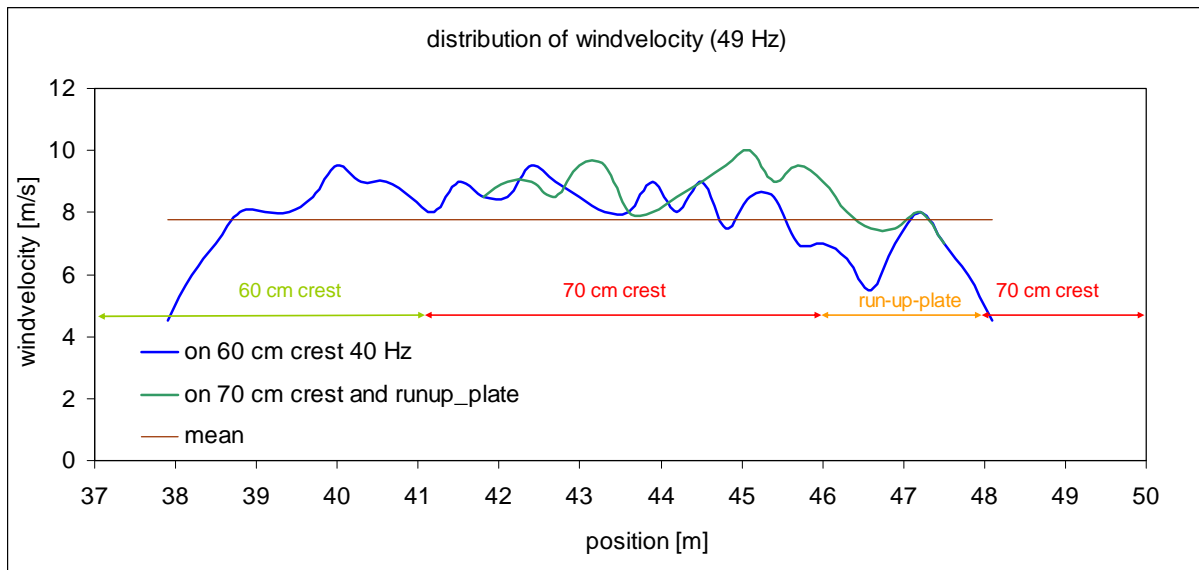


Figure 3.17 Wind velocity distribution for a frequency of 49 Hz (FlowDike 2)

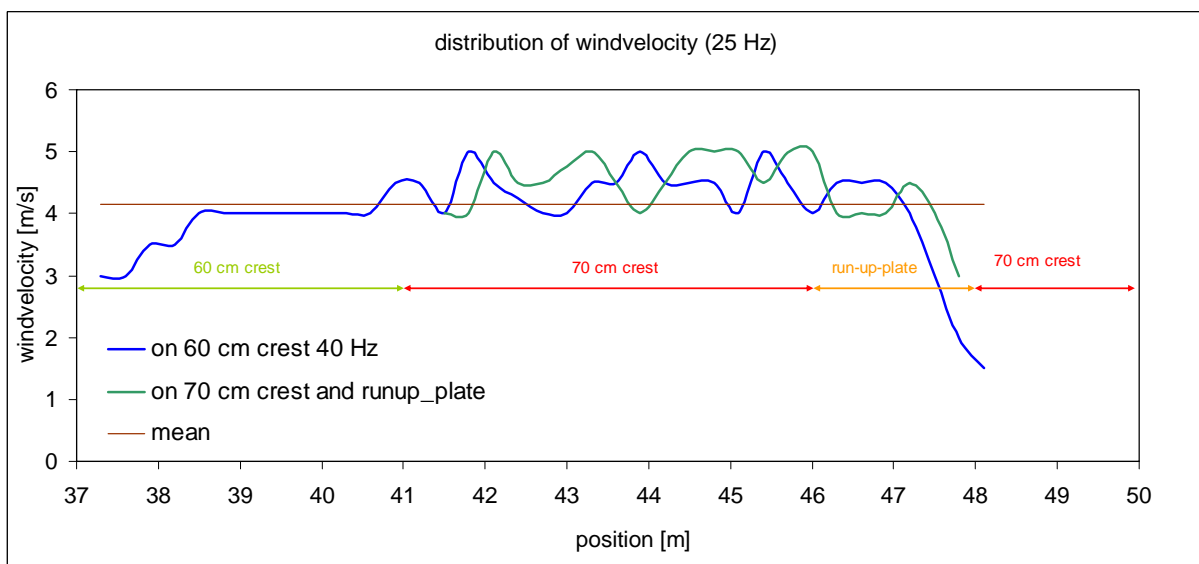


Figure 3.18 Wind velocity distribution for a frequency of 25 Hz (FlowDike 2)

### 3.2.5 Current (Weir, ADV, Micro propeller)

#### FlowDike 1

For constant water depth of 0.5 m within the channel a stabilised current of approximately 0.3 m/s was achievable with the maximum pump capacity of 1.12 m<sup>3</sup>/s. This limited the range for applicable currents and only a second one was chosen for the data set. This current was taken to be 0.15 m/s. Here, the pump capacity needed to be reduced to 0.6 m<sup>3</sup>/s and the weir changed in its height from 32.16 cm to 38.66 cm above the ground.

Current velocities were controlled with two ADV's and two big micro propellers. All these devices were fixed on a beam, which was situated 2 m before the upstream edge of the wave machine (Figure 3.19). The velocity was measured at 1/3 below the water surface (circa 33 cm from the bottom) where an average velocity within the depth profile is assumed. Both ADV's were placed in a distance of 2 m and 3.5 m from the dike toe. For a better knowledge of the velocity distribution in the cross section two micro propellers were installed additionally, within a distance of 1.5 m, besides the ADV's.



Figure 3.19 Beam upstream the wave machine; ADV; Micro propeller (FlowDike 1)

#### FlowDike 2

The current control did not change a lot from the latest investigations in FlowDike 1. The beam sustaining all mounted current devices was installed at the same position of 55 m in the basin (2 m further upstream than the wave maker). However, the distances between the instruments and from the dike toe were reduced because of the restriction in channel width. Their positions are listed below in Figure 3.20

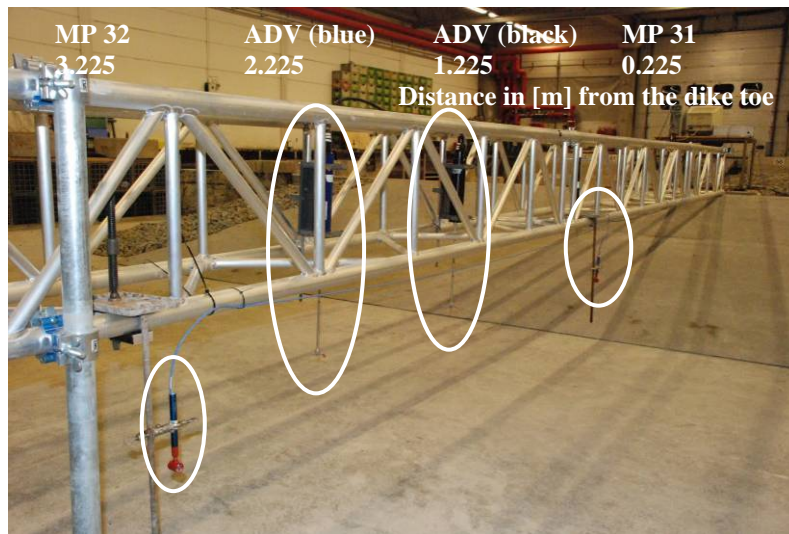


Figure 3.20 Beam upstream the wave machine with current devices (FlowDike 2)

The measuring point within the velocity profile did not change. For a better comparability and with regards to the above stated assumptions, the sampling volumes were kept at a position of approximately 33 cm from the bottom of the channel (like in FlowDike 1).

Due to the narrower channel a new maximum current of 0.40 m/s could be adjusted for the constant water level of 0.55 m. Therefore a weir height of 33.7 cm and a pump capacity of 1.1 m<sup>3</sup>/s were used. The mean velocity of 0.3 m/s was controlled with a discharge of 0.83 m<sup>3</sup>/s and a weir height of 38.2 cm. A current of 0.15 m/s was still induced for the comparison of some test series, although the influence was assumed to be negligible from the elder analysis. Here fore the weir was positioned at 44.2 cm from the bottom for a capacity of 0.43 m<sup>3</sup>/s.

At the beginning of each test day, the velocity measurements of all probes were recorded when the current was stabilised. If the average of the mean values did not deviate more than 5 cm/s from each other, the current was assumed to be correct.

### 3.2.6 Run-up (Capacitive gauge, Camera, Step gauge)

#### 3.2.6.1 Wave run-up plate

##### **FlowDike 1**

The dike height of 0.6 m and 0.7 m was chosen to measure wave overtopping. For wave run-up measurements the dike was too low.

Therefore a 2 m wide and 2.5 m long ply wood plate was installed as an extension of the dike slope (Figure 3.21). Its surface was covered with sand which was fixed by means of shellac to provide a similar surface roughness as of concrete slope.

The capacitive gauge was mounted in the middle of the run-up-plate. At the right side an adhesive tape with a black and yellow pattern was put on as the gauge board. The gauge board had two different scales. The original scale with its 1 cm long sections showed the oblique wave run-up height. The distances at the second scale were multiplied with 10<sup>0.5</sup> and represented the vertical run-up height.



Figure 3.21 Wave run-up plate and rack with both digital cameras

To get films with a better contrast the wave run-up board was enlightened by a 2000 W-spotlight which was positioned such as the light met the run-up plate within an angle of  $120^\circ$  to the optical axis of the digital cameras.

For the purpose of synchronizing all measurements a digital radio controlled clock with a  $0.4 \times 0.4$  m display was positioned on the left side of the run-up plate (Figure 3.21).

### FlowDike 2

The run-up board was reused after cutting the legs to achieve the slope inclination of 1:6, thus a new scale had to be pasted onto it.

#### 3.2.6.2 Wave run-up gauge

### FlowDike 1 and FlowDike 2

The wave run-up height was measured using a capacitive gauge. As schematically shown in Figure 3.22 the required equipment contained a submerged capacitor, a transducer and an A/D-converter.

The two electrodes of the capacitor (Figure 3.23) were formed by one isolated and one non isolated wires each 3.5 m long. They were mounted on the run-up plate orthogonally to the dike base. One end was installed about 0.25 m above the bed which is equal to 0.25 m below still-water-level (SWL). The other end was fitted at the highest point of the run-up plate. Thus it is possible to measure both the wave run-up and the run-down. To avoid a water film between the two electrodes after a wave runs down several rubber bands assure a constant distance of about 5 mm between the two wires.

The air or the water between the two wires is the dielectric fluid. Because the permittivity of water is 80 times greater than that of air, the variation of the water level produces a measurable variation of the electrical value of the capacitor.

The transducer allows loading and unloading the capacitor 25 times per second which is equal to a measurement frequency of 25 Hz. Each value of the time constant of the capacitor  $\tau$  would be transmitted to the A/D-converter as a voltage value. The scale of the voltage value ranged from 0 V to 5 V. The digital signal which came out of the A/D-converter would be transmitted to the data collection unit and put in storage together with the signals of the other measurement equipment.

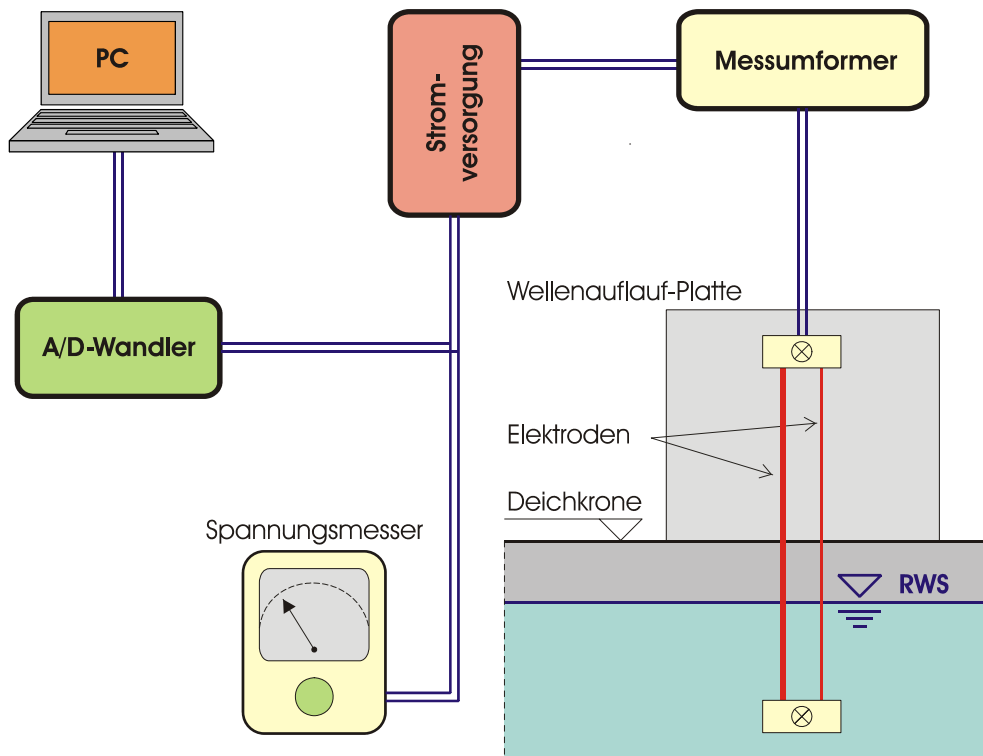


Figure 3.22: Schema of data collecting using the capacitive wave run-up gauge

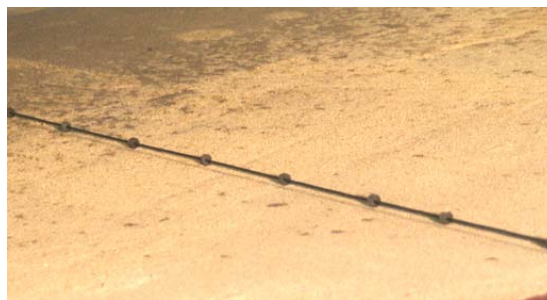


Figure 3.23: Capacitive wave run-up gauge on the dike slope– detailed view with the two electrodes and distance pieces.

In addition to the capacitive gauge the wave run-up height was measured by two digital gauges (*step-gauges*) each 1.5 m long. They were mounted at the 0.7 m high dike slope within a distance of 2.2 m. With these gauges it is only possible to measure the wave run-up till the dike crest.

### 3.2.6.3 Digital video cameras

#### FlowDike 1

In addition to the capacitive wave run-up gauge two digital video cameras were used to record the wave run-up (Figure 3.24). Both were mounted on a rack about 4 m above the ground (Figure 3.21). The rack was fixed at a laboratory crane to make the positioning of the two cameras very easy.

One digital camera was a compact, professional USB 2.0 camera from VRmagic GmbH which is suitable for industrial purposes. The used model VRmC-3 + PRO contained a 1/3 inch-CMOS-sensor which could record 69 frames per second. The picture resolution of 754 x 482 pixels was adequate for measurement purposes in the model tests presented herein.

The camera was suitable for recording very fast motions like wave run-up on slopes. One benefit of this camera was the possibility to transmit the data to the computer directly by the high speed USB 2.0 interface and without any additional frame grabber hardware. The recorded films were AVI-files. These files should be automatically analysed after the end of the model tests.



Figure 3.24: Left: USB-camera, Right: Both cameras mounted on a rack in the model setup

The other digital camera was a SONY Camcorder (Model: *DCR-TRV900E PAL*), with a 3CCD (*Charge Coupled Device*, 1/4 inch). The objective had a focal distance between 4.3 mm and 51.6 mm and a 12 times optical zoom.

The camcorder was employed as a redundant system in the event of a USB-camera malfunction. The camcorder used mini cassettes to store its films. Choosing the LP-modus record time of the mini cassettes could be extended to 90 minutes. Because of test durations between 17 and 34 minutes the cassettes were able to storage films between 2 and 4 test films.

For analysis purposes we have to transform the films on mini cassettes into AVI-files. This is very time expensive and that is why USB camera was chosen as the main system though the SONY camcorder has a better resolution.

## FlowDike 2

In FlowDike 2 both cameras were replaced with two others, which have a better resolution. Since the image-processing algorithm works with grey-level images, one colour camera was replaced with a more powerful monochrome camera (1/2" Progressive-scan-CCD sensor (*Charge Coupled Device*, 1/2 inch) JAI CM-140 GE of Stemmer Imaging). Its resolution of 1392 x 1040 pixels with 4.65  $\mu\text{m}$  pixel size allows producing pictures of the run-up plate with a precision of 0.5 mm.

The second camera (a colour area scan camera) was used for documentation purpose only. It had the same features like the monochrome one but the output-files are three times greater (about 2.6 GB/min). The same objectives as in FlowDike 1 were reused.

A benefit of these cameras was their Gigabit Ethernet (C3 series) interface, which allowed to place the laptop, connected with a 30 m cable, in the office room outside the very humid hall. Also the transfer rate was thus increased on about 3 times. The MATLAB algorithm was upgraded to considering the new format by the analysis of the output-files.

### 3.2.6.4 Step gauge

During FlowDike 2 the step gauges, which were not analysed for FlowDike 1, have been left out. There is no analysis available concerning the step gauges yet.

### 3.2.7 Overflow velocity and layer thickness (Micro propeller, Wave gauge, Pressure sensor)

## FlowDike 1

From the interest in flow velocities and flow depths on the crest during an overtopping event *Schiltknecht* micropropellers and small wave gauges (with a length of 20 cm) were used. As indicated in Figure 3.25 two small micropropellers combined with two wave gauges were situated in every testing section (60 cm and 70 cm crest) between both overtopping boxes. They measured the velocities and water depths on the front and the backward edge of the dike crest. The signals given in Figure 3.26 demonstrate the measurements of wave gauges and micro propeller during single overtopping events – wave by wave.

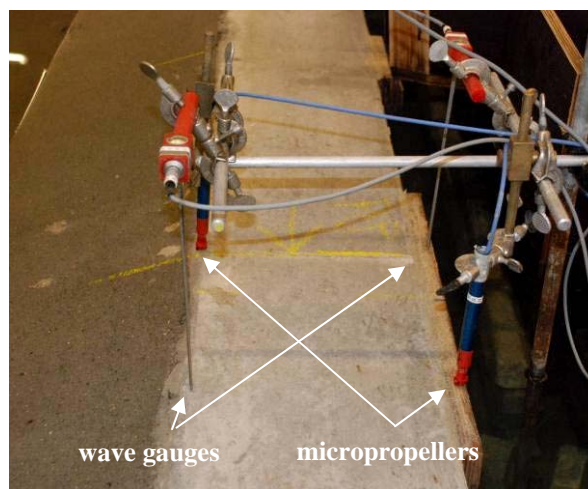


Figure 3.25 Measurement of velocity and depth of flow on the crest

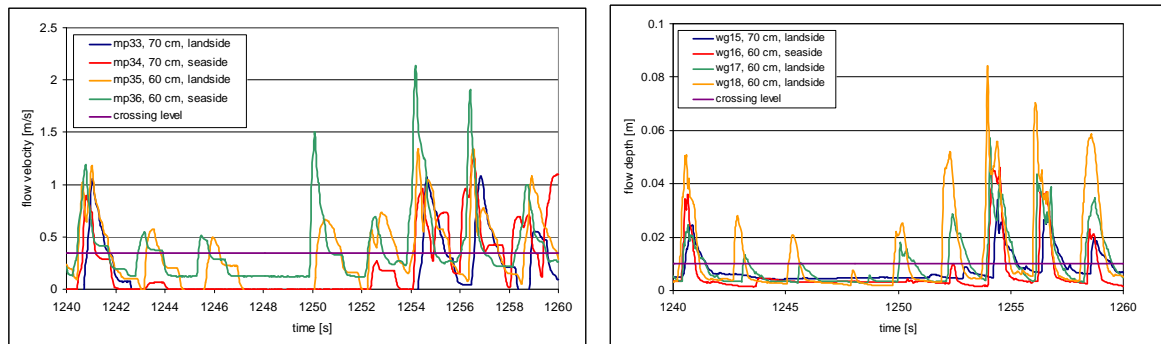


Figure 3.26 Micropropeller (left) and wave gauge (right) measurement for a sequence (s1\_03\_30\_w5\_00\_00)

## FlowDike 2

In FlowDike 1 only wave gauges were used to measure the layer thickness. For FlowDike 2 pressure sensors were used additionally. This new device and the purpose to avoid the influence of the crest edges (drop of water level) induced a change in order for all instruments on the dike. Instead of installing them at the edges all devices were situated 3 cm from each side of the crest, so a distance of 24 cm was kept between the aligned seaward and landward devices. To investigate the influence of the front edge (between the slope and crest), another wave gauge was placed perpendicular onto the slope. Measurements on the wave or the flow depth of the up rushing wave were taken in a horizontal distance of circa 12 cm before the edge (Figure 3.27).

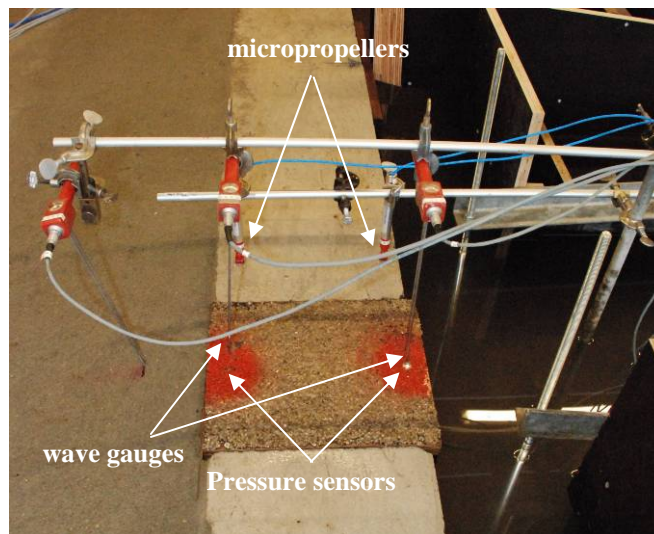


Figure 3.27 Measurement of pressure, velocity and depth of flow on the crest

### 3.2.8 Overtopping (Load cell, Pump)

#### FlowDike 1

Wave overtopping was measured by four similar overtopping boxes - two per crest section. One unit constituted an overtopping tank (35 cm x 75 cm x 75 cm) mounted on a load cell of 10 cm height. This load cell was placed on the bottom of a separate dry box (55 cm x 102 cm x 118 cm), which was built to avoid uplift of the overtopping tanks and load cells, when the basin is flooded. A channel of 10 cm inner width led a part of the incoming wave into the tank, where the weight of water was constantly recorded by the load cell. The inlet was not really 10 cm in width. Because of the thick

plywood parts (1.8 cm) it was not clear whether there were any influences on the overtopping amount. Therefore the edges of the channel were sharpened after the first test series. For data redundancy a wave gauge (60 cm) was placed in every tank to measure the water elevation. Annotation: wave gauges could not be used to detect the single wave events as it records only the water level within the overtopping tank, which is not constant, due to the incoming wave events and the pumping during testing.

For the tests huge amounts of overtopping water were expected, especially for w5 the amount was planned to reach 30 litres at the end of the test. This showed that the dimensions of the tank were not capable to capture them during one test of approximately 30 min. Therefore a pump (standard pump) with a predetermined sufficient flow (i.e. 1.733 l/s) was placed within each tank. All four of them were connected with the data acquisition via a switch, so start and end time of pumping could easily be detected. In special tests each pumping curve was recorded, this allowed to recalculate the lost amount of water during the pumping time. After every test the tanks had to be emptied to ensure that pumping was done not more than necessary. This practice regarded the loss of data for the single event detection during pumping.



Figure 3.28 Overtopping boxes with channel and measurement devices for flow depth and flow velocity measurements

In Figure 3.29 the overtopping amount measured during one test is displayed. Here the descending part indicates the pumping of water. The signals given in Figure 3.30 demonstrate the measurements of the load cells for wave by wave overtopping during 20 seconds.

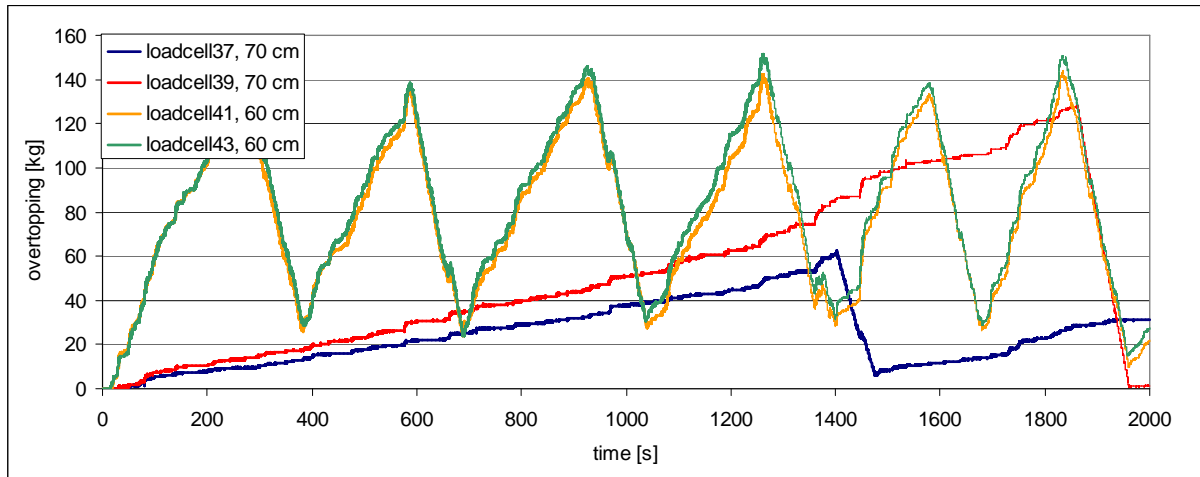


Figure 3.29 Overtopping measurement a whole test (s1\_03\_30\_w5\_00\_+00)

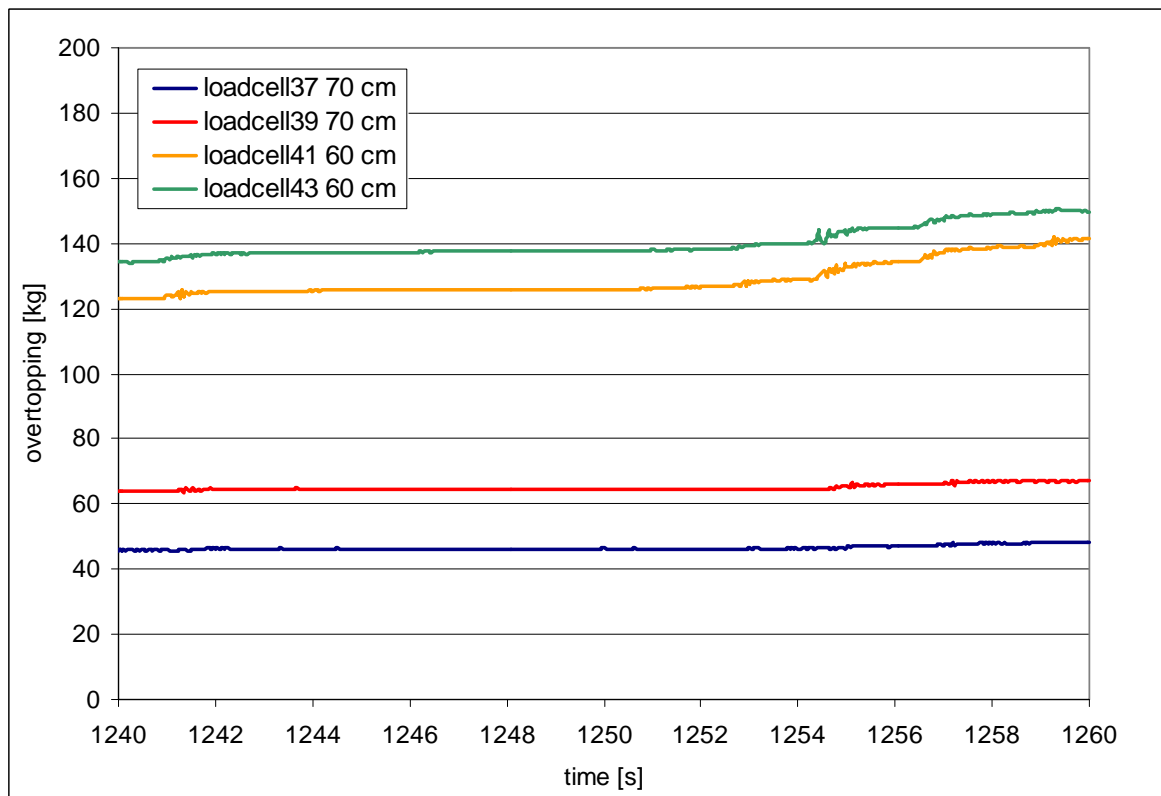


Figure 3.30 Overtopping measurement for a sequence of 20 s (s1\_03\_30\_w5\_00\_+00)

### FlowDike 2

For the second phase of investigations, the retained overtopping unities of FlowDike 1 were reused. Only new channels with sharpened edges had to be rebuilt. Although the overtopping amount on a 1:6 dike decreases due to the inclination of the slope and breaking wave conditions, the garden pumps were still needed for the largest waves in period and wave height.

### 3.3 Calibration

#### 3.3.1 Gauge scale adaptation

After fixing the adhesive gauge tape on the run-up plate the scale was longer because of its elasticity. In order to control possible changes, a post measurement was conducted. As a result the label of 2.9 m was placed in a distance of 2.923 m to the zero-point which is equal to an extensibility of 0.8%. In the end the measured wave run-up is too short and has to be corrected.

Assuming a linear correlation between the original and the extended scale the following formula was obtained to match both:

$$\text{length}_{\text{correct}} = 1,0087 \cdot \text{length}_{\text{gauge board}} \quad (3.1)$$

The even little difference has to be considered in the post processing and the data analysis using AVI-files from the camera.

#### 3.3.2 Capacitive run-up gauge calibration

The measurement results of the 18 resistance wave gauges were influenced by water temperature and salinity. That's why one had to calibrate these gauges twice a day.

Otherwise the capacitive gauge was non-sensitive to these environmental conditions. The calibration was conducted only one time before the test start. Therefore three tests with regularly waves with a mean wave height of  $\bar{H} = 0.1; 0.15$  and  $0.2$  were run. Data analysis considered the measured values  $x$  in Volt together with the still-water-level and the maximum water level during wave run-up (WS in meters) from video films.

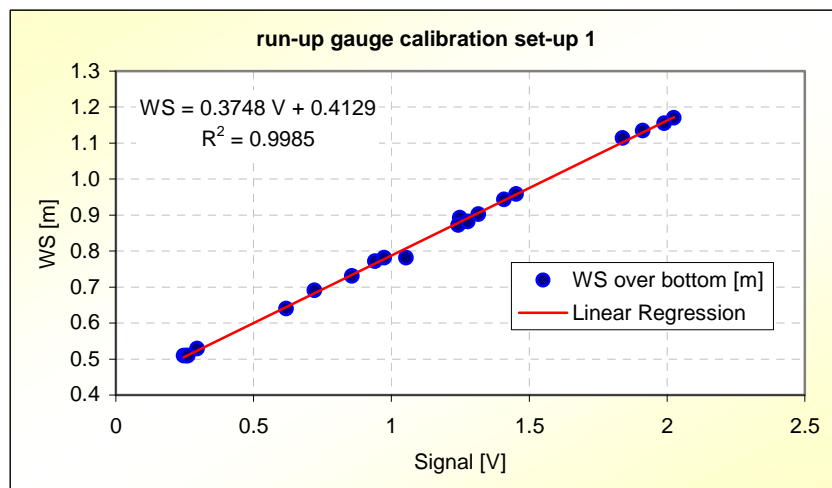


Figure 3.31 Run-up gauge calibration (set-up 1)

The result of data analysis considering equation (3.1) shows Figure 3.31. As the result of a linear regression with 20 values ( $R^2 = 0.9985$ ) the following equation was obtained:

$$\text{WS} = 0.3748 \cdot x + 0.4047 \quad (3.2)$$

Then the wave run-up height  $h_r$  could be calculated as the difference between WS and the still-water-level  $h_{sw}$ :

$$h_r = WS - h_{sw} \quad (3.3)$$

Equation (3.2) depends on the model set-up especially on the wire length and the mounting height. That's why the calibration has to be repeated for each model set-up (see equation (3.4) and (3.5)).

$$WS = 0.3674 \cdot V + 0.2279 \quad (R^2 = 0.9977, \text{ set-up 2}) \quad (3.4)$$

$$WS = 0.3708 \cdot V + 0.4095 \quad (R^2 = 0.9977, \text{ set-up 3}) \quad (3.5)$$

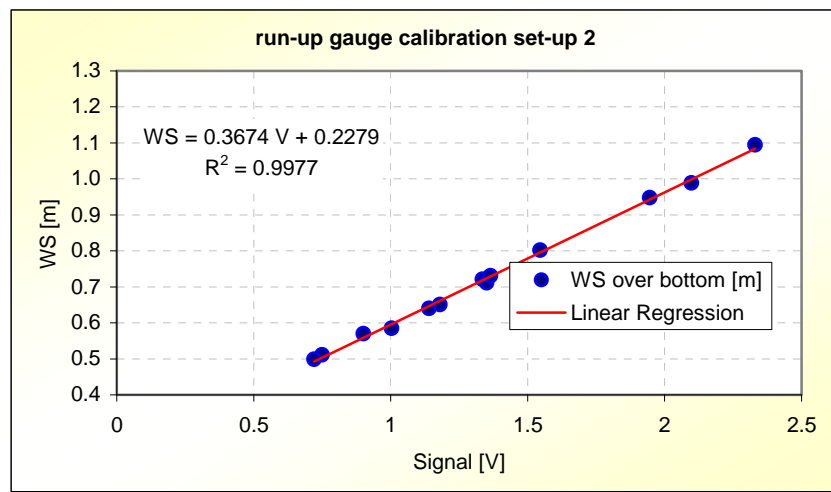


Figure 3.32 Kalibrierung des kapazitiven Auflaufpegels beim Setup 2

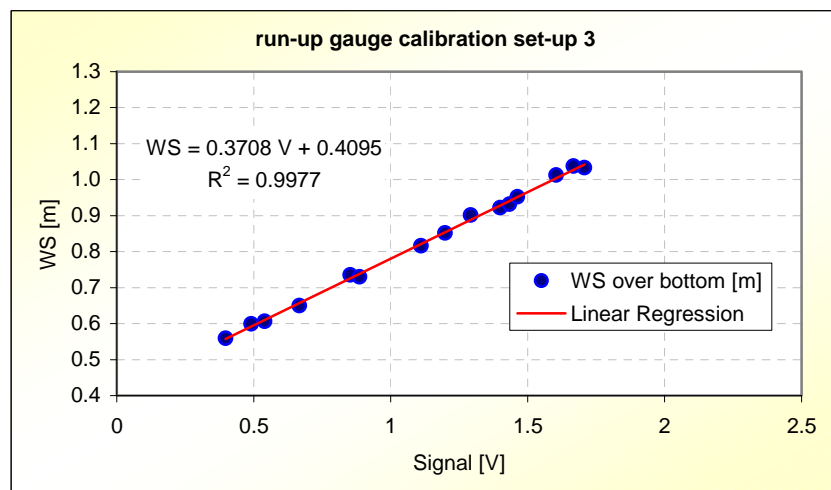


Figure 3.33 Kalibrierung des kapazitiven Auflaufpegels beim Setup 3

## 4 Literature review

### 4.1 State of the Art

Wave run-up and wave overtopping are the most important parameters for freeboard design. Analyses were performed mostly for coastal areas in the past. First investigations have been carried out before 1935 (see WASSING, 1957 and GIBSON, 1930). In the meantime, many experimental, numerical, theoretical and field investigations were performed. Extensive studies on perpendicular wave run-up and overtopping and some investigations on oblique wave run-up are available.

SCHÜTTRUMPF (2003) summarised these studies:

*“The objective of many investigations in the past was the determination of the reduction coefficient  $\gamma_\theta$  for wave run-up or wave overtopping with oblique wave attack. WASSING (1957) conducted first experiments on wave run-up with oblique wave attack and regular waves. More experiments on wave run-up or wave overtopping with regular waves were performed by ISHIHARA (1960), HOSOI & SHUTO (1964), OWEN (1980) and TAUTENHAIN (1982) resulting in different formulas for  $\gamma_\theta$ .*

*Model tests on wave run-up or wave overtopping with long crested waves were performed by DAEMRICH (1991), JUHL & SLOTH (1994), FRANCO (1995), VAN DER MEER & DE WAAL (1990), SAKAKIYAMA & KAJIMA (1996) and HEBSSGAARD (1998) for different structures resulting in other expressions for  $\gamma_\theta$ .*

*FRANCO (1995), VAN DER MEER & DE WAAL (1990), SAKAKIYAMA & KAJIMA (1996) and HIRAISHI (1996) performed model tests with short crested waves and found differences in wave run-up and wave overtopping to long crested waves. Finally, some results are available from field experiments (WAGNER & BÜRGER, 1973).”*

The different regression functions for influence of obliqueness are given in Figure 4.1.

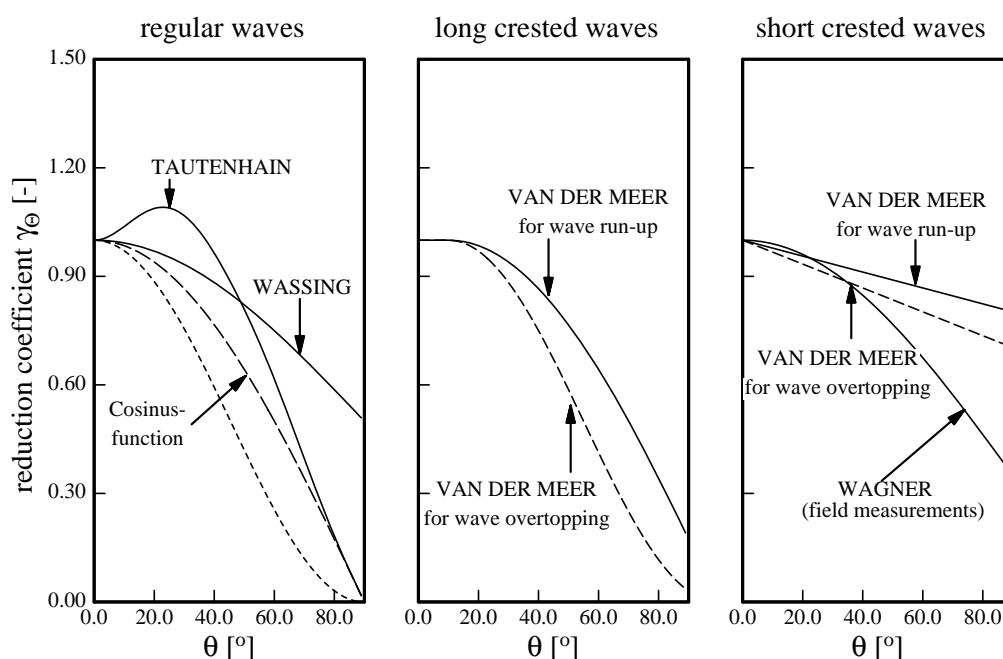


Figure 4.1 Reduction Factor ( $\gamma_\theta = \gamma_B$ ), Reference: SCHÜTTRUMPF (2003)

The well-known formulae by VAN DER MEER ET AL. (1998) are recommended nowadays by many international and national guidelines to calculate the wave run-up height  $R_{u2\%}$ , which is exceeded by 2% of the incoming waves, and the average overtopping rate  $q$ . The effects of oblique wave attack, berms, surface roughness and crown walls are considered in these formulae as well by simple reduction factors. The most recent work, however, is the EUROPEAN OVERTOPPING MANUAL (EUROTOP) (2007). It includes the aforementioned formulae and gives a good overall view of the present situation of crest level design for coastal structures.

Strong winds may have multiple effects on wave run-up and wave overtopping, like deformation of incoming wave field, generation and transport of spray, direct influence on wave run-up and wave overtopping (GONZALEZ-ESCRIVA, 2006). Therefore, the influence of wind should not generally be neglected under typical design conditions. Especially for small overtopping rates and vertical structures the effect of wind might be significant (DE WAAL ET AL., 1996). On the other hand, the influence of wind can be neglected for high overtopping rates and/or low wind velocities (WARD ET AL., 1996) but information on wind influence is still scarce. The main problem to consider wind experimentally and to quantify its effect is the inaccurate scaling of wind in small scale model tests. YAMASHIRO ET AL. (2006) recommend scaling the prototype wind by a factor 1/3 but the experiments are restricted to a model scale of 1/45.

By now, for the effect of currents on wave run-up and wave overtopping no systematic investigations are available. JENSEN & FRIGAARD (2000) performed a small number of model tests (about 10) to investigate the influence of introducing a longshore current on wave run-up for a model of the Zeebrugge breakwater site. Their results indicate an increase of the wave run-up height of about 20% by introducing a longshore current of 1m/s in the model.

The combined effect of currents and wind on wave run-up and wave overtopping has not been investigated before. Thus, the effect of wave run-up and wave overtopping due to a current and wind is an issue still not solved for a reliable based design of river, estuarine and also coastal dikes.

Nowadays, the research on wave run-up and wave overtopping intends to describe also the flow processes on the crest. SCHÜTTRUMPF (2001) and VAN GENT (2002) describe these processes related to wave run-up and wave overtopping by flow parameters such as flow depth  $h_c$  and flow velocity  $v_c$ . Experimental investigations on the overtopping flow parameters were performed in small and large wave flumes but the three dimensionality of the process was not investigated so far.

## 4.2 Influencing variables

First of all, the EUROTOP-MANUAL (2007) will be taken as a basis for the present investigation. Here it should be mentioned, that the adapted formulae in this work are stated for short crested waves, but for testing only long crested waves could be used, although they do not exist. This has to be considered for comparison of the analysis.

Usually the influence of different factors on wave run-up height or overtopping could be determined using a formula which was originally suggested by Hunt (1959) or the upgraded version in EUROTOP-MANUAL (2007) and different correction parameters:

$$\frac{R_{u2\%}}{H_{m0}} = C_1 \cdot \gamma_b \cdot \gamma_f \cdot \gamma_\beta \cdot \xi_{m-1,0} \quad (4.1)$$

with its maximum value

$$\frac{R_{u2\%}}{H_{m0}} = \gamma_f \cdot \gamma_\beta \cdot \left( c_2 - \frac{c_3}{\sqrt{\xi_{m-1,0}}} \right) \quad (4.2)$$

Descriptions:

- $R_{u2\%}$  wave run-up height which will be exceeded by 2% of all waves [m]
- $c_1$ ,  $c_2$  and  $c_3$  are empirical parameters with  $c_2 = c_1 \cdot \xi_{tr} + c_3 / \xi_{tr}$  [-]
- For a prediction of the average  $R_{u2\%}$ ,  $c_1 = 1.65$ ;  $c_2 = 4.0$  and  $c_3 = 1.5$  should be used.
- $\xi_{tr}$  surf parameter describing the transition between breaking and non breaking waves [-]
- $\gamma_b$  parameter which covers the influence of a bench or a dike surface with at least two different slopes [-]
- $\gamma_f$  parameter which covers the influence of surface roughness [-]
- $\gamma_\beta$  parameter which covers the influence of wave direction (angle  $\beta$ ) [-]

For the average overtopping discharge  $q$  EUROTOP-MANUAL (2007) gives the following formula for breaking conditions (2.8), which is limited by the non-breaking conditions as a maximum (2.9):

$$\frac{q}{\sqrt{g} \cdot H_{m0}^3} = \frac{0.067}{\sqrt{\tan \alpha}} \cdot \gamma_b \cdot \xi_{m-1,0} \cdot \exp\left(-4.75 \frac{R_c}{\xi_{m-1,0} \cdot H_{m0} \cdot \gamma_b \cdot \gamma_f \cdot \gamma_\beta \cdot \gamma_v}\right) \quad (4.3)$$

$$\frac{q}{\sqrt{g} \cdot H_{m0}^3} = 0.2 \cdot \exp\left(-2.6 \frac{R_c}{H_{m0} \cdot \gamma_f \cdot \gamma_\beta}\right) \quad (4.4)$$

Descriptions:

- $q$  average wave overtopping discharge [ $m^3/(s \cdot m)$ ]
- $R_c$  freeboard height [m]
- $\xi_{m-1,0}$  Breaker parameter [-] (also: Iribarren number or surf similarity parameter) defined as followed:

$$\xi_{m-1,0} = \frac{\tan \alpha}{\sqrt{H_{m0} / L_{m-1,0}}} \quad (4.5)$$

with:

- $\alpha$  = angle of the outer dike slope [°]
- $H_{m0}$  = significant wave height of the swell at the dike base [m] ( $\approx H_s = H_{1/3}$ )
- $L_{0m,-1,0}$  = wave length in deep water [m]:

$$L_{0m,-1,0} = \frac{g \cdot T_{m-1,0}^2}{2\pi} \quad (4.6)$$

with:

- $T_{m-1,0}$  = spectral period based on  $m_{-1}/m_0$ [s]
- $g$  = acceleration due to gravity [ $m/s^2$ ]

The aim of the research project is to introduce and to verify experimentally the influence of dike parallel currents and wind on wave run-up  $R_{u2\%}$  and on the wave overtopping rate  $q$ . Following variables have to be generated and measured:

- velocity and direction of wind and current
- water level
- reflection coefficient and wave spectrum
- individual values of wave run-up height
- mean overtopping rate and individual values of overtopping volume
- flow depth on dike crest
- flow velocity on dike crest

## 5 Data processing

### 5.1 Remarks

An evaluation of the measured raw data of the wave field, run-up and overtopping is necessary intending to analyse and present the results in order to develop or modify the existing design formulae. As described previously the raw data are available from a digitalisation with  $\Delta t = 0.04$  sec ( $f_s = 25$  Hz) for FlowDike 1 and  $\Delta t = 0.025$  sec ( $f_s = 40$ Hz) for FlowDike 2. In order to reduce their extent to characteristic parameters, analyses driven by time domain or by frequency domain were used.

As data processing tools the Wave Synthesizer from the DHI software package Mike Zero was used for reflection and crossing analysis. For calculation of the average overtopping volumes a MATLAB script was created, that uses the available ascii files (\*.daf).

At this point it has to be mentioned, that the processed data files only exist completely for the setups 1 to 3 of FlowDike 1. The data processing of FlowDike 2 has not been finished yet and only the parameters of interest for the basic analysis on overtopping, such as average overtopping rate  $q$  and the incoming wave parameters at the toe of the structure were processed.

### 5.2 Evaluation methods

Wind and current as main influencing variables were controlled separately from the data acquisition before starting the tests. A significant reason is that during testing the current recording would be influenced by the wave distribution, thus the length of the channel is limited. The wind could only be determined in one point; hence the distribution along the dike crest had to be validated before testing.

In frequency domain the wave parameters were analysed using a reflection analysis. Herein the reflection coefficient  $C_r$  is determined at the same time. The time-series of water level elevation is transformed and analysed by a FOURIER-transformation giving the spectral energy density  $S(f)$  for incident and reflected wave and their average. Based on the moments  $m_n$  of the spectral densities, the following characteristic wave parameters can be calculated:

- wave height  $H_{m0} = 4 \cdot \sqrt{m_0}$  [m]
- wave period  $T_{m0,1} = \frac{m_0}{m_1}$  [s]
- wave period  $T_{m0,2} = \sqrt{\frac{m_0}{m_2}}$  [s]
- peak period  $T_p$  [s]

Since  $T_{m-1,0}$  could not be calculated with the used program, the relation between spectral and peak period for uniform single peaked spectra  $T_p = 1.1 \cdot T_{m-1,0}$  is used (EUROTOP, 2007).

Determining the wave field in time domain, a zero-down crossing was applied, whereby single wave events were defined. From the certain quantity  $N$  of the measured surface elevation, related average values for the maximum wave height  $H_{\max}$  (peak to peak decomposition) and the mean wave period  $T_m$

(event duration), can be calculated. These values are the average of all wave gauges contributing to one of the wave arrays. Other averages for characteristic height parameters, such as the significant wave height  $H_s = H_{1/3}$ , have not been analysed yet.

Wave run-up events are the maximum elevations of the run-up tongue from the still water level. The wave run-up height is determined with a crossing analysis using a threshold level different from zero. Therefore a different number of events results compared to the number of wave events. The calculation of statistical wave run-up characteristics has to be related to the number of incoming waves. In the following the analysis of the wave field and wave overtopping will be discussed.

The overtopping is calculated by adding the lost pump volumes (recalculation from known capacity and working period) to the collected amount within the tank. By dividing the overtopping amount with the channel width of 0.1 m (0.118 m before sharpening the edges of the inlet) and the testing duration an average overtopping rate  $q$  in l/(s·m) is determined for each tank.

Crossing analysis with a defined threshold is done as well for the measurement devices on the crest. Here the micro propellers were measuring the flow velocity on the crest at the seaward  $v_{C,s}$  and the landward edge  $v_{C,l}$ , while the wave gauges gave the signals for the layer thickness  $h_{C,s}$  and  $h_{C,l}$ . As described earlier, statistical characteristics were determined as a relation of detected events and number of waves.

For data analysis the following parameters were distinguished to be analysed in a first step:

- Evaluation from wave measurements:
  - Frequency domain:  $H_{m0}$ ,  $T_p$ ,  $T_{m0,1}$ ,  $T_{m0,2}$ ,  $T_p$ ,  $C_r$ ,  $T_{m-1,0}$
  - Time domain:  $H_{max}$ ,  $T_m$ ,  $N$
  - Plots: time series, energy density, reflection function
- Analysis on wave run-up and wave overtopping:
  - Time domain:  $R_{u2\%}$   
percentage of wave overtopping the freeboard heights:  $P_{OW-60}$ ,  $P_{OW-70}$   
average overtopping rate  $q$
  - Plots: time series, exceedance curves
- Analysis on flow velocity and flow depth:
  - Time domain:  $v_{C0.1\%}$ ,  $v_{C2\%}$ ,  $v_{C5\%}$ ,  $v_{C10\%}$  each for seaward and landward edge  
 $h_{C0.1\%}$ ,  $h_{C2\%}$ ,  $h_{C5\%}$ ,  $h_{C10\%}$  each for seaward and landward edge
  - Plots: time series, exceedance curves

### 5.3 Data processing of the reference test, wave 1

#### 5.3.1 Wave field

In the previous chapters it was mentioned, that a JONSWAP spectrum was used for the investigations. A typical raw data is illustrated in Figure 5.1. The red line is the fixed crossing level at the SWL when the wave gauges should give no surface elevations. The shift between the peaks of each wave gauge is due to the defined distances within the alignment of 0 - 0.4 - 0.75 - 1.0 - 1.1 in the wave array. These

defined distances have to be specified within MikeZero for the reflection analysis. For oblique wave attack the array was not changed in position to a perpendicular attack of the long crested waves, so the distance was recalculated with a factor of the cosine of the angle of wave attack. From the crossing analysis the maximum of detected events of all wave gauges is taken as number of waves  $N$ .

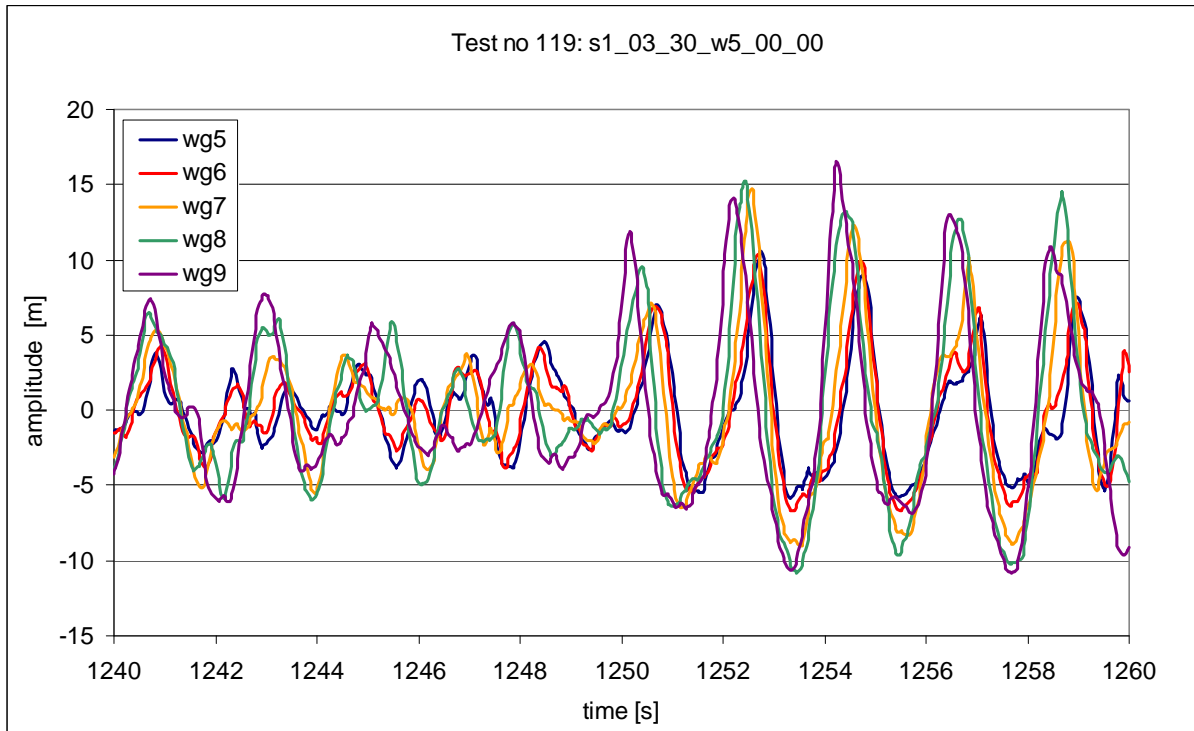


Figure 5.1 Raw data for the wave gauge array of gauges 9-5

To validate the application of a homogenous JONSWAP-spectrum, the results from reflection and crossing analysis were evaluated. From the reflection analysis, which is done in frequency domain, the plotted distribution of energy density in Figure 5.2 corresponds to the theoretical assumption for a JONSWAP spectrum to be single peaked.

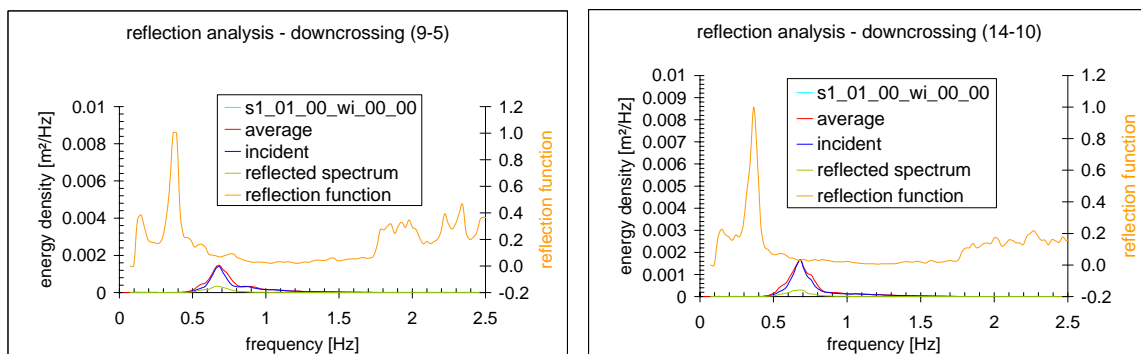


Figure 5.2 Results for spectral energy density (frequency domain); FlowDike 1

As a result of the crossing analysis in time domain, Figure 5.3 depicts the Raleigh distribution of wave heights for both wave arrays, as it is common JONSWAP spectra in for deep water. Here it is applied on the cumulative distribution of the wave height  $H_{m0}$ . The abscissa is fitted to a Raleigh scale by means of the relation:

$$x' = (-\ln(1 - (100\% - x\%)/100))^{0.5} \quad (5.1)$$

The fit is the reason why a linear curve is found. The similarity of their shape indicates the homogeneous arrangement for both crest heights.

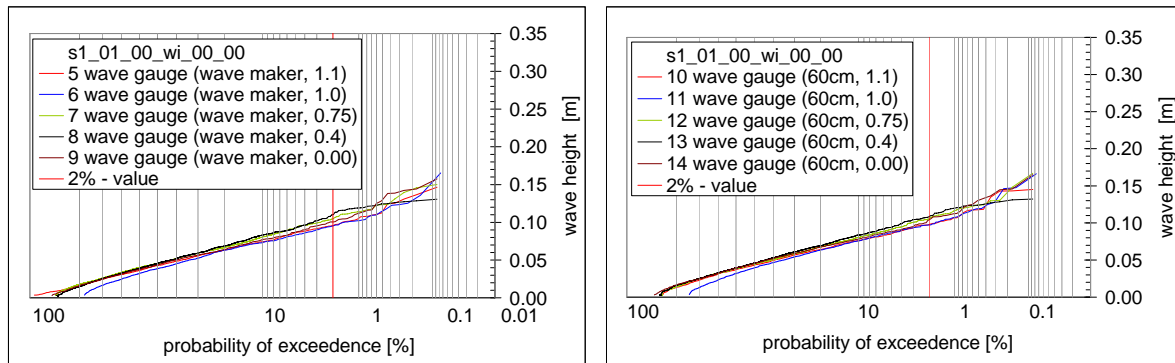


Figure 5.3 Linear distribution of wave height  $H_{m0}$  over a Raleigh scale for a Jonswap spectrum for wave gauge array 9-5 (left) and wave gauge array 14-10 (right); FlowDike 1

## 5.3.2 Run-up

### 5.3.2.1 Video analysis

Stored video data had a compacted AVI-format (*Codec VRMM*) with 10 frames per second. To detect the highest wave run-up height for each frame a MATLAB procedure has been used. In order to get the run-up time series we have to assign the recording time of each frame to the detected run-up in it.



Figure 5.4 MATLAB interface which was used to analyse video films

In the first step of the procedure we have to find in which parts (pixel) of the frame a movement has taken place which is visible by changes in pixel brightness. Therefore the difference between two pictures in sequence was calculated. The difference is equal zero if there was no movement and unequal zero if there was a movement. A variable threshold (threshold for image difference, see “Parameter” in Figure 5.4) has been used to adjust the sensitivity in detection of pixels with significant brightness difference.

In a next step the value “1” (white) was assigned to pixels with significant brightness difference and the value “0” (black) to all others.

After that we have to determine that pixel region of a certain width (min. wave crest width = 5 pixel) and height (min. wave crest height = 1 pixel) which was located at the highest level within one frame. The setting of these two parameters is possible within the left section “Parameter” of the designed MATLAB interface (see Figure 5.4). It was necessary to determine a minimum wave crest width to avoid false detection of reflections on the rough surface of the run-up board or due to water drops as wave tip. A min. wave crest width of 5 pixels was sufficient in most cases.

Now the level value [pixel] of all white regions wider than or equal to min. wave crest width was determined. At the end the region with the global maximum of all level values was identified.

Before one could start the procedure several parts of the pictures have to be excluded from analysis due to several reasons. The size and the location of the excluded picture regions have to be determined for each model test because it could be possible that the location of the camera had been changed between two model tests.

The parts at the left and the right side of the pictures for instance are not necessary within the analysis because they only include things which are located behind the run-up board. These parts were “cut out” by means of a tool which was integrated in the designed MATLAB interface (left below in Figure 5.4). These parts are marked with a darker colour in Figure 5.5.

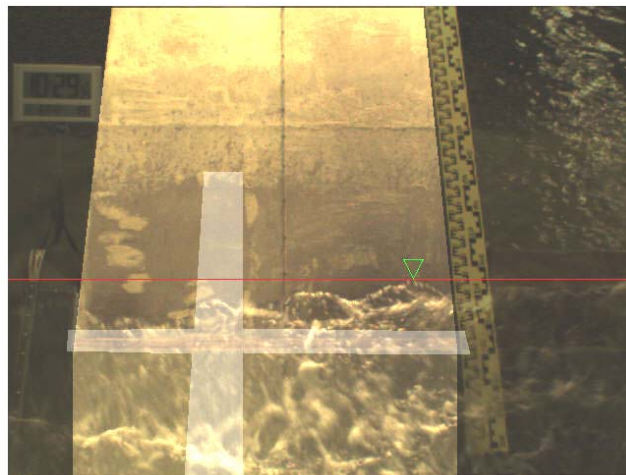


Figure 5.5 Detected position of the highest wave tip on the run-up plate (red line with green triangle)

Another almost perpendicular bar, which is marked with a lighter colour in Figure 5.5 was excluded due to frequent reflections caused by the light of a ceiling lamp which occurred still after the waves run down. The third region is shaped like a horizontal bar and is also marked with a lighter colour in Figure 5.5. This bar covers the boundary between the dike slope and the run-up board. Water drops

remain there due to very small roughness elements and could be detected as wave tips although the wave runs already down.

In order to get a photo documentation of the model tests every single test and every device has been photographed during test program. Due to its smooth surface camera flash lights were reflected by the gauge scale and false detections of wave run-up could be created. That's why the gauge scale at the right side of the run-up plate was excluded from analysis too.

The detected wave run-up height can be visualised within the video in order to verify the detection process. This is marked with a red line and a green triangle in Figure 5.5. During the video analysis every picture was transformed into grey scale and there was no visualisation on the screen in order to get a higher detection speed. Therefore the procedure was started in batch modus.

The last step in the procedure was to calculate the run-up height value in meter out of the run-up height in pixel. There was a nonlinear function due to the optical distortion within the camera lens and due to the effects of perspective because the image plane was not parallel to the run-up board.

This nonlinear function has to be determined for each model test before the analysis was conducted. Therefore several data are used. At first one has to click on the gauge scale in the picture displaced within the designed MATLAB interface. The obtained data set [cm; pixel] is visible as a table in the left and below corner in Figure 5.4 ("gauge scale"). Another used value was the still-water-level. One has to determine its height above level zero of the gauge scale in the set "Parameter" as "SWL" (see Figure 5.4, left and middle). Another needed parameter was the dilatations correction factor. Its determination has been described in chapter 3.3. All these data has been used to obtain a polynomial function of degree 3 to calculate  $R$  [m] out of  $R$  [pixel].

#### 5.3.2.2 Measurement results of the run-up-gauge

The values measured by the capacitive gauge has been stored with all values from other devices as wave gauges, anemometers, micro propellers and ADV in central data storage directly. The unit of these values is Volt and the time series format is \*.dsf0. The latter is a binary code developed by DHI.

Functions (3.2) to (3.5) have been used to calculate the run-up height in meter according to the model set-up.

During the analysis it has been found that the still-water-level in some test records was higher at the end of the test ( $t = t_{\text{END}}$ ) than at the beginning ( $t = t_0$ ). The difference was about 1 cm. The reason was that after the first waves run up little water remained between the two wires above the ring-shaped distance pieces. This was only visible when the water had enough time to evaporate from the wires for instance over night and the wires were totally dry before the tests began. This effect was easily identifiable and has been considered within the data analysis.

#### 5.3.2.3 Determination of $R_{2\%}$

As wave run-up height the value  $R_{2\%}$  is often used within literature. This is the run-up height which has been exceeded by 2 % of all arriving waves of a wave spectrum. Another MATLAB procedure has been used to calculate  $R_{2\%}$  on basis of run-up time series (see chapter 5.3.2.1).

Within the procedure a zero-down-crossing has been used to get the maximum height of each wave run-up. These  $n$  maximum values were then sorted in descending order.

In a second step the number  $m$  of all waves which run up the slope during one model test has been determined. The number of  $m$  could differ from  $n$ .

The value of  $R_{2\%}$  was equal to that wave run-up height which has been exceeded by more than  $k = 0.02 \cdot m$  wave run-ups.

### 5.3.3 Overtopping

For the following analysis the amount of overtopping water was calculated. It occurs that the amounts of both overtopping boxes per crest heights differ a lot from each other. This would be noticeable as scattering in the analysis. Since for analysis an averaged amount of both tanks is used, this information will be lost in the analysing chapter.

The Figure 5.6 (left) shows the raw signal for the evaluated overtopping. This time no pumping was applied and the single events are visible, as well as the final overtopping amounts (65 kg for load cell 43). A total amount of overtopping is calculated from this raw data at the end of the test series. The load in kg (or l) is divided by the test duration and the width of the inlet channel. So, in this case the calculation for load cell 43 is:  $q = 65 \text{ l} / (1350 \text{ s} \times 0.118 \text{ m}) = 0.408 \text{ l}/(\text{s}\cdot\text{m})$ .

The accuracy of the load cell is within a non-linearity of  $< 0.05\%$ . This means for a maximum measuring range of approximately 220 kg (2150 N) this gives a detectable load of 0.11 kg. For the demonstrated test series, with generated wave spectra  $w1$ , the overtopping amount on the 70 cm crest is so small that it would not be taken into account in the analysis. As definition for “detectable” overtopping amounts, a value beneath  $0.02 \text{ l}/(\text{s}\cdot\text{m})$  will be assumed to be negligible.

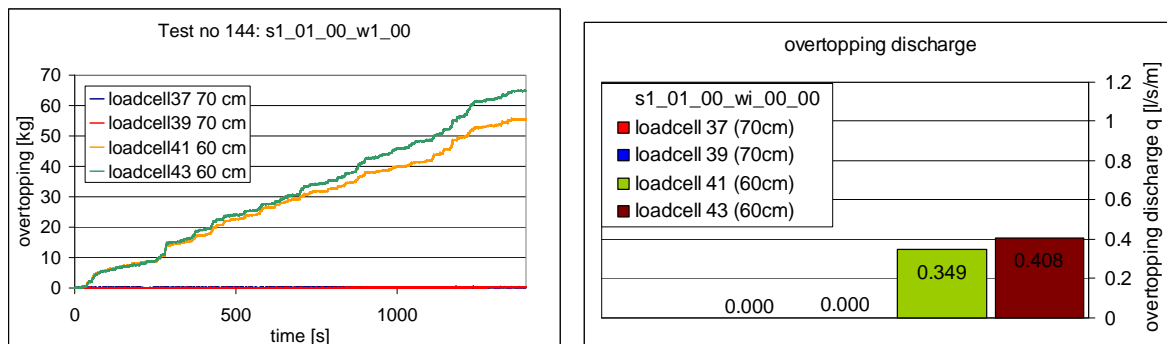


Figure 5.6 Overtopping raw data (left) and calculated overtopping discharge (right)

### 5.3.4 Flow velocity on the crest

In future the main interest will focus on the analysis and description of the single overtopping events. Therefore, also the process of the overtopping on the crest will be analysed in detail. The micro propellers are processed in the same way as the run-up. Threshold levels (0.1 Volt and 1 Volt, see Figure 5.7) were selected to identify the number of events.

Afterwards the measured velocities are displayed within an exceedance curve (see Figure 5.8). Here, values are calculated by adding the threshold and multiplication of the voltage readings with the defined calibration factor (see Annex). The 2%-value for the velocities on the 60 cm are 1.2 m/s (mp 35) and 1.33 m/s (mp 36). For the 70 cm only for the seaward side some items were detected, but do not give any useful results. This fits well with the results from the overtopping.

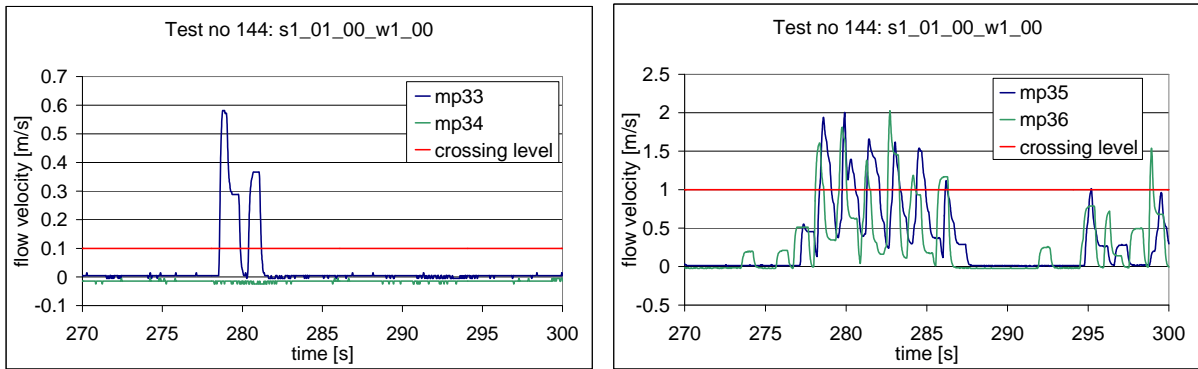


Figure 5.7 Raw data with crossing level - micro propellers on 70 cm crest (left); micro propeller on 60 cm crest (right)

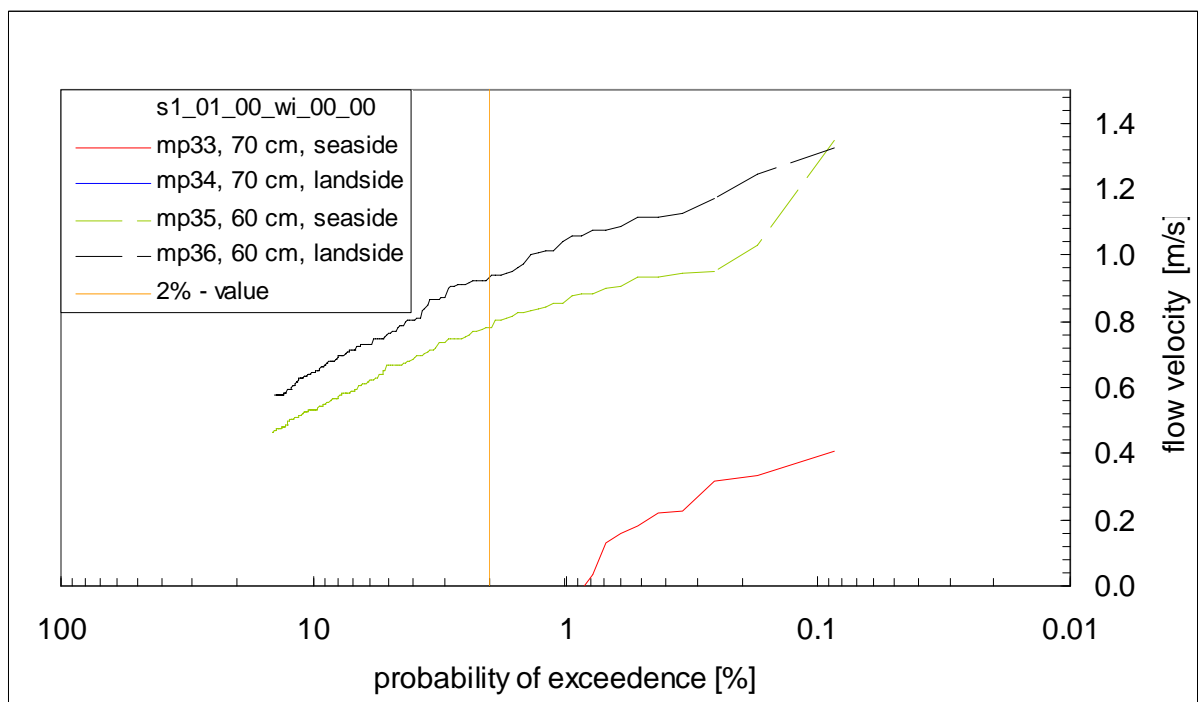


Figure 5.8 Exceedance curves for micro propellers

### 5.3.5 Flow depth on the crest

The procedure in processing remained the same for the layer thickness, as it was done for run-up and flow velocities. The data from the DHI Wave Synthesizer was already given in m, therefore no calibration had to be added on it.

As mentioned above for the micro propellers, items for the 70 cm crest are detected (see the raw data in Figure 5.9), but the exceedance curves do not even reach the 2%-value. This illustrates Figure 5.10; the flow depths for both crest heights are given. Due to the different freeboard heights, the layer thickness on the 70 cm crest is lower than on the 60 cm crest. It can be remarked that the flow depth decreases over the width of the crest, since the wave gauges on the landward edge give smaller values than the ones on the seaward side. The 2%-values of the layer thickness on the 60 cm crest are 0.017 m (wg 17) and 0.026 m (wg 16).

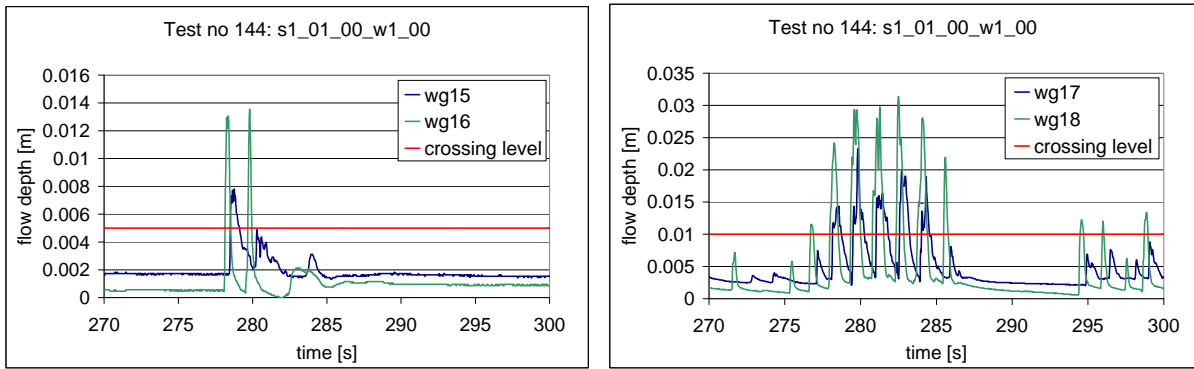


Figure 5.9 Raw data with crossing level – wave gauges on 70 cm crest (left); wave gauges on 60 cm crest (right)

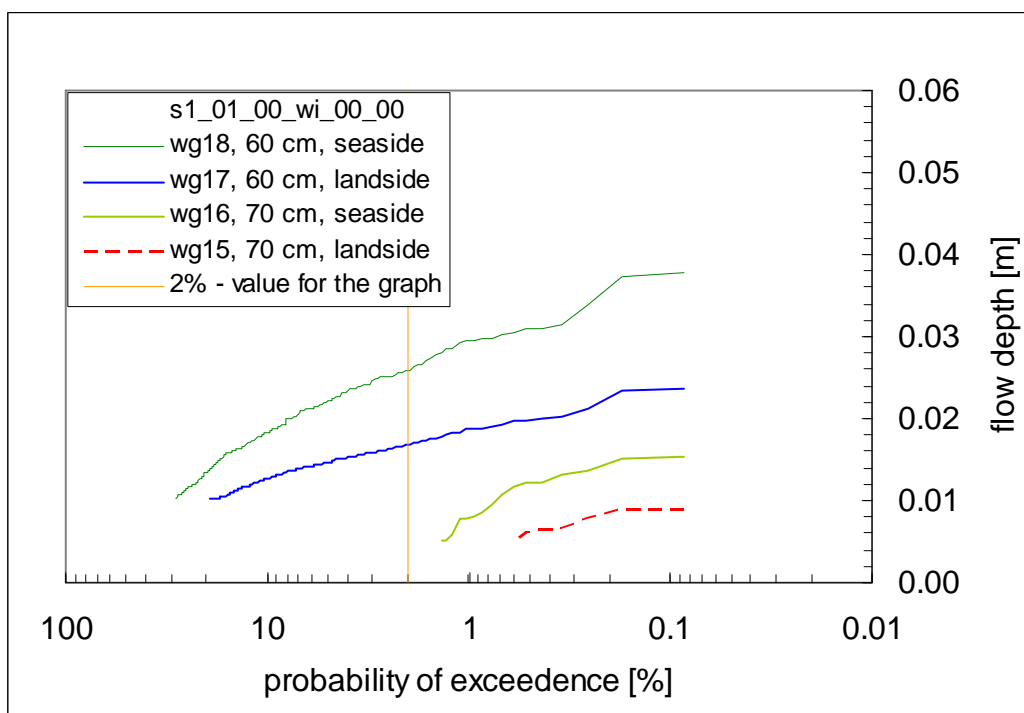


Figure 5.10 Exceedance curves for wave gauges

## 6 Analysis of wave field

### Significant wave height $H_{m0}$

The result analysis considers the relative wave run-up height  $R_{2\%}/H_{m0}$ . That's why this chapter focuses on the deformation of the wave spectrum during its propagation from the wave maker to the dike toe.

The significant wave height is one parameter which has to be determined in the start file of the wave maker (see  $H_{WM}$  in Table 2.1). The values were  $H_{WM} = 0.07$  m (Spectrums 1 and 2); 0.1 m (spectrums 3 and 4) and 0.15 m (spectrums 5 and 6).

The wave spectrum was measured by two sets of 5 wave gauges (see chapter 3.2.3 and 3.2.4). The first set was situated in front of the 70 cm-high model dike (gauge 5-9) and the second set was located in front of the 60 cm-high model dike (gauge 14-10). In Figure 6.1 the calculated values  $H_{m0}$  for the reference test condition are shown. Values are calculated for each wave gauge of the two wave gauge sets and differ a little.

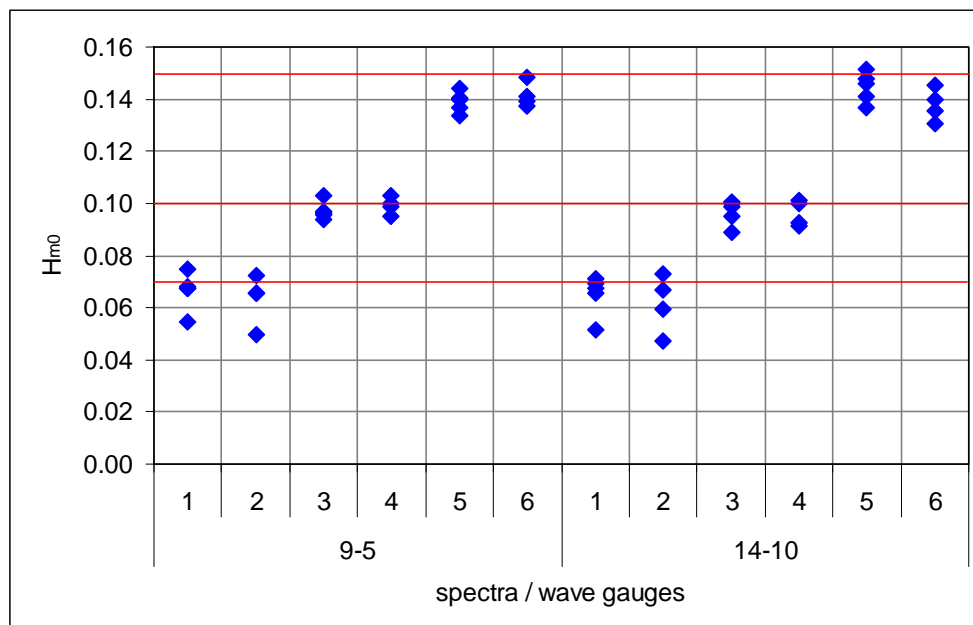


Figure 6.1 Significant wave height  $H_{m0}$  for the reference model test calculated at each wave gauge of the two sets of wave gauges (no. of wave spectrum see Table 2.1)

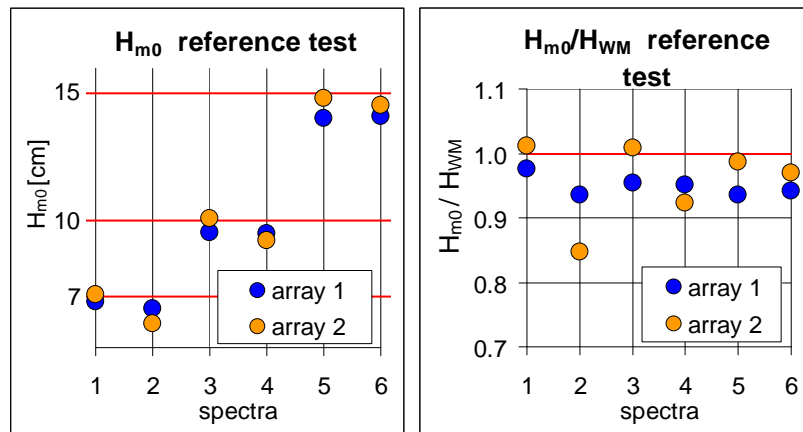


Figure 6.2 Significant wave height  $H_{m0}$  of the attacking spectrums, results from the reference model tests (left:  $H_{m0}$  [cm], right:  $H_{m0}$  relative to the wave height created by the wave maker  $H_{WM}$ )

After cross correlation under consideration of wave reflection only one value  $H_{m0}$  for each reference model test was obtained. These values are presented in Figure 6.2 (left figure). In addition relative values  $H_{m0}/H_{WM}$  are presented (right figure).

The relative values cover a range between 0.94 and 0.98 (wave gauge set 1) and 0.85 and 1.01 (wave gauge set 2). Results from wave gauge set 1 are more consistent. Figure 6.3 presents the energy density depending on frequency for wave spectrum 2 which shows the highest discrepancy for the relative values in Figure 6.2. The energy density of the superposed spectrum (average) measured by wave gauge set 2 is considerable lower than values obtained by wave gauge set 1. Because  $H_{m0}$  is proportional to energy  $H_{m0,2}$  is lower than  $H_{m0,1}$ . Further analysis is required to interpret this effect.

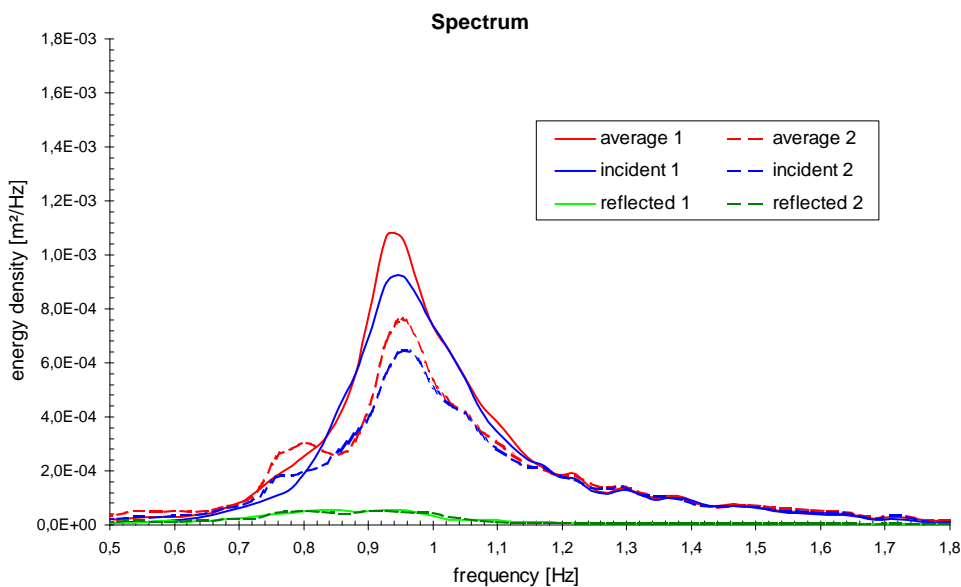


Figure 6.3 Energy density versus frequency: values of the incident, reflected and superposed spectrum calculated for the two sets of wave gauges (reference model test, avi-file no. 145 (see Table A 1) and wave spectrum no. 2)

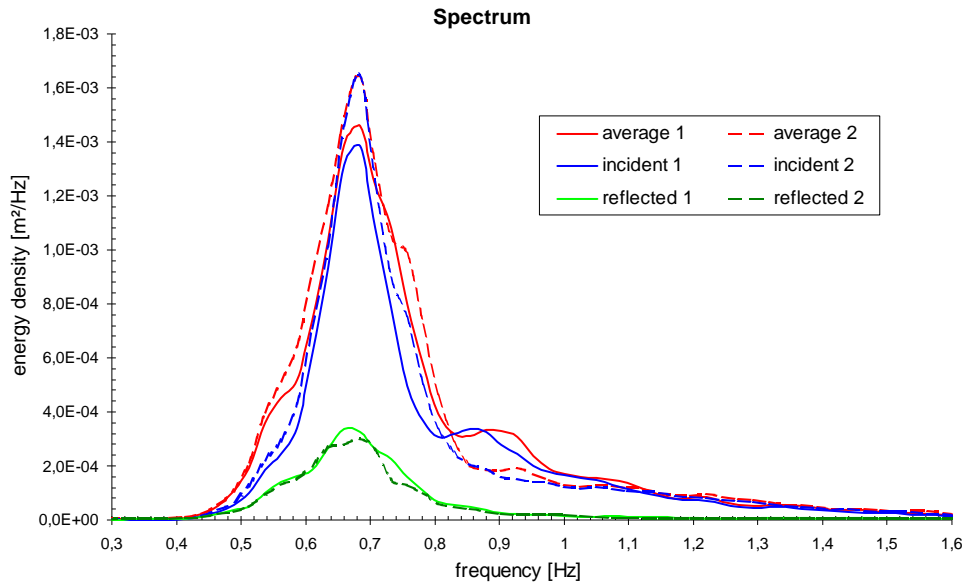


Figure 6.4 Energy density versus frequency: values of the incident, reflected and superposed spectrum calculated for the two sets of wave gauges (reference model test, avi-file no. 144 (see Table A 1) and wave spectrum no. 1)

Figure 6.4 presents the energy density depending on frequency for wave spectrum 1 in Figure 6.2 as another example. Besides the energy density of the superposed spectrum (average) measured by wave gauge set 2 and wave gauge set 1 shows different peaks the region bounded by the curves are very similar. That's why the obtained values  $H_{m0}$  are very similar too.

Results indicate a deformation during wave propagation. Therefore  $H_{m0}$  based on measurements was used to determine the relative wave run-up height in the following analysis.

The following diagrams present the influence of wind, current and wave direction on significant wave height (Figure 6.5 and Figure 6.6) and on wave period (Figure 6.7 and Figure 6.8).

Values measured by wave gauge set 1 lead to little higher factors in best fit line functions obtained by linear regression. Increased values  $H_{m0}$  are caused by oblique wave attack.  $H_{m0}$  is 1.28-times bigger in model tests with  $\theta = 45^\circ$  than the values obtained in reference model tests. Comparison between angles of wave attack with positive and negative sign is possible because only model tests without current were included in the analysis.

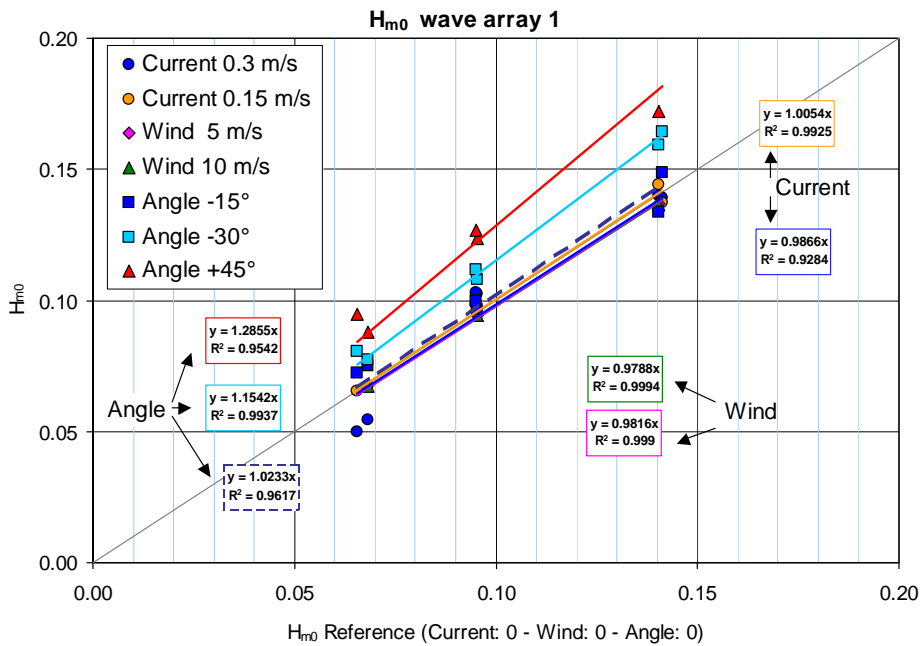


Figure 6.5 Significant wave height measured by wave gauges no. 1: comparison between reference tests and model tests with only one different influencing parameter (wind, wave direction, current)

The influence of wind on significant wave height is very small ( $< -2\%$ ). A lower current velocity  $v = 0.15$  m/s has no decisive effect either ( $\pm 1\%$ ).

If we consider a mean value of measurement results of wave gauges set 1 and 2 the significant wave height decreases under the influence of a higher current velocity  $v = 0.3$  m/s ( $-5\%$ ).

Figure 6.7 and Figure 6.8 present a comparison between wave period determined in reference model test and in model test with only one parameter (wind, current, wave direction) different.

Results indicate no decisive effect by wind.

A oblique wave attack creates little deformation in wave period ( $< -4\%$ )

Although there is no deformation effect with slow current  $v = 0.15$  m/s ( $-1\%$ ) the faster current velocity  $v = 0.3$  m/s produces significant shorter wave periods ( $8\% - 9\%$ ).

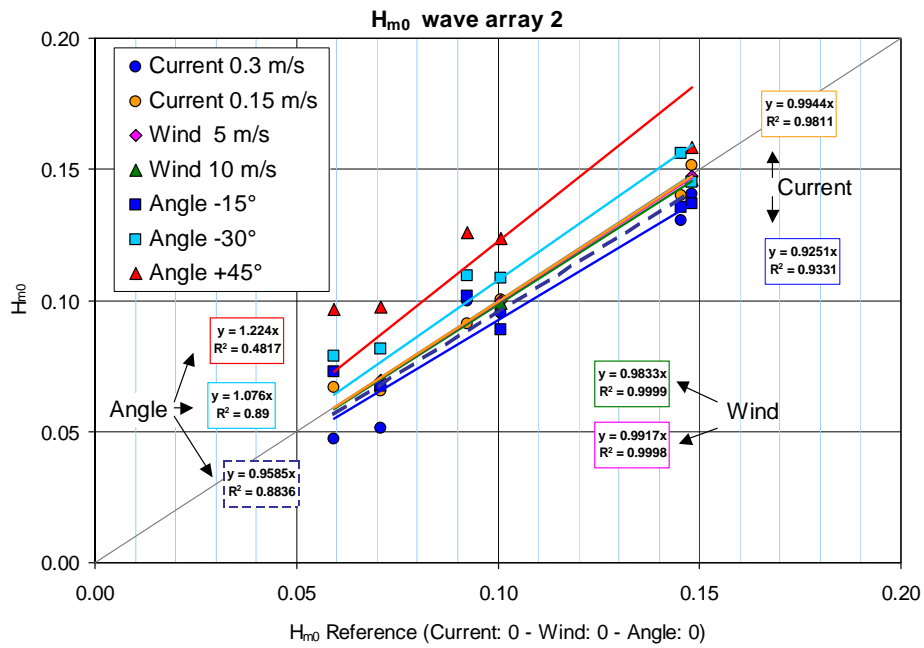


Figure 6.6 Significant wave height measured by wave gauges no. 2: comparison between reference tests and model tests with only one different influencing parameter (wind, wave direction, current)

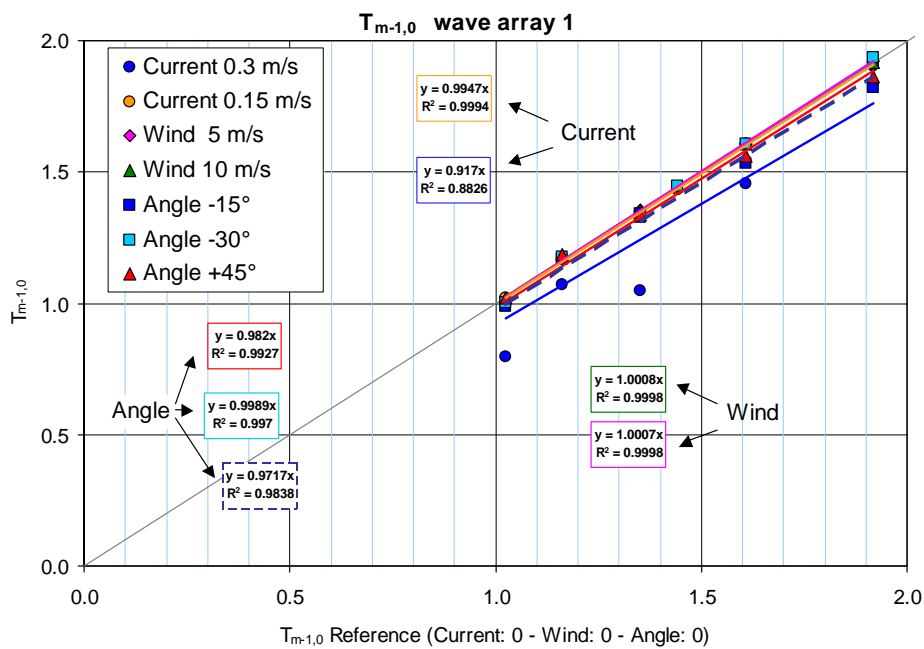


Figure 6.7 Wave period measured by wave gauge set 1: comparison between reference tests and model tests with only one different influencing parameter (wind, wave direction, current)

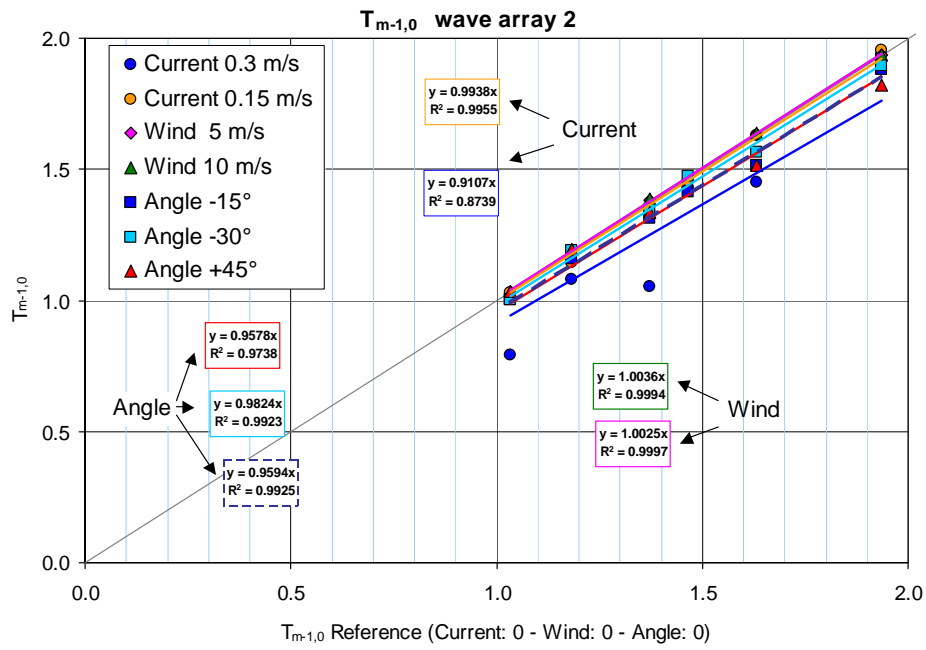


Figure 6.8 Wave period measured by wave gauge set 2: comparison between reference tests and model tests with only one different influencing parameter (wind, wave direction, current)

## 7 Analysis on run-up

### 7.1 Remarks

The main objectives of measurement analysis are to estimate the influence of each parameter considered (current, wind, direction of wave attack) on the wave run-up height and to determine correction factors using in equation (4.1).

The following analysis includes generally these model tests which differ from reference tests (without wind, without current, wave attack orthogonal to the dike crest) only by one parameter (wind, wave direction, current).

### 7.2 Comparison between capacitive gauge and video

Figure 7.1 shows the run-up height depending on time obtained by both measurement facilities – the capacitive gauge and video camera (model test 155). Obviously there is a good agreement and both measurement techniques are suitable to determine wave run-up.

As mentioned before video analysis could only determine wave run-up in regions without reflection. So the run-up peaks at time  $t = 33$ ; 53 and 58 seconds (marked with black ellipses) represent only the lowest boundary of that region which was excluded during video analysis (see chapter 5.3.2.1). The capacitive gauge gives the right values. But this has no effect on  $R_{2\%}$  because the error affects only the smaller run-up heights.

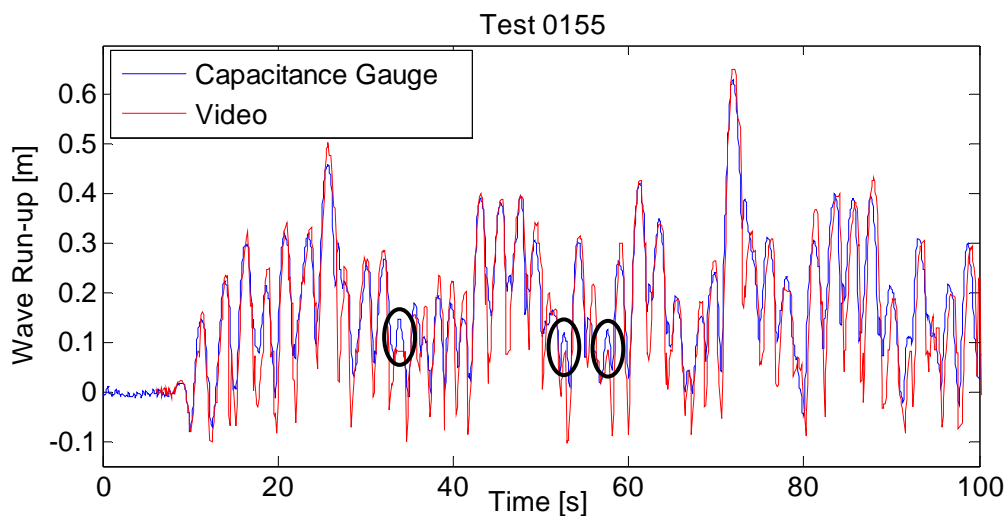


Figure 7.1 Wave run-up depending on time measured by capacitive gauge and video, model test 155

A comparison between calculated values of  $R_{2\%}$  for both measurement facilities for all model tests is presented in Figure 7.2. Designation is the same as in Table 2.2. The first number is equal to the setup number and the second number marks the model test.

The values on basis of capacitive gauge measurement are almost all lower than the values obtained by video analysis. The difference is up to 5 cm and in the case of oblique wave attack up to 7 cm. This is because the capacitive gauge was situated in the middle of the run-up plate and could only measure the wave run-up there although the run-up height differed along the plate width. Result from video analysis captured always the maximum run-up height independent of its location on the run-up plate

(see chapter 5.3.2.1). The wider amplitude of the video measurement results in Figure 7.1 is caused by these characteristics of the used measurement facilities.

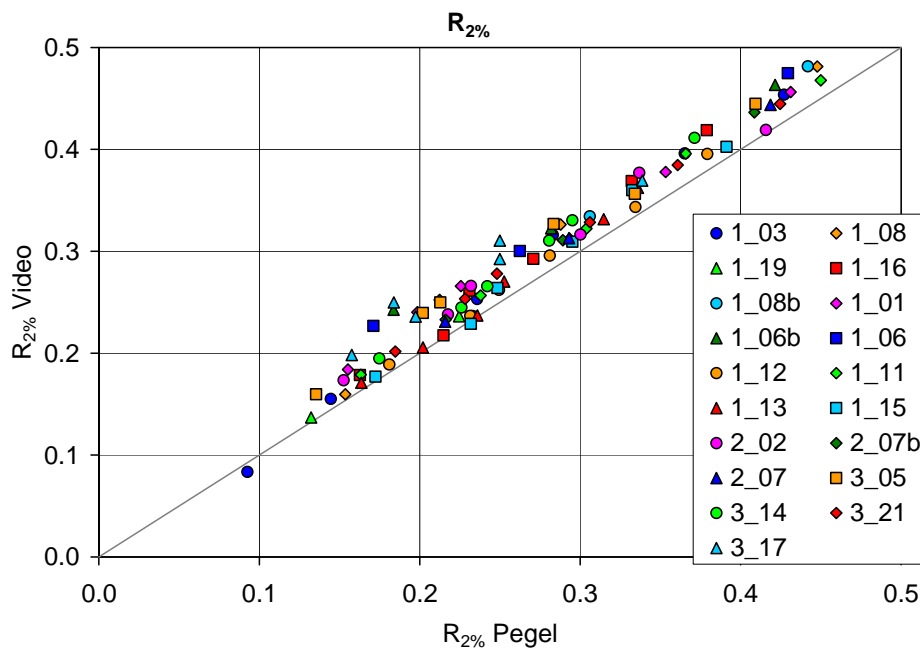


Figure 7.2 Wave run-up height  $R_{2\%}$  (percentile 2%) for all model tests: comparison between values on basis of video analysis and capacitive gauge measurement

The following discussion includes only  $R_{2\%}$ -values obtained by video analysis.

### 7.3 Run-up height $R_{2\%}$ and relative run-up height $R_{2\%}/H_{m0}$

Figure 7.3 and Figure 7.4 show calculated values of relative wave run-up height  $R_{2\%}/H_{m0}$  versus Iribarren number  $\xi_{m-1,0}$  for all model tests. The annotation numbers refer to Table 2.2. First number is equal to the model setup number and second number describes the model test (column “Testserie”). Two functions have been added to the figures, on the one side the function by EUROTOP 2007 (equation (4.1) and (4.2)) and on the other hand function presented by POHL & HEYER 2005. Reference model tests (without current, without wind, wave attack orthogonal to the dike crest) are marked with “+”. Values for  $H_{m0}$  were obtained by analysis of wave spectrums measured by the wave gauge set 1 (gauge 5 – 9) because these gauges are situated nearer to the run-up plate.

Relative run-up of reference model tests in Figure 7.3 (values from video analysis) is higher than the function by EUROTOP 2007. This is due to video analysis routine which detects the highest run-up for each time step. EUROTOP 2007 refers to mean values of wave run-up.

Relative run-up of reference model test in Figure 7.4 (values measured by capacitive gauge) is lower than expected by EuroTop 2007. This is explicable because the function of EUROTOP 2007 is only valid for smooth dike slopes. The rougher surface of the dike slope in the model setup causes lower wave run-up heights.

Iribarren number is  $\xi_{m-1,0} > 1.3$  for all model tests and  $> 2$  for the most. That is why breaking waves in the model test could be described as plunging breakers. Still surging breakers are also possible.

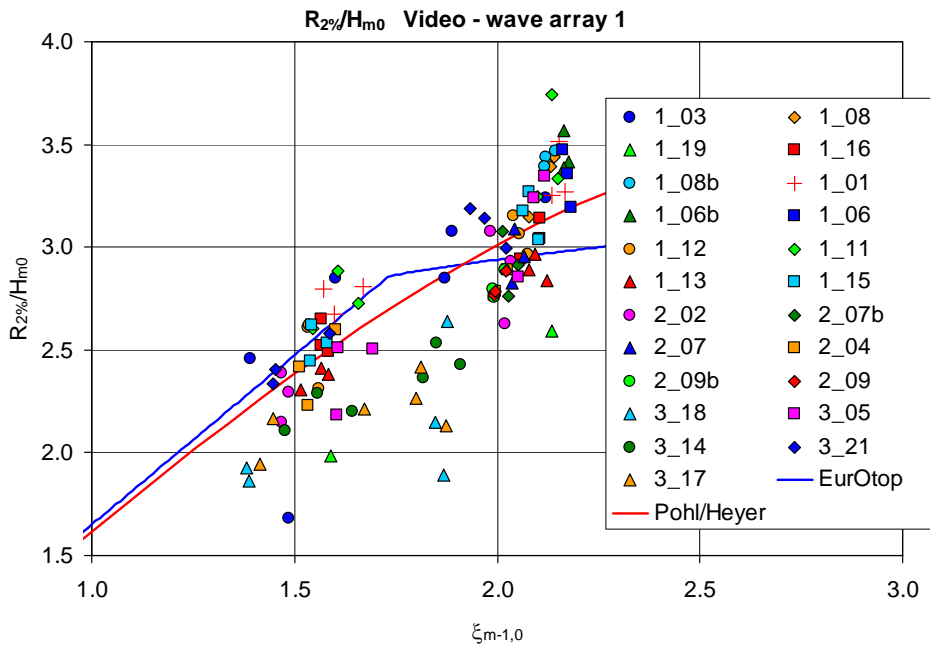


Figure 7.3 Relative run-up height  $R_{2\%}/H_{m0}$  versus Iribarren number  $\xi_{m-1,0}$  (results from video analysis;  $H_{m0}$  measured at wave gauge set 1; see Table 2.2 for annotation numbers)

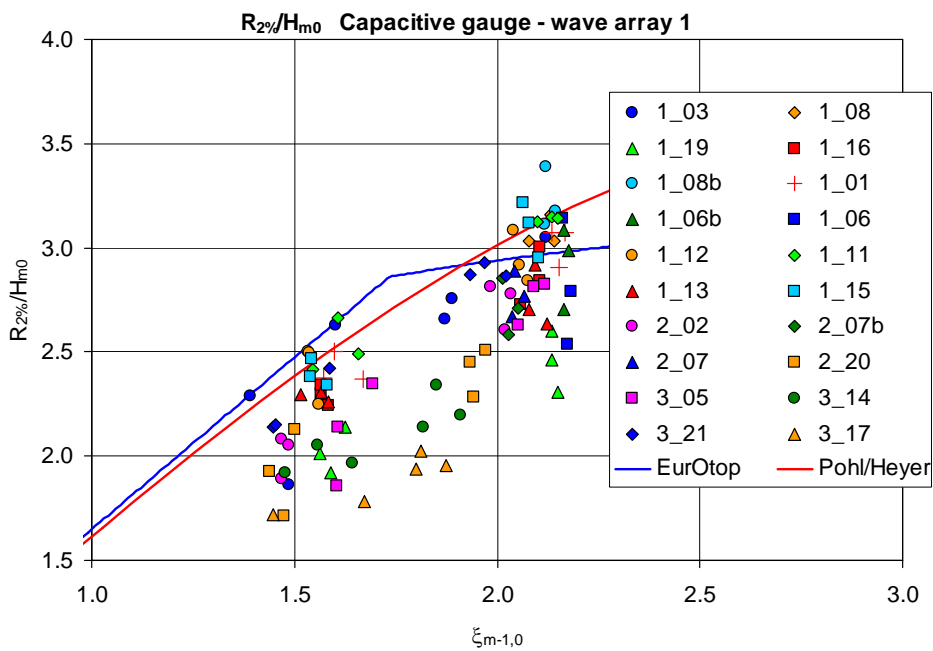


Figure 7.4 Relative run-up height  $R_{2\%}/H_{m0}$  versus Iribarren number  $\xi_{m-1,0}$  (results from capacitive gauge;  $H_{m0}$  at wave gauge set 1; see Table 2.2 for annotation numbers)

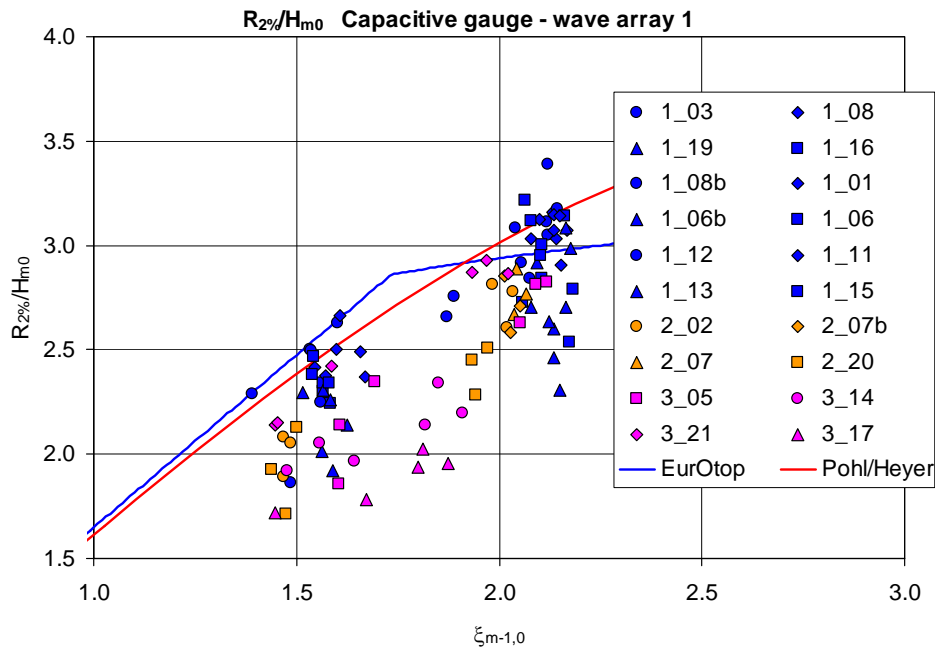


Figure 7.5 Relative run-up height  $R_{2\%}/H_{m0}$  versus Iribarren number  $\xi_{m-1,0}$  (results from capacitive gauge;  $H_{m0}$  at wave gauge set 1; each setup is marked by different colour; see Table 2.2 for annotation numbers)

Figure 7.5 shows the same diagram as Figure 7.4 but each setup is marked by different colour. It is visible that the model test with setup 1 and 2 are characterised by a smaller number of  $\xi_{m-1,0}$ . Model test with setup 3 include tests with  $\theta = 30^\circ$  and  $45^\circ$  and current. That's why the deformation of each wave spectrum is stronger.

Figure 7.6 presents the calculated values based on measurements by capacitive gauge. The diagram shows the relative wave run-up height  $R_{2\%}/H_{m0}$ .  $H_{m0}$  is the significant wave height of the attacking wave spectrum measured at the dike toe (70 cm high reach) by wave gauge set 1. In the diagram relative run-up of reference tests has been compared to model tests with only one different influencing parameter (wind, wave direction, current). Best fit lines obtained by linear regression for each parameter investigated have been added to the diagram.

As expected wave run-up caused by oblique wave attack is lower than by orthogonal wave direction ( $\theta = 0^\circ$ ). The result gives a decrease of about 2% if  $\theta = 15^\circ$  and of about 12% if  $\theta = 30^\circ$ .

A current of  $v = 0.15$  m/s leads to an increasing wave run-up (4%). This effect is also perceptible considering the absolute values  $R_{2\%}$  (see Figure 7.8) and independent from deformation of wave spectrums. The influence is in the same order of magnitude as errors in measurement techniques. That's why further analysis is required to check these results.

Model tests with current  $v = 0.3$  m/s lead to a decreasing wave run-up (6%). But some test configurations result in increasing wave run-up.

The number of model test with wind is too small (only 3 wave spectrums with steepness of 0.025) to obtain satisfactory conclusions about its influence on wave run-up.

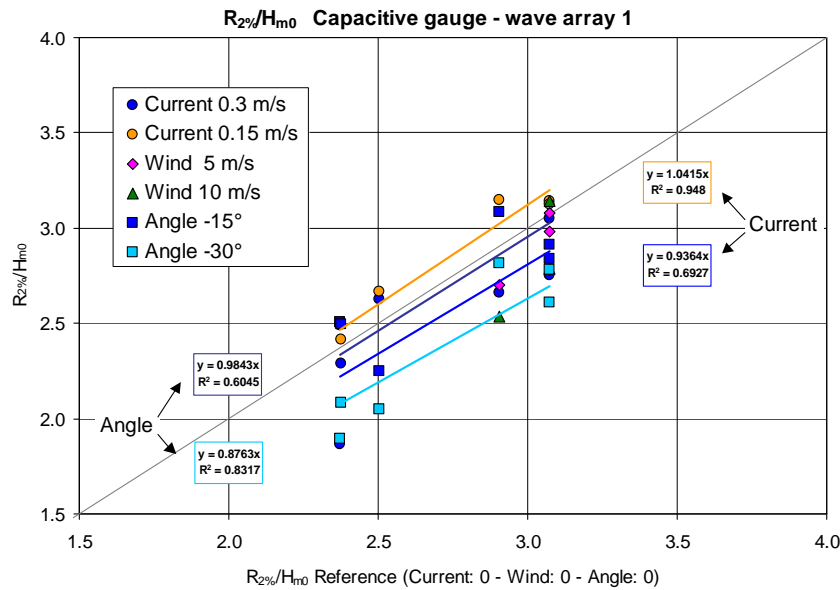


Figure 7.6 Relative run-up measured by capacitive gauge: comparison between reference tests and model tests with only one different influencing parameter (wind, wave direction, current)

Figure 7.7 shows the analogous diagram to Figure 7.6 but with values of relative run-up on the basis of video analysis. The slope of best fit line is smaller considering model tests with current as well as oblique wave attack. That means that the influence on the highest wave tip determined in the video analysis is stronger than on a mean run-up height measured by capacitive gauge<sup>3</sup>. Wave run-up height under oblique wave attack with an angle of  $\theta = -45^\circ$  are lessened by 33% in average.

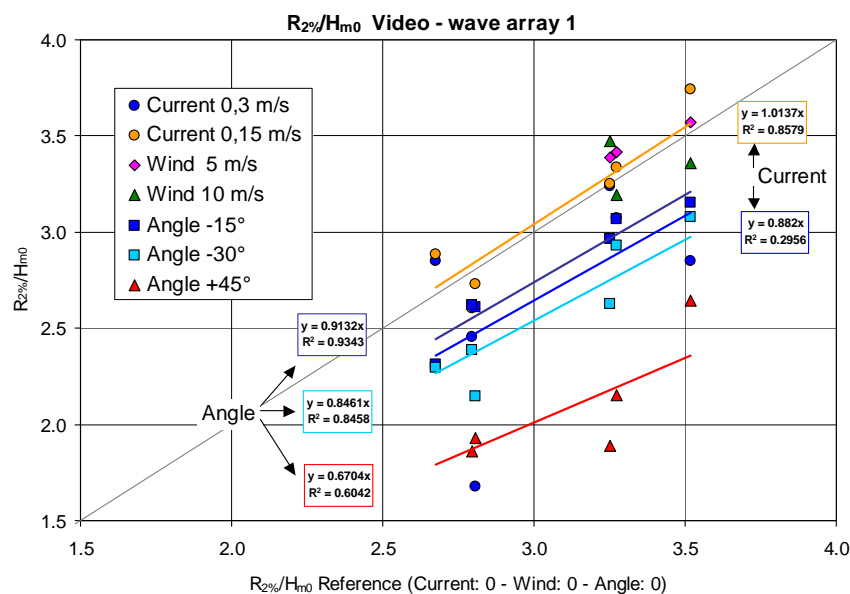


Figure 7.7 Relative run-up height from video analysis: comparison between reference tests and model tests with only one different influencing parameter (wind, wave direction, current)

<sup>3</sup> Measurement results from the capacitive gauge are supposed to be mean values because of the random variation of wave run-up about the width of the run-up plate. During video analysis the highest wave tip for each time step was detected.

A comparison between the values of run-up height measured by capacitive gauge for reference tests versus model tests with one different influencing parameter (wind, wave direction, current) each is shown in Figure 7.8. In all cases the deviation is less than 5 % which indicates that the influence of wind, wave direction and current is marginal within the investigation area.

Figure 7.9 shows an analogous diagram but with results from video analysis. As mentioned in reference to relative run-up height the decrease of highest run-up (results from video analysis) is bigger than in the case of mean run-up (results from capacitive gauge). The model test with wind don't show any influence on wave run-up.

All results of linear regression show higher values of  $R^2$  considering the absolute run-up height  $R_{2\%}$  than in respect to relative run-up  $R_{2\%}/H_{m0}$ . This means that conclusions referring to  $R_{2\%}$  are more reliable.

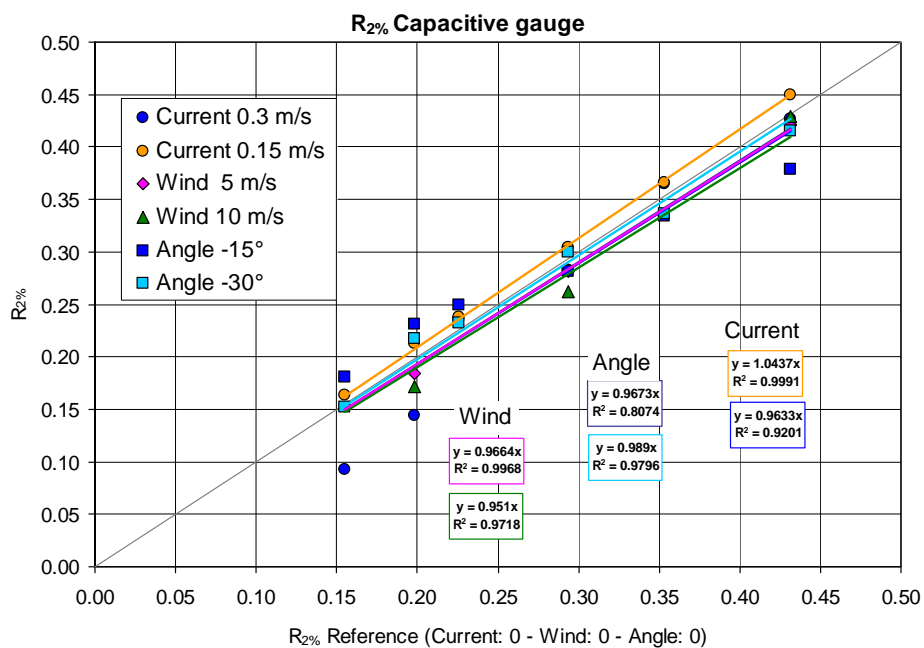


Figure 7.8 Run-up height measured by capacitive gauge: comparison between reference tests and model tests with only one different influencing parameter (wind, wave direction, current)

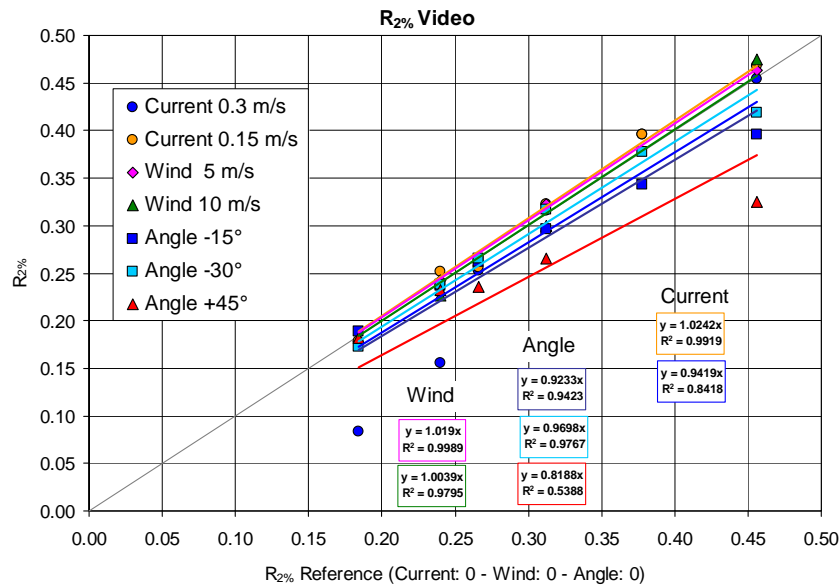


Figure 7.9 Run-up height from video analysis: comparison between reference tests and model tests with only one different influencing parameter (wind, wave direction, current)

### 7.3.1 Influence of the wave direction $\theta$

To analyse the influence of the direction of wave propagation the ratio  $\gamma_\theta$  between relative run-up height of oblique waves and waves with a propagation direction orthogonal to the dike crest was considered:

$$\gamma_\theta = \frac{(R_{2\%}/H_{m0})_\theta}{(R_{2\%}/H_{m0})_{orth}} \tag{7.1}$$

Figure 7.10 shows calculated values of  $\gamma_\theta$  in dependence of the angle of wave attack  $\theta$ . These values are equal to the derivative of  $\gamma_\theta$  with respect to  $\theta$  or the slope of the linear best fit line in Figure 7.6.

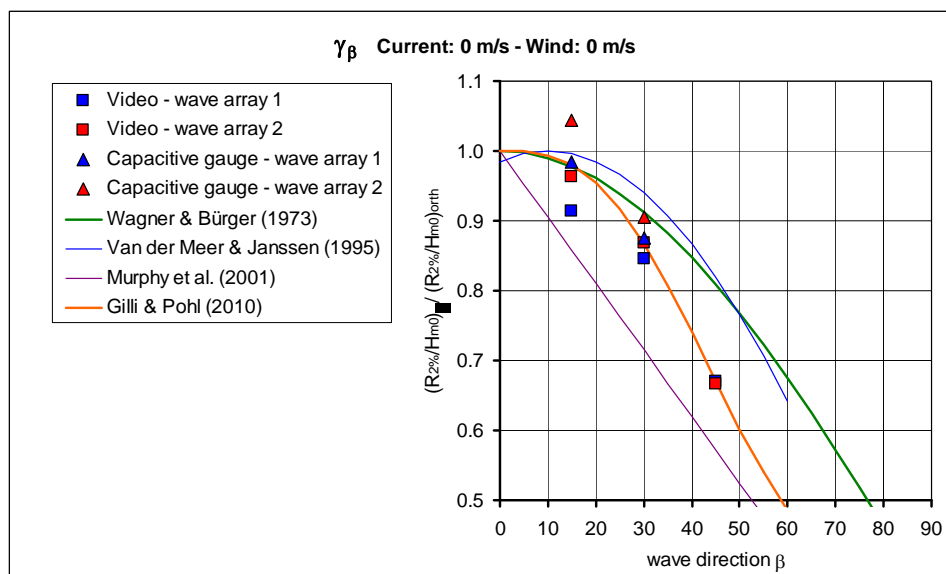


Figure 7.10 Ratio  $\gamma_\theta$  between relative run-up height of oblique waves and waves with a propagation direction orthogonal to the dike crest (results from model test without current)

It is evident that the bigger the angle of wave direction the smaller the ratio  $\gamma_\theta$ . Obviously the relation between  $\gamma_\theta$  and  $\theta$  is nonlinear.

Some function of older investigations has been added to the calculated values in Figure 7.10. On the one hand the formula of WAGNER & BÜRGER 1973 agree to the own results for smaller values of  $\theta$ . But on the other hand the bigger the angle of wave attack the bigger the discrepancy to the values on the basis of measurements.

The following function of best fit line has been obtained:

$$\gamma_\theta = a + b \left[ (1 + \theta') e^{-\theta'} \right]^{c\theta'} \quad (7.2)$$

with  $\theta' = \frac{\theta}{90}$  and  $\theta$  [degree] and the following coefficients:

$$a = 0.35; b = 0.65 \text{ and } c = 15.0$$

Function (7.2) has been added to Figure 7.10 too. The function is only valid for  $\theta < 50^\circ$  considering the model tests. A validation with model test including angle of wave attack  $\theta > 45^\circ$  is desirable.

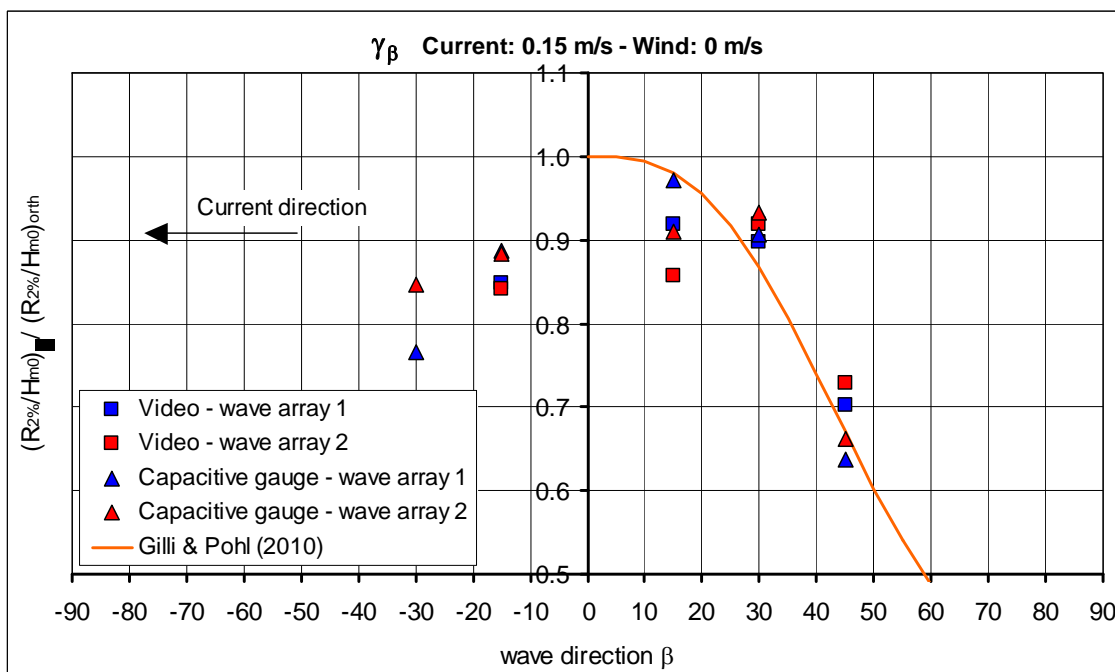


Figure 7.11 Ratio  $\gamma_\theta$  between relative run-up height with oblique waves ( $\theta = -30; -15; 15; 30; 45^\circ$ ) and waves with a propagation direction orthogonal to the dike crest (current velocity  $v = 0.15$  m/s, (—) GILLI & POHL 2010, see Figure 7.10)

Figure 7.11 presents the calculated ratio  $\gamma_\theta$  between the relative run-up height with oblique waves and a wave direction orthogonal to the dike crest. Only model test with current  $v = 0.15$  m/s are considered. A comparison between the values of  $\gamma_\theta$  based on model test with current (dots in Figure 7.11) and without current (orange line, see also Figure 7.10) shows that a current has a significant influence only in model test with a negative wave direction which means an oblique wave propagation against the current.

### 7.3.2 Influence of current

To analyse the influence of current the ratio  $\gamma_v$  between the relative run-up height with and without current was considered:

$$\gamma_v = \frac{(R_{2\%}/H_{m0})_v}{(R_{2\%}/H_{m0})_0} \quad (7.3)$$

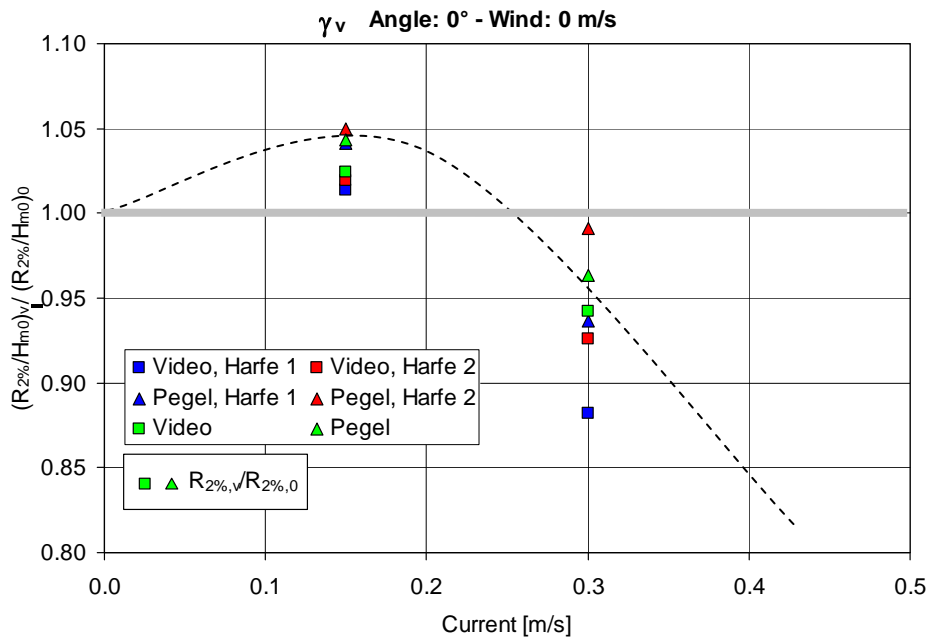


Figure 7.12 Ratio  $\gamma_v$  between relative wave run-up height from model tests with current ( $v = 0.15$  and  $0.30$  m/s) and without current

Figure 7.12 shows the calculated values  $\gamma_v$  for all model tests differing only by current ( $v \neq 0$ ) from reference model test ( $v = 0$ ). Furthermore the ration  $\gamma_{v,abs}$  between absolute values of run-up height with and without current

$$\gamma_{v,abs} = \frac{R_{2\%,v}}{R_{2\%,0}} \quad (7.4)$$

has been added to the figure. These values are independent of  $H_{m0}$  at the dike toe but the deformation of the wave spectrum during propagation from the wave maker to the dike slope may be included within these values.

Each dot in the diagram represents a mean value of all 6 model test with the same boundary conditions and one of the 6 spectrums considered (see Figure 7.6 and Figure 7.9). It is obvious that the decrease of  $\gamma_v$  considering the highest run-up height (results of video analysis) is bigger than the decrease considering mean run-up height (results from capacitive gauge).

On the assumption that  $\gamma_{v,rel} = \gamma_v = 1$  if  $v = 0$  and besides the only few measurement results one could conclude that the function between  $\gamma_{v,rel}$  or  $\gamma_v$  and  $v$  has a non-linear character (dotted line). Measurement results indicate first an increasing and then a decreasing function. Further investigation should carry out to validate this result.

Finally results indicate a non-linear decreasing effect on wave run-up caused by current.

## 8 Analysis on overtopping

### 8.1 Introduction

This chapter describes the analysis on the influence of wind, currents and oblique wave attack on wave overtopping. The studied data set includes different combinations of all influencing parameters, but can be subdivided in four main sub sets:

- Perpendicular wave attack – as reference test
- Wind influence on wave attack
- Current influence on wave attack
- Oblique wave attack

The basic set for perpendicular wave attack and the sub set for oblique wave attack are used for a first comparison of the tests to the currently applied formulae, summarised in the EUROTOP-MANUAL (2007), and former investigations made i.e. by OUMERACI ET AL. (2001). This is done first to validate the applied evaluation method. In addition the newly introduced variables, such as current and wind, are analysed and compared to the basic tests. As a first step, analysis on current and wind influence are done for perpendicular wave attack and will be followed by an analysis of their influence on oblique wave attack.

The considered parameters are defined as following:

- wind velocity  $u$ :                5 m/s (only FlowDike 1) 10 m/s
- current velocity  $v$ :            0.15 m/s 0.3 m/s 0.4 m/s (only FlowDike 2)
- angle of wave attack  $\beta$ :     $0^\circ$   $-15^\circ$   $+15^\circ$   $-30^\circ$   $+30^\circ$   $+45^\circ$

Negative wave angles are with the current and positive ones against it.

### 8.2 Methods

In the EUROTOP-MANUAL (2007) probabilistic formulae are given for the “design and prediction or comparison of measurements ( $\xi_{m-1,0} < 5$ )“. These formulae are mentioned in 4.2. Analyses start with distinguishing the set of results in breaking and non-breaking conditions. Therefore the formulae (4.3) and (4.4) are used to calculate the average overtopping discharge  $q$  from the given or measured boundary conditions. As the non-breaking condition limits the overtopping discharge as a maximum value, see formula (4.4), the smallest of both results should be taken as governing condition. Here the wave heights and overtopping amounts are given for each crest from different overtopping devices.

After the distinction in breaking and non-breaking waves, the dimensionless parameter for overtopping discharge  $Q_*$  and freeboard height  $R_*$  are calculated. These parameters differ, depending on the breaking condition, and are displayed as parameter groups in the overtopping graphs. Formulas for breaking (8.1) and non-breaking (8.2) conditions determine two dimensionless parameter groups  $Q_*$  and  $R_*$ :

$$Q_* = \frac{q}{\sqrt{g \cdot H_{m0}^3}} \cdot \sqrt{\frac{s_{m-1,0}}{\tan \alpha}} \quad R_* = \frac{R_c}{H_{m0}} \cdot \sqrt{\frac{s_{m-1,0}}{\tan \alpha}} \quad (8.1)$$

$$Q_* = \frac{q}{\sqrt{g \cdot H_{m0}^3}} \quad R_* = \frac{R_c}{H_{m0}} \quad (8.2)$$

Description:

- $Q_*$  = dimensionless overtopping rate [-]
- $R_*$  = dimensionless freeboard [-]
- $H_{m0}$  = significant wave height [m]
- $s_{m-1,0}$  = wave steepness [-]
- $\alpha$  = slope of the front face of the structure [°]

The dimensionless factors correspond to the exponential relationship used for the calculation of the average overtopping rate, as given in EUROTOP-MANUAL (2007):

$$Q_* = Q_0 \cdot \exp(-b \cdot R_*) \quad (8.3)$$

Description:

- $Q_0$  = interception with the y-axis [-]
- $b$  = inclination of the graph [-]

This relation gives the probabilistic curves for overtopping calculation using the following factors (see also the graphs in the EUROTOP-MANUAL (2007) :

- breaking waves:  $Q_0 = 0.067$ ;  $b = -4.75$
- non-breaking waves:  $Q_0 = 0.2$ ;  $b = -2.6$

Furthermore, reduction factors for obliqueness  $\gamma_\beta$  can be determined by comparison of the different exponential coefficients  $b$ . The exact procedure is to divide the slope coefficient of the perpendicular wave attack by the slope coefficient for the considered angle of wave attack.

$$\gamma_\beta = \frac{b(\beta = 0)}{b(\beta)} \quad (8.4)$$

In a first step this analysing method will be adapted as well for the influence of current and wind.

The following chapters will break down the different combinations, which were investigated, and combine them to the given theories. At this point it should be mentioned; that an average overtopping rate  $q$  per crest calculated from both tanks was used for the determination of the dimensionless factor  $Q_*$ . The influence of this method will be discussed later.

### 8.3 Influence of wave direction

Oblique wave attack has been investigated before, so this chapter will only be an adaptation and verification. This is done with regard to the following analyses, which will consider the combined effects of obliqueness, currents and wind.

#### Oblique wave attack – FlowDike 1

In the following figures (Figure 8.1 and Figure 8.2) all test results for oblique wave attacks are given. The trend lines have been determined with fixed interception for each angle of wave attack.

Again the data points lay very well around their exponential regression. Only the points for non-breaking with  $-15^\circ$  oblique waves seem to scatter too much. There is an obvious trend in both graphs, where the increase of obliqueness results in a reduction of overtopping. For the larger angles the reduction increases, this means between  $0^\circ$  and  $15^\circ$  the reduction is lower than between  $30^\circ$  and  $45^\circ$ .

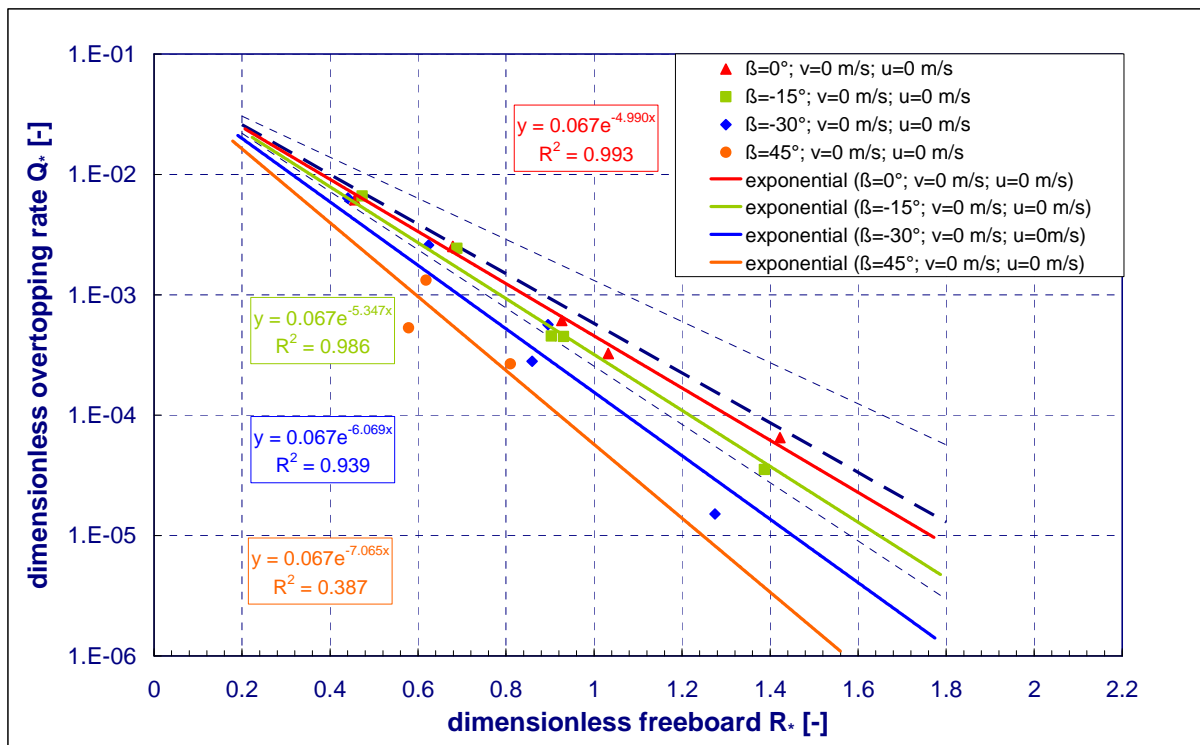


Figure 8.1 Oblique wave attack; FlowDike 1 (breaking conditions)

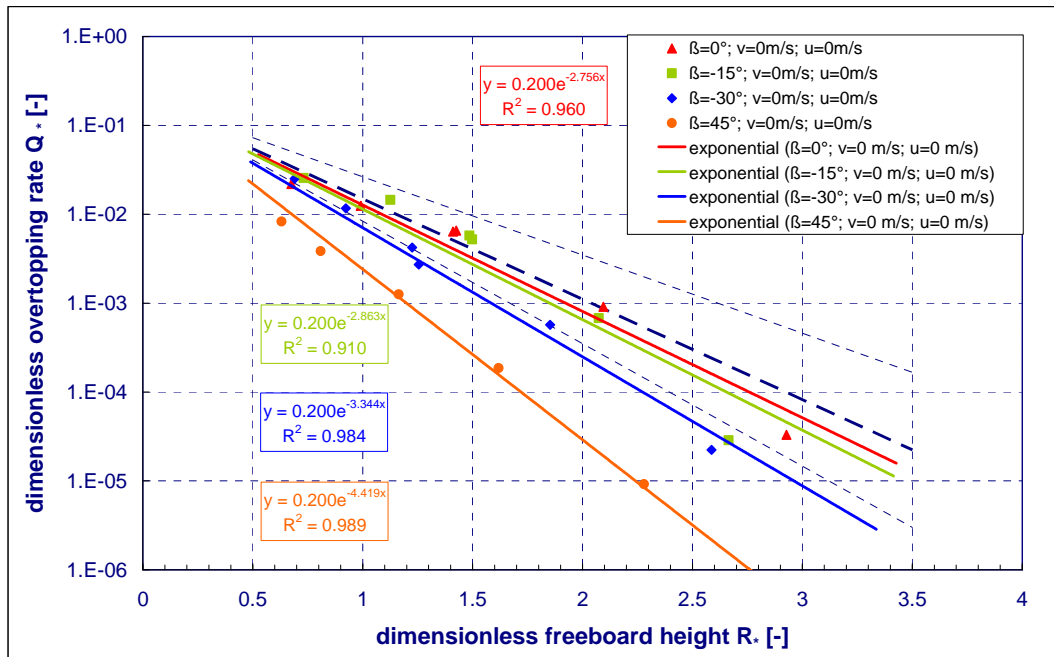


Figure 8.2 Oblique wave attack; FlowDike 1 (non-breaking conditions)

### Oblique wave attack – FlowDike 2

For FlowDike 2 the trend lines and results for oblique wave attack for the breaking conditions are illustrated in Figure 8.3. Still the trend is followed that an increase in obliqueness results in the reduction of overtopping, but this time the reduction, especially between  $30^\circ$  and  $45^\circ$ , is not as large as for the 1:3 sloped dike. It was mentioned before those small overtopping amounts were expected and also recognised during testing due to the slope inclination. An explanation for less difference in the overtopping graphs for FlowDike 2 could be as well the smoother slope of the dike that leads to early breaking on the dike.

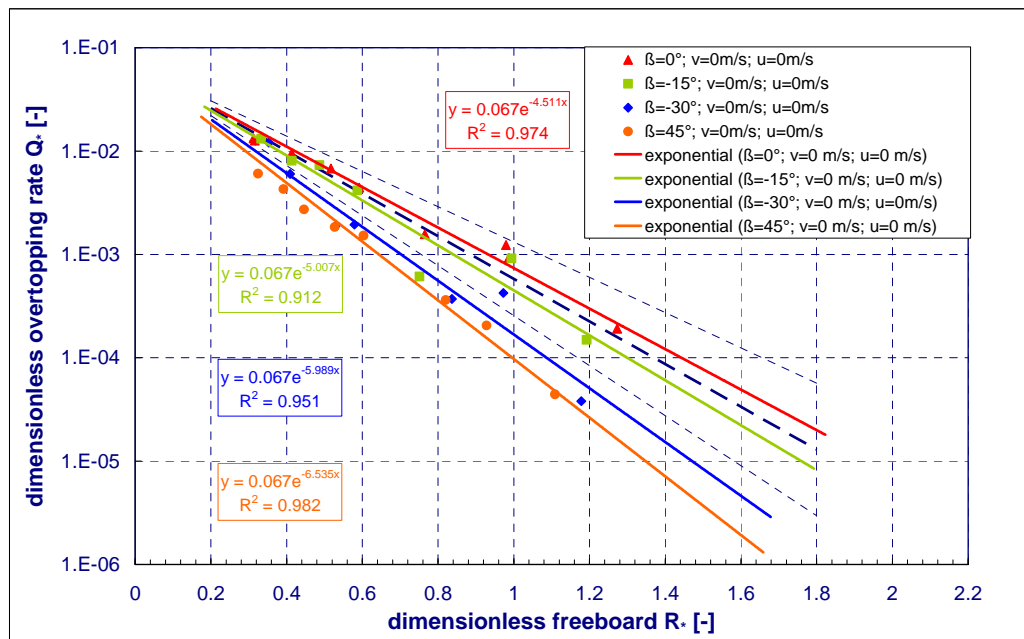


Figure 8.3 Oblique wave attack; FlowDike 2 (breaking conditions)

### Relation of the slopes 1:3 and 1:6

A closer look at the coefficient  $b$  shows that for all different angles of wave attack a shift between the 1:3 slope and the 1:6 slope is noticeable. The shift was already perceived for the perpendicular waves (section 8.4) and will stay the same through the whole analysis. Comparing the inclinations of the slope ( $b_{1:6}/b_{1:3}$ ), all of them are decreasing about 7% - 10%; only for the 30° angle this relation is not followed. Here the inclination remains approximately the same  $(-5.989/-6.069) = 99\%$ .

### 8.4 Analysis of the reference test serie

In a first step the results from the basic test without wind or current are compared to the existing formulae from the EUROTOP-MANUAL (2007). The results for FlowDike 1 and FlowDike 2 are illustrated below, together with the formulae for breaking and non-breaking waves ((4.3) and (4.4)) and their 90% confidence interval.

First the results for both configurations fit well within the 5% upper and lower confidence limits, which are displayed as dotted lines in the graphics. Most of the points fall below the average probabilistic trend (dashed blue line) from the EUROTOP-MANUAL (2007), but validate altogether the formulae.

An easier comparison for the following analysis is given by adding a “trend line”, in Excel for the results. Here an exponential trend is chosen due to the relation between dimensionless overtopping discharge  $Q_*$  and freeboard height  $R_*$ , given earlier in formula (8.3).

After fitting the trend for the basic reference test, all following analysis will be done by regression analysis. For this purpose the inclinations of the slope  $b$  for each test series trend are compared to the inclination  $b$  of the basic test. This method is explained more detailed in the summarising chapter on reduction factors 8.8.

The analysis on wave overtopping were done with averaged overtopping volumes, due to this applied method the scattering of data points is not visibly. It has to be mentioned, that this scatter occurs and might be due to the narrow width of the channels compared to the length of the dike. This has to be kept in mind for the reliability of the analysis.

#### Perpendicular wave attack – FlowDike 1

Two different trend lines are chosen to be compared. First a simple regression for the best fit was used. Secondly, for better comparison with the formulae from the EUROTOP-MANUAL (2007), a regression with a fixed crossing on the y-axis was applied. The fixed interception  $Q_0$  remains the same as the y-axis crossing from formulae (8.3) for each breaking condition.

In contrast to (8.3) the dimensionless factors found for the best fit (black line) are:

- breaking waves:  $Q_0 = 0.057; \quad b = -4.836$
- non-breaking waves:  $Q_0 = 0.265; \quad b = -2.901$

With a fixed interception the following trend (red line) is found:

- breaking waves:  $Q_0 = 0.067$ ;  $b = -4.990$
- non-breaking waves:  $Q_0 = 0.2$ ;  $b = -2.756$

The regression coefficient  $R^2$  gives the accuracy of the applied trend line. Here the regression coefficients for both graphs do not deviate a lot from each other. They are  $R^2 = 0.994$  (best fit) and  $R^2 = 0.993$  (with fixed  $Q_0$ ) for breaking conditions and  $R^2 = 0.963$  (best fit) and  $R^2 = 0.960$  (with fixed  $Q_0$ ) for non-breaking conditions.

In each case the results follow an average trend, which is just a bit lower than the stated equation from the EUROTOP-MANUAL (2007). The regression coefficient shows that both fitted trends do not deviate a lot from one another. Concluding for the analysis on wind, current and oblique wave attack, the crossing with the y-axis of the basic reference test can remain the same as in the formulae from EUROTOP-MANUAL (2007), but the inclination of the slope  $b$  will increase. This factor will influence the designated comparison of the results, as it is used to determine the influence of each variable within a parametric study.

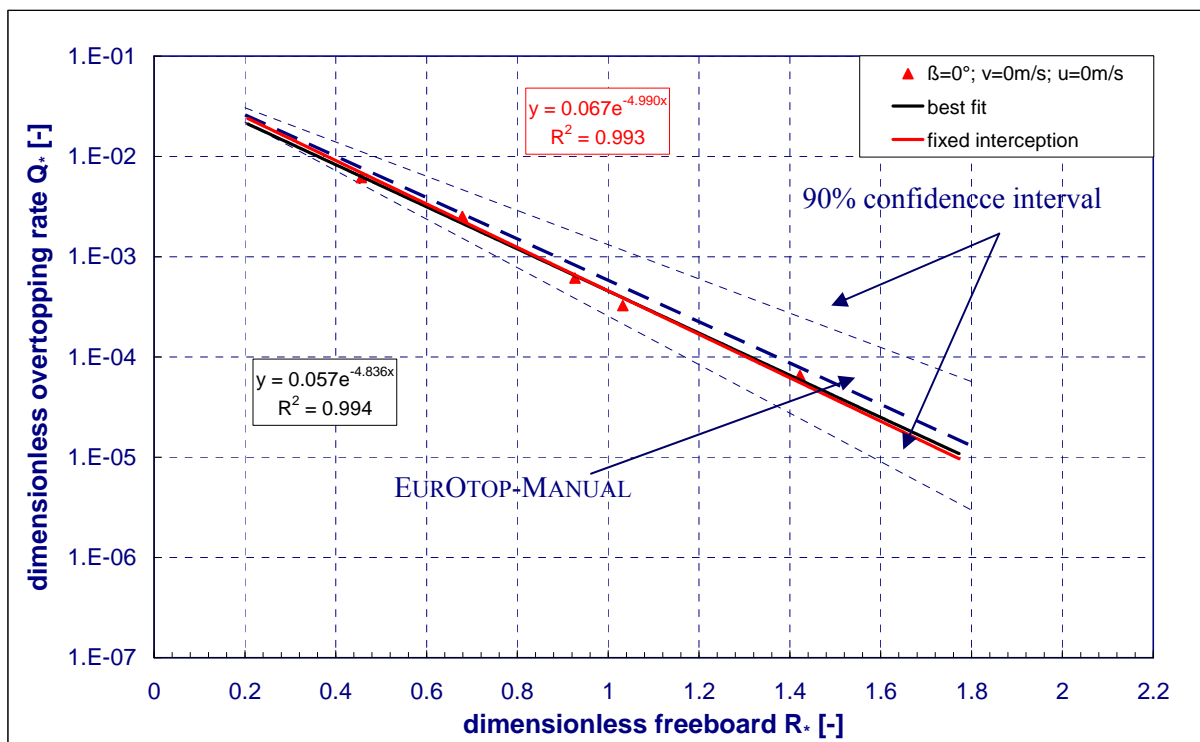


Figure 8.4 Reference test; FlowDike 1 (breaking condition)

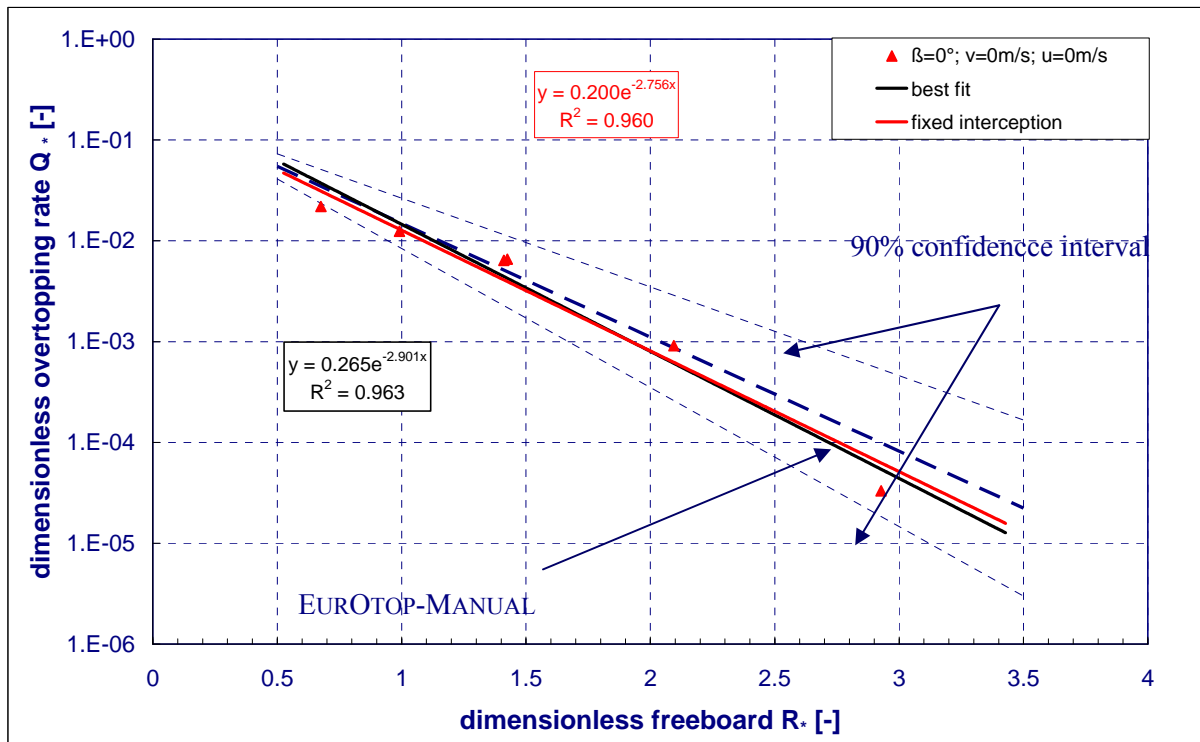


Figure 8.5 Reference test; FlowDike 1 (non-breaking condition)

### Perpendicular wave attack – FlowDike 2

For FlowDike 2 the same procedure was applied as explained in the chapter above. The only difference is in the breaking conditions, as for a 1:6 sloped dike only breaking conditions exist, due to the influence of the slope.

Also for the 1:6 sloped dike the averaged overtopping amount fit well in the 90% confidence interval. Though the trend lines chosen for the regression analysis reveal an average trend that is close to the probabilistic line, it is slightly higher than the overtopping formula.

The dimensionless factors found for the best fit (black line) are:

- breaking waves:  $Q_0 = 0.052$ ;  $b = -4.214$

With a fixed interception the following trend (red line) is found:

- breaking waves:  $Q_0 = 0.067$ ;  $b = -4.511$

The regression coefficient are  $R^2 = 0.980$  (best fit) and  $R^2 = 0.974$  (with fixed  $Q_0$ ) for breaking conditions. Due to this fact and for better comparison the analysis will remain based on a regression curve with fixed interception, as described for the 1:3 slope.

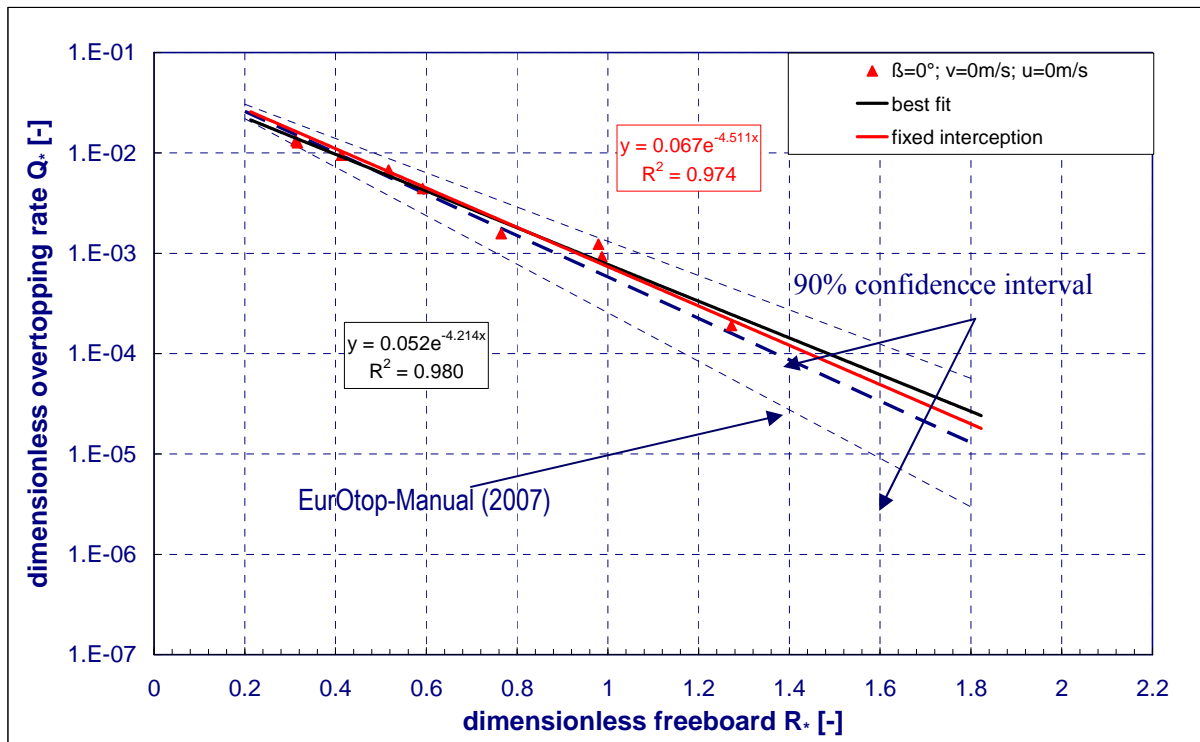


Figure 8.6 Reference test; FlowDike 2 (breaking condition)

### Relation of the slopes 1:3 and 1:6

Summarising the first conclusions drawn in this chapter, it can be stated that:

- The results validate well the theory applied in EUROTOP-MANUAL (2007).
- The overtopping formula overestimate slightly the results found in FlowDike 1, but underestimates those of FlowDike 2.
- The trend lines with fixed interception show an acceptable accuracy compared to the “best fit”.
- The basic trend lines used for regression analysis of the following parametric set can be fixed on the y-axis to the interception values of formulae (8.3).
- Between the results of FlowDike 1 and FlowDike 2 a shift will remain during the analysis. This variance is about 10% conferring the slope inclinations  $(b_{1:6}/b_{1:3}) = (-4.511/-4.990) = 90\%$ .

### 8.5 Influence of wind

From the test program it can be seen that the test series on wind contain merely the wave spectra w1, w3 and w5 with a steepness of 0.025. The steepness is a limiting factor for the breaker parameter and affects as well the overtopping formulae. Due to this is the reason, the generated waves for wind tests give only results for non-breaking conditions during FlowDike 1. For FlowDike 2 the influence of the slope was governing and still only breaking waves occurred. Another difference between FlowDike 1 and FlowDike 2 is the missing wind tests on  $u = 5\text{m/s}$ , only two tests on this wind speed exist, but have not been evaluated yet.

### Perpendicular wave attack with wind influence – FlowDike 1

Though the effect in overtopping could be measured, the detected events marked as points in the graphs show almost no influence for high overtopping events (lying on the points of the reference test). For smaller amounts an increasing trend for the average overtopping can be established. This coincides well with the statements from WARD ET AL. (1996) and DE WAAL ET AL. (1996)

It is remarkable in Figure 8.7 that the trend lines stay within the confidence interval. As the trend lines are all above the reference trend from the basic test, it can be concluded that the overtopping increases for wind influence. For both investigated wind velocities the resulting regression is very close, as the inclinations of the slope  $b$  do not differ a lot. This effect could be explained with the small difference between the measured velocities. As the scaling of the wind is a very complex issue (GONZALEZ-ESCRIVA, 2006) and only two different velocities were applicable, the parametric range is very small.

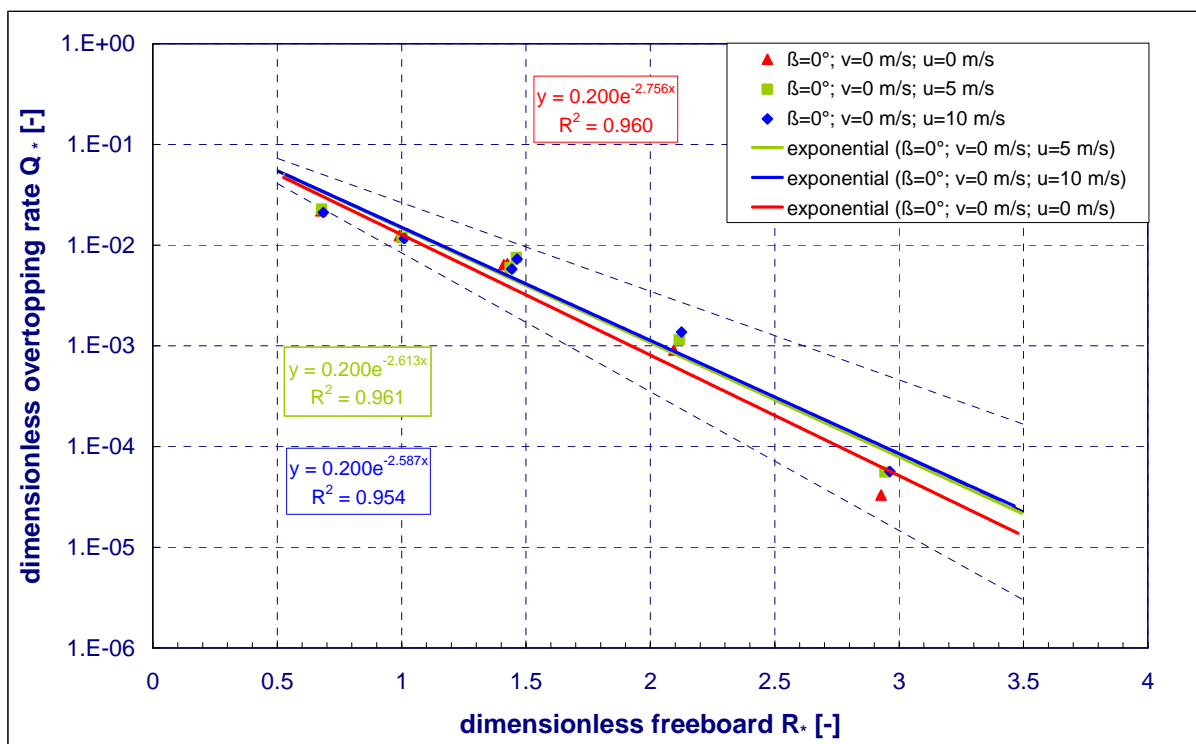


Figure 8.7 Wind influence; FlowDike 1 (non-breaking conditions)

### Perpendicular wave attack with wind influence – FlowDike 2

For FlowDike 2 the effect of increasing average overtopping amounts for the smaller wave spectra, such as  $w_1$  can be stated again. The first data points for high waves in the graph match again the points from the reference test, but for smaller overtopping amounts the influence is visible. Here the increasing effect of wind is calculated from the relation of the inclination of the graphs  $b$   $(-4.249/-4.511) = 1.062$  (about 6%).

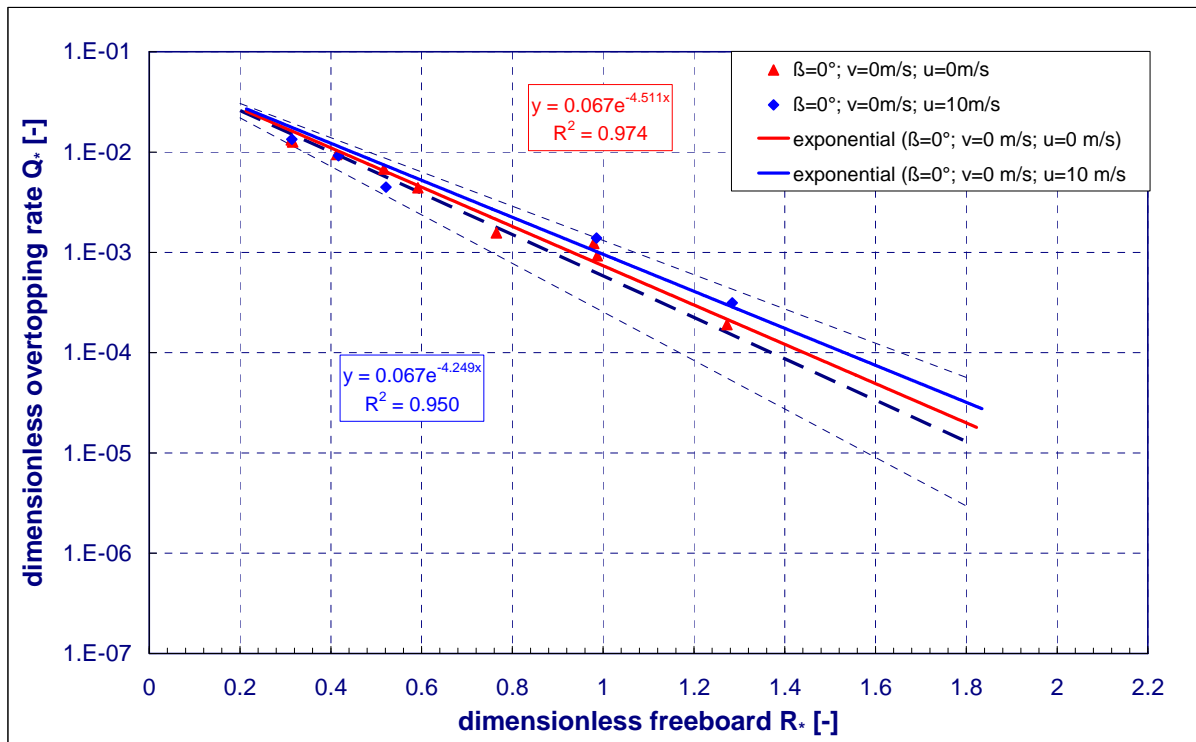


Figure 8.8 Wind influence; FlowDike 2 (breaking conditions)

### Relation of the slopes 1:3 and 1:6

Although the wind velocities differed by a factor two, the calculated factors  $\gamma$  show that their influence on the overtopping did not deviate a lot. For wind speeds of 5 m/s an increase of 5.5% for the overtopping was designated in FlowDike 1, but for 10 m/s the influence increased only about 1% to 6.5%. FlowDike 2 only contained the tests for a wind speed of 10 m/s. This test led to a factor of 6.2% so a little lower than in FlowDike 1.

### 8.6 Influence of current

The current effect on wave overtopping was investigated on two different velocities during FlowDike 1. In FlowDike 2 it was possible to apply another higher current of 0.40 m/s. This enlarged the data sets and reflects more on real situations. As described for the wind tests, also for current effects, the smaller wave spectra give a good impression of the influence on overtopping. Nevertheless it has to be investigated if the influence on overtopping is negligible for high overtopping events as well.

#### Perpendicular wave attack with current influence – Flow Dike 1

Illustrated in Figure 8.9 and Figure 8.10 are the results for breaking and non-breaking conditions. Both graphics show that in summary the data points drop below the reference curve. For the non-breaking conditions the current of 0.15 m/s seems to be a bit too high compared to the effect within the breaking conditions, where the regressions for 0.15 m/s and 0.30 m/s are closely aligned. The marked data point in the graph seems to be a little bit too high, but still the graph fits well.

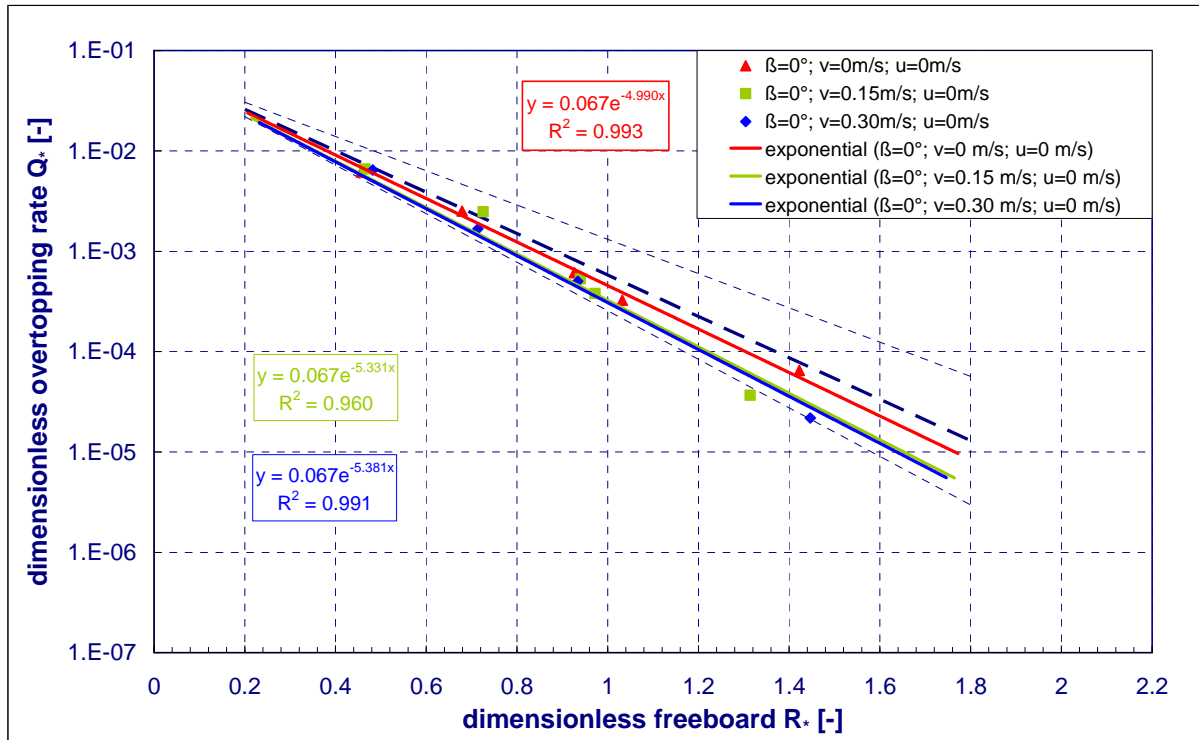


Figure 8.9 Current influence; FlowDike1 (breaking conditions)

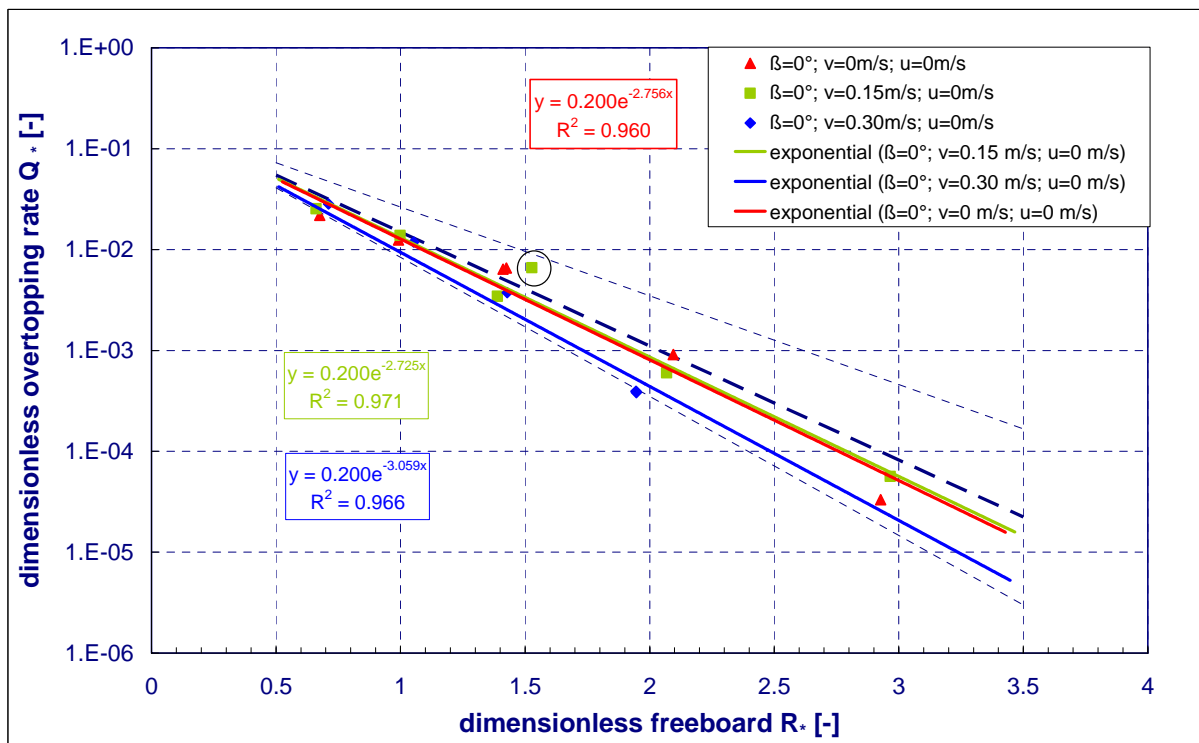


Figure 8.10 Current influence; FlowDike1 (non-breaking conditions)

**Perpendicular wave attack with current influence – Flow Dike 2**

A different idea of the influence of currents on wave overtopping depicts Figure 8.11. Here all of the trend lines are below the reference test, thus they are all aligned close to each other. It is visible that the inclination of the slope for the current of 0.15 m/s is too low ( $b = -4.639$ ) compared to the

inclinations for  $v = 0.30$  m/s and  $v = 0.40$  m/s ( $b = -4.583$ ) and ( $b = -4.616$ ). Although the effects are small, it still seems to be reliable that there is an influence on the overtopping.

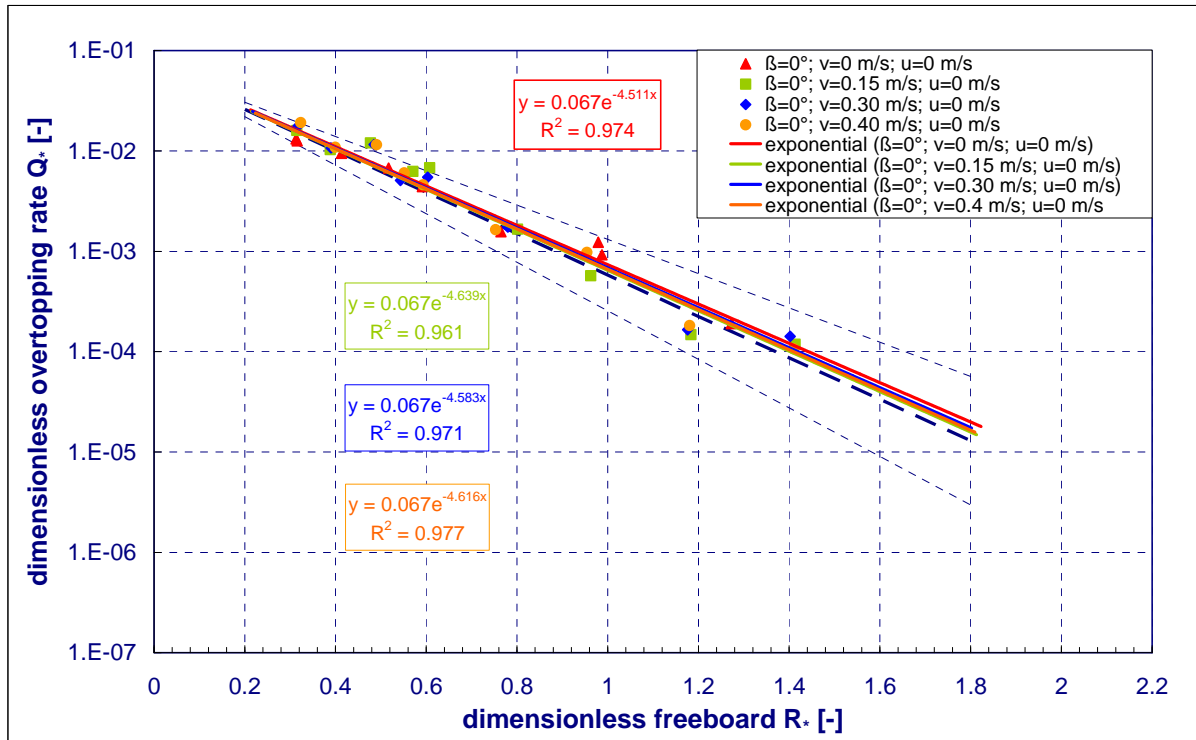


Figure 8.11 Current influence; FlowDike 2 (breaking conditions)

### Relation of the slopes 1:3 and 1:6

Parallel currents effect the overtopping in that the propagation of the waves in the channel in front of the dike will be displaced with the current direction. The influence might depend as well on the general incident direction of the waves, but this would be a matter for further investigations. Comparing the results from FlowDike 1 and FlowDike 2 for the current influence, it is questionable whether the difference in the alignment is due to the effect of the slope or if errors occurred during one of the data processing.

### 8.7 Influence of with wind and current

The combined effects of wind and current should be compared to the tests only on wind or current effect. In chapter 8.5 the limit of applied wave spectra to  $w_1$ ,  $w_3$ ,  $w_5$  and their effect on displaying the results were already mentioned.

### Perpendicular wave attack with wind and current influence – FlowDike 1 and FlowDike 2

Comparison of the combined results in Figure 8.12 with the ones for the individual influencing parameters wind and current (sections 8.5 and 8.6) lead to the impression that the wind influences is neutralising the current effect partly. This is reasonable, as the influences have an opposite effect on the overtopping. Further analysis on the integrated combination of both parameters has not been evaluated yet.

For FlowDike 2 Figure 8.13 depicts the results, but here only measurements on a wind velocity of  $u = 10$  m/s are available. The influence of wind (that was about 6 % in section 8.5) is not constant in the results of the combined effect. Here for the current of 0.15 m/s it increases the overtopping but more than expected and for the 0.30 m/s it even decreases combined to Figure 8.11 and the slope for the 0.40 m/s do not change particularly.

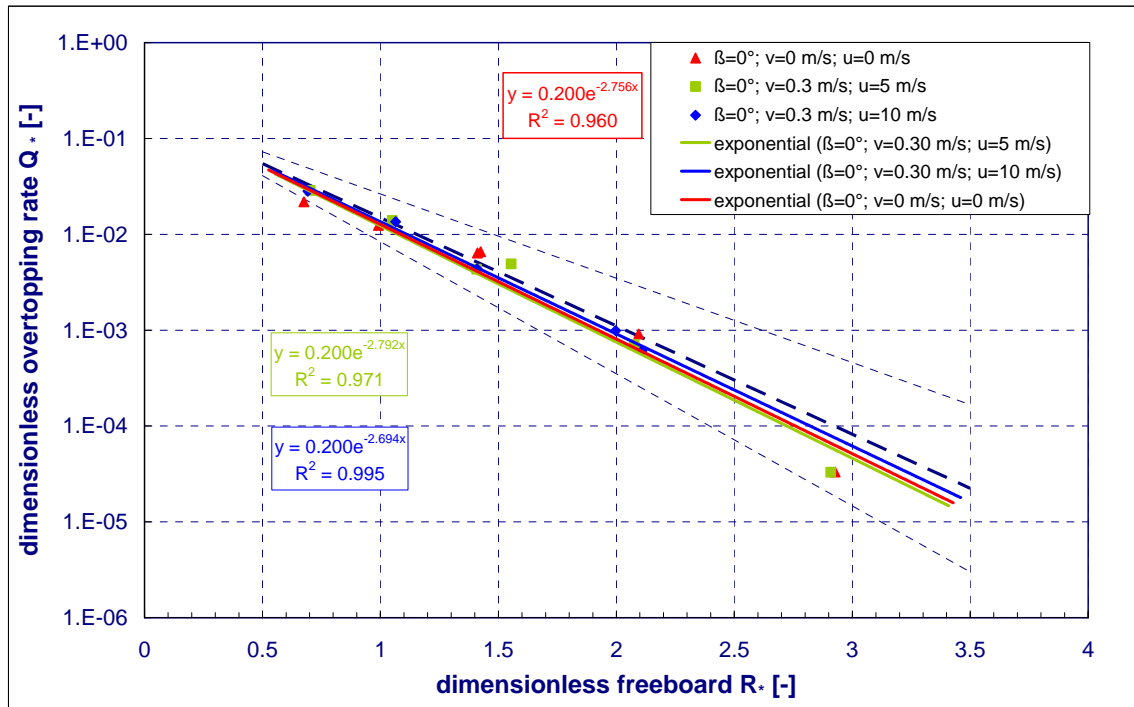


Figure 8.12 Wind and current influence; FlowDike 1 (non-breaking conditions)

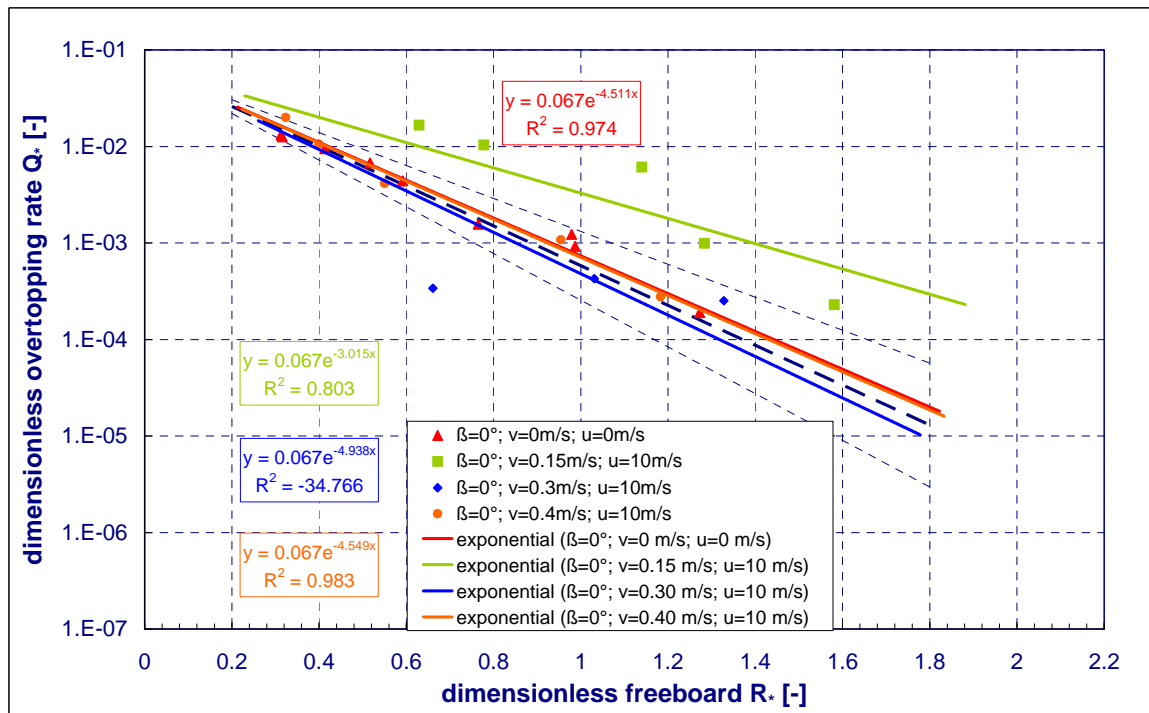


Figure 8.13 Wind and current influence; FlowDike 2 (breaking condition)

## 8.8 Reduction factors

This section summarises the factors for reduction, or in case of the wind an increase of the overtopping by means of a regression analysis as it is explained in chapter 8.2. The tables listed below give the parametric studies on the influences of interest. For every data set the variable of the slope inclination  $b$  and the determined influencing factor  $\gamma$  are given.

Basic trends can be assumed for the influencing parameters, such as:

- The effect of wind is recognisable as an increase in overtopping and it is in the same range for both investigations (compared factor for 10m/s).
- Currents have a decreasing effect. In FlowDike 2 the effect is much less than it is in FlowDike 1. If this is due to the slope, or whether it should have less recognisable influence on perpendicular wave attack for the 1:3 slope is not predictable yet.
- For the combined effects neither the analysis can be completed nor is a trend really noticeable. It can be stressed out that both variables have an opposite influence. First the influences for every single parameter should be analysed, before the adaption and range of mutual influence can be distinguished.
- The oblique wave attack is reducing the overtopping and validates therefore the former investigations.

Table 8.1 Slope inclination b and reduction factors ( $\gamma$ ) for influencing variables (wind and current influence)

|              |          | wind              |                   | current           |                   |          |                   |
|--------------|----------|-------------------|-------------------|-------------------|-------------------|----------|-------------------|
|              |          | 0 m/s             | 5 m/s             | 10 m/s            | 0 m/s             | 5 m/s    | 10 m/s            |
|              |          | 1:3               | 1:3               | 1:3               | 1:6               | 1:6      | 1:6               |
| breaking     | 0.00 m/s | -4.99<br>(1.000)  | -<br>(-)          | -<br>(-)          | -4.511<br>(1.000) | -<br>(-) | -4.249<br>(1.062) |
|              | 0.15 m/s | -5.331<br>(0.936) | -<br>(-)          | -<br>(-)          | -4.639<br>(0.972) | -<br>(-) | -3.015<br>(1.496) |
|              | 0.30 m/s | -5.381<br>(0.927) | -<br>(-)          | -<br>(-)          | -4.583<br>(0.984) | -<br>(-) | -4.938<br>(0.914) |
|              | 0.40 m/s | -<br>(-)          | -<br>(-)          | -<br>(-)          | -4.616<br>(0.977) | -<br>(-) | -4.549<br>(0.992) |
| non-breaking | 0.00 m/s | -2.756<br>(1.000) | -2.613<br>(1.055) | -2.587<br>(1.065) | -<br>(-)          | -<br>(-) | -<br>(-)          |
|              | 0.15 m/s | -2.725<br>(1.011) | -<br>(-)          | -<br>(-)          | -<br>(-)          | -<br>(-) | -<br>(-)          |
|              | 0.30 m/s | -3.059<br>(0.901) | -2.792<br>(0.987) | -2.694<br>(1.023) | -<br>(-)          | -<br>(-) | -<br>(-)          |
|              | 0.40 m/s | -<br>(-)          | -<br>(-)          | -<br>(-)          | -<br>(-)          | -<br>(-) | -<br>(-)          |

Table 8.2 Slope inclination b and reduction factors ( $\gamma_b$ ) for oblique wave attack

|                      |      | slope of the dike |                   |
|----------------------|------|-------------------|-------------------|
|                      |      | 1:3               | 1:6               |
| angle of wave attack |      |                   |                   |
| breaking             | 0°   | -4.99<br>(1.000)  | -4.511<br>(1.000) |
|                      | -15° | -5.347<br>(0.933) | -5.007<br>(0.901) |
|                      | -30° | -6.069<br>(0.822) | -5.989<br>(0.753) |
|                      | +45° | -7.065<br>(0.706) | -6.535<br>(0.690) |
| non-breaking         | 0°   | -2.756            | -<br>(-)          |
|                      | -15° | -2.863<br>(0.963) | -<br>(-)          |
|                      | -30° | -3.344<br>(0.824) | -<br>(-)          |
|                      | +45° | -4.419<br>(0.624) | -<br>(-)          |

For both investigations (either 1:3 dike and 1:6 dike) model tests were already performed and their results are described in the final report of the KFKI- project "Schräger Wellenaufwurf an Seedeichen". In Figure 8.14 the results from FlowDike 1 and FlowDike 2 are depicted to be compared to the model tests in Canada (1:6 dike) and Hannover (1:3 dike). The non linear regression formulae given by OUMERACI ET AL. (2001) are:

$$\gamma_{\beta} = 0.65 \cdot \cos(\beta) + 0.35 \quad (1:3 \text{ dike, Hannover}) \quad (8.5)$$

$$\gamma_{\beta} = 0.9 \cdot \cos(\beta) + 0.1 \quad (1:6 \text{ dike, Canada}) \quad (8.6)$$

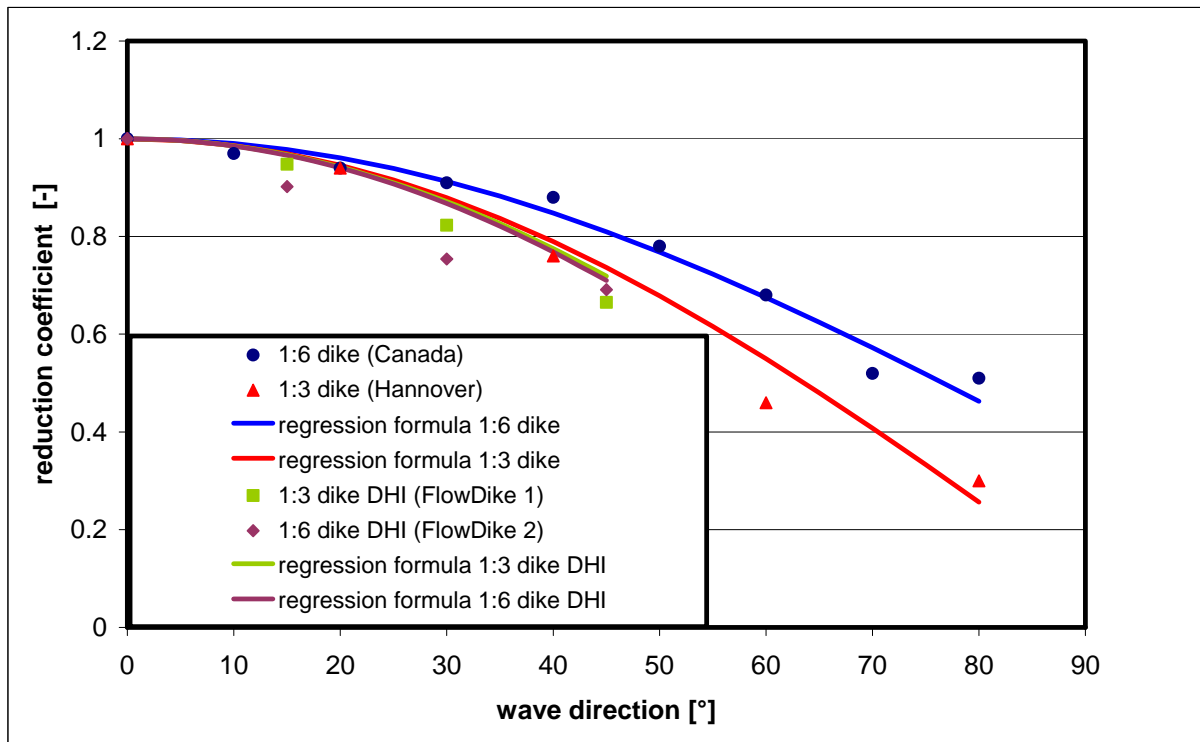


Figure 8.14 Comparison of reduction factors for obliqueness - FlowDike 1 and FlowDike 2 with investigations by OUMERACI ET AL. (2001)

The results of FlowDike 1 validate well the trend of the former results. All data points fall a little bit below the regression; this is why another formula for FlowDike 1 was calculated to:

$$\gamma_{\beta} = 0.96 \cdot \cos(\beta) + 0.04 \quad (\text{FlowDike 1}) \quad (8.7)$$

$$\gamma_{\beta} = 0.99 \cdot \cos(\beta) + 0.01 \quad (\text{Flow Dike 2}) \quad (8.8)$$

For FlowDike 2 the results drop significantly compared to the regression. This drop would not have been expected compared to the results found in Canada. The regression calculated for FlowDike 2 (8.8) has no perceivable difference to the 1:3 sloped dike. Here further analysis should be done to verify the results, before starting the analysis on current influence on oblique wave attack.

## 9 Conclusion

The investigations of FlowDike 1 and FlowDike 2 concentrate on the effects of wind and parallel current on wave run-up and wave overtopping for perpendicular and oblique wave attack. These variables were two of the missing effects in freeboard design and therefore a main interest for design purposes. Model tests were carried out in the shallow water wave basin at DHI (Denmark) and included the configuration of a 1:3 sloped dike (FlowDike 1) and a 1:6 sloped dike (FlowDike 2).

The tests on perpendicular wave attack without influencing parameter validated the existing wave overtopping formulae from the EUROTOP-MANUAL (2007). For both model tests the data points of the reference tests fit well within the 90% confidence interval of the formula. In FlowDike 1 the general trend is a little lower and for FlowDike 2 it is a bit higher than the equation. A comparison of the results for both model tests gives a variance in the trend of circa 10%. This should be remarked in the further comparison of both model tests.

All wind tests on wave overtopping confirmed the stated assumptions by GONZALEZ-ESCRIVA (2006) and DE WAAL ET AL. (1996) concerning the significant wind impact on small overtopping discharge. For high overtopping discharges practically no influence is noticeable as the data points for wind match those of the reference test, this validates the stated theory of WARD ET AL. (1996). No distinctions can be made on the deviations between the different slopes, and even for the two different wind velocities no significant variation can be found.

The current effects can be assumed to have a reducing influence on the wave overtopping. Although FlowDike 1 as well as FlowDike 2 give reasonable results, some of them do not validate the average trend. For example the 0.15 m/s for non-breaking conditions in FlowDike 1 and for breaking conditions in FlowDike 2, this might depend on the small current and should be analysed more detailed. The main difference in the results of FlowDike 1 and FlowDike 2 for current effects is the difference in the deviation of the trend lines from the reference test. Here the flatter and also longer slope could be an influencing factor, as it governs the breaker parameter.

Tests on combined effects of wind and current showed a superposition of the opposite influences of both parameters (FlowDike 1). The results for FlowDike 2 have a high variation, so conclusions on their effect and differences in the related tests for 1:3 and 1:6 sloped dikes can not be pointed out here.

The influence of oblique waves on overtopping was analysed as a last resort. In a first attempt the results found for both investigations validate the trend for obliqueness to reduce wave overtopping. The reduction factors found for FlowDike 1 validate well the regression trend found for former investigations by OUMERACI ET AL. (2001), but the slope of 1:6 does not.

For all comparable test series it was found that for the flatter slope of 1:6 the average overtopping discharges increases. In theory the change of the slope from 1:3 to 1:6 should affect the average overtopping in the way that it will be decreased. So in assumption the deviation of the results from FlowDike 1 and FlowDike 2 has to be verified, whether there was a mistake in the evaluations.

From the analysis it can be stated that an average trend of increasing overtopping volumes were determined for wind application, as well as decreasing trend for volumes of test series with currents or oblique waves. A summary of the above mentioned conclusions on influencing parameters is included

---

within the preliminary correction factors for wind, current, combined effects and obliqueness  $\gamma_\beta$ . These were designated for each investigation phase.

Finally the combined effects for wind, current and obliquity are still a matter of further analysis; especially the adoption of the factors by formulas has to be investigated. In addition, more theoretical work is required to determine the effect of currents on wave evolution and the resulting wave run-up and wave overtopping processes, which was presented in a first step in the data processing

## Glossary

**Average wave:** The average wave is a superposition of the incident and reflected wave and therefore it is the actual visible wave.

**Breaking waves (plunging) and non-breaking waves (surging):** A certain type of breaking is given by the combination of structure slope and wave steepness for the deep water conditions. On sloped structures it can be defined by the breaker parameter  $\xi_{m-1,0}$  with breaking waves  $\xi_{m-1,0} > 2 - 3$  and non-breaking waves  $\xi_{m-1,0} < 2 - 3$ . The transition between plunging and surging waves is known as collapsing.

**Crossing analysis:** For most of the processed data a crossing analysis (up or down crossing) was used in time domain. Both options use a defined crossing level within the raw data signal to detect single events and their parameter, such as peak to peak value or event duration. The difference between up or down crossing is the starting direction within the analysis, whether it starts to detect an event first when it is crossing the threshold in upward direction or downwards.

**Exceedance curve:** An exceedance curve is one tool to visualise the distribution of any parameter, such as run-up heights. The percentage of exceeding is calculated from the number of detected events related to the number of waves  $N$ . The curve simply relates the percentage of events to i.e. the run-up height.

**Incident wave:** The incident wave describes the wave coming from the sea before it hits the structure. In the model tests it is the incidental generated wave from the wave maker without reflection influences.

**JONSWAP-spectra:** The Joint North Sea Wave Project – spectra describes the empirical distribution of energy with frequency within the ocean. It is one of the most frequently applied spectra and was applied for many model tests before; thus it was used for comparability.

**Long crested waves:** Surface waves that are nearly two-dimensional, in that the crests appear very long in comparison with the wave length, and the energy propagation is concentrated in a narrow band around the mean wave direction. They do not exist in nature, but can be generated in the laboratory.

**Oblique wave attack:** Waves that strike the structure at an angle.

**Perpendicular wave attack:** Waves that strike the structure normally to its face.

**Raleigh distribution:** A Raleigh distribution is a continuous probability distribution that can be used to describe the fitting of a density function.

**Reflection analysis:** The reflection analysis done in frequency domain is used to determine the moments of spectral density for incident and reflected waves.

**Reflection coefficient:** The reflection coefficient is determined during reflection analysis and describes the intensity of a reflected wave relative to an incident wave.

**Reflected wave:** Waves that hit the structure and are reflected seaward with little or no breaking. The wave height and wave length decreases depending on the type of structure.

**Return period:** The average length of time between sea states of a given severity.

**Significant wave height:** The average height of the highest of one third of the waves in a given sea state.

**Short crested waves:** Waves that have a small extent in the direction perpendicular to the direction of propagation. Most waves in natural state are short-crested.

**Spectral energy density:** It describes how the energy (or variance) of a signal or a time series is distributed with frequency.

**Wave run-up and wave overtopping:** The run-up is the rush of water up a structure as a result of wave attack. Wave overtopping is the mean discharge of water in  $l/(s \cdot m)$  that passes over a structure due to wave attack and should be limited to a tolerable amount.

**Wave steepness:** The wave steepness is defined as the ratio of wave height to wave length ( $H/L$ ). It includes therefore information about the characteristic and history of the wave. Distinction can be made into swell sea ( $s_0 = 0.01$ ) and wind sea ( $s_0 = 0.04$  to  $0.06$ ).

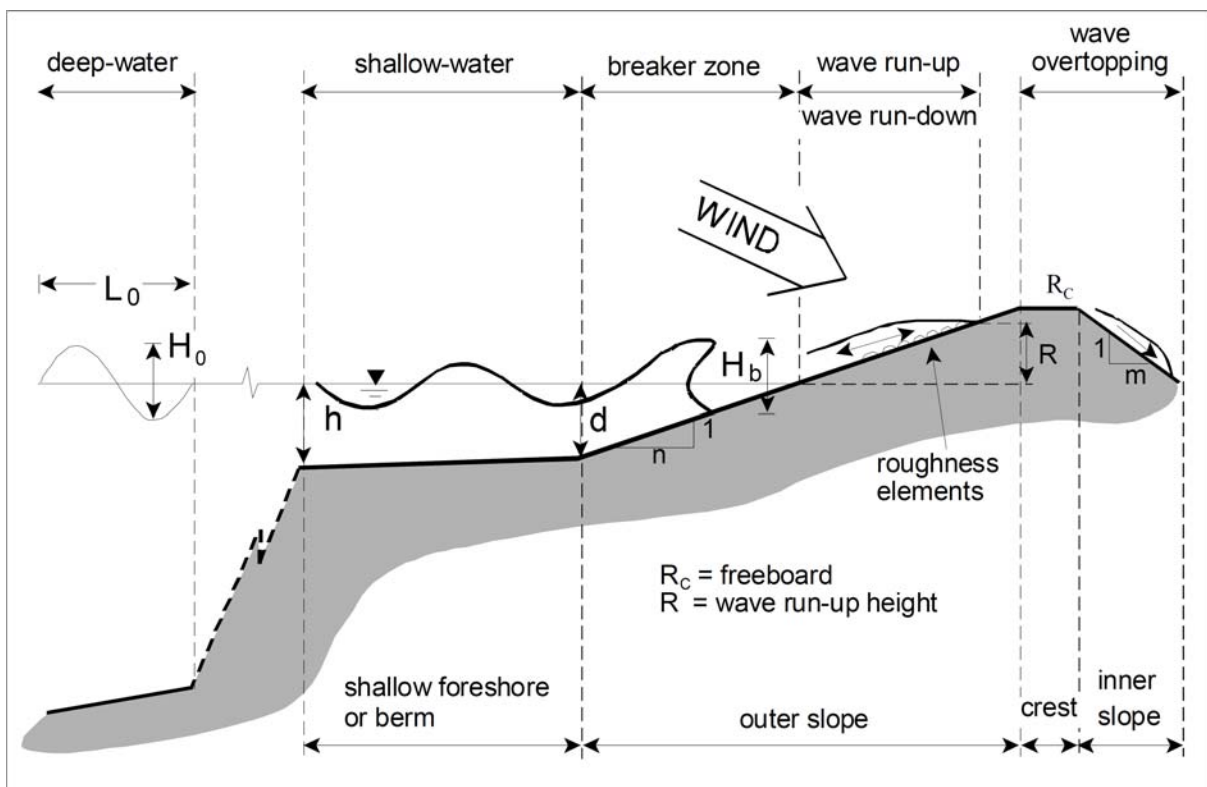


Figure A 1 Definition sketch for wave run-up and wave overtopping (Reference: OUMERACI ET AL. (2001))

## Notation

### Capital letter

|              |  |     |
|--------------|--|-----|
| $C_r$        | average reflection coefficient                                       | [-] |
| $H$          | wave height  | [m] |
| $H_{m0}$     | estimate of significant wave height from spectral analysis           | [m] |
| $H_{max}$    | measured maximum wave height   | [m] |
| $H_s$        | significant wave height defined as highest one-third of wave heights | [m] |
| $H_{WM}$     | wave height, adjusted at the wave machine                            | [m] |
| $L$          | wave length measured in direction of wave propagation                | [m] |
| $L_{0m-1,0}$ | deep water wave length based on $T_{m-1,0}$                          | [m] |
| $N$          | number of waves  | [-] |
| $P_{OW}$     | probability of overtopping per wave                                  | [-] |
| $Q_0$        | interception with the y-axis   | [-] |
| $Q^*$        | dimensionless overtopping discharge                                  | [-] |
| $R_c$        | crest freeboard of structure   | [m] |
| $R_u$        | run-up level, vertical measured with respect to the SWL              | [m] |
| $R_{ux\%}$   | run-up level exceeded by x% of incident waves                        | [m] |
| $R^*$        | dimensionless freeboard  | [-] |
| $T$          | wave period  | [s] |
| $T_m$        | average wave period (here: from time-domain analysis)                | [s] |
| $T_{m0,1}$   | average wave period defined by $m_0/m_1$                             | [s] |
| $T_{m0,2}$   | average wave period defined by $\sqrt{m_0/m_2}$                      | [s] |
| $T_{m-1,0}$  | average wave period defined by $m_{-1}/m_0$                          | [s] |
| $T_p$        | spectral peak wave period  | [s] |

**Lower case letter**

|                |  |                        |
|----------------|--|------------------------|
| b              | inclination of the slope   | [-]                    |
| f              | frequency  | [Hz]                   |
| $f_p$          | spectral peak frequency  | [Hz]                   |
| g              | acceleration due to gravity (= 9.81)   | [m/s <sup>2</sup> ]    |
| h              | water depth at the toe of the structure  | [m]                    |
| $h_c$          | layer thickness (flow depth) on the dike crest                                   | [m]                    |
| $m_n$          | nth moment of spectral density   | [m <sup>2</sup> /sn]   |
| q              | mean overtopping discharge per meter structure width                             | [m <sup>3</sup> /(sm)] |
| s              | wave steepness = H/L   | [-]                    |
| $s_{m-1,0}$    | wave steepness with L0 based on $T_{m-1,0}$                                      | [-]                    |
| u              | wind velocity  | [m/s]                  |
| v              | current velocity   | [m/s]                  |
| $v_c$          | overtopping velocity (flow velocity) on the dike crest                           | [m/s]                  |
| $\alpha$       | angle between structure slope and horizontal                                     | [°]                    |
| $\beta$        | angle of wave attack relative to normal on structure                             | [°]                    |
| $\gamma$       | correction factor  | [-]                    |
| $\gamma_b$     | correction factor for a berm   | [-]                    |
| $\gamma_f$     | correction factor for surface roughness  | [-]                    |
| $\gamma_\beta$ | correction factor for oblique wave attack  | [-]                    |
| $\theta$       | direction of wave propagation  | [°]                    |
| $\xi_{m-1,0}$  | breaker parameter based on $s_{m-1,0}$   | [-]                    |
| $\xi_{tr}$     | surf parameter describing the transition between breaking and non breaking waves | [-]                    |

### Annex

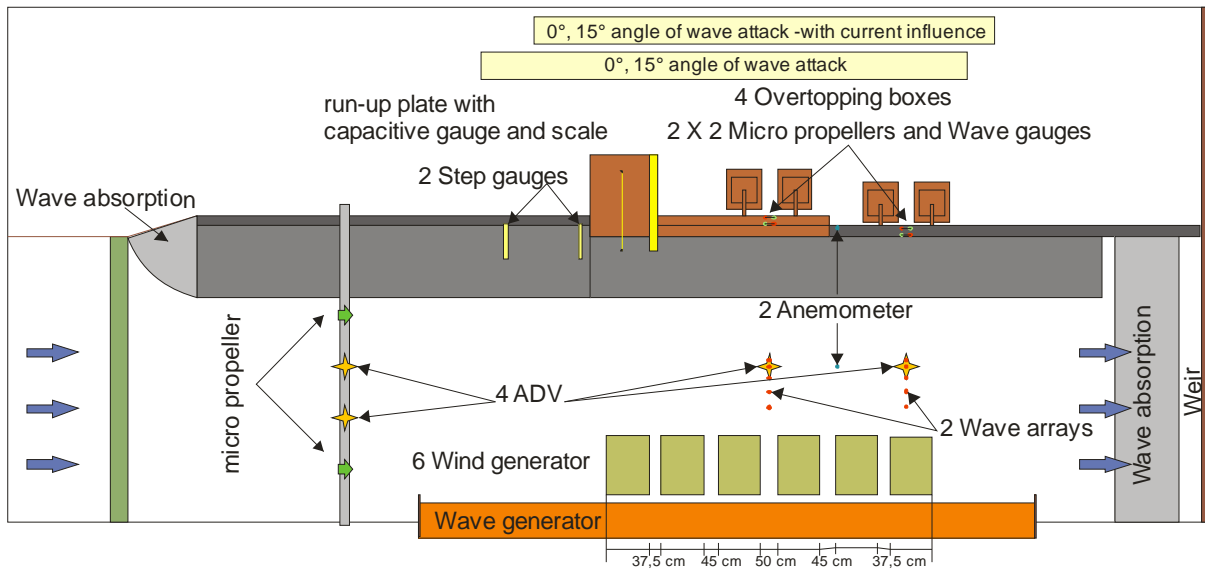


Figure A 2 Setup 1 - angles of wave attack 0°, +15° und -15°(FlowDike 1)

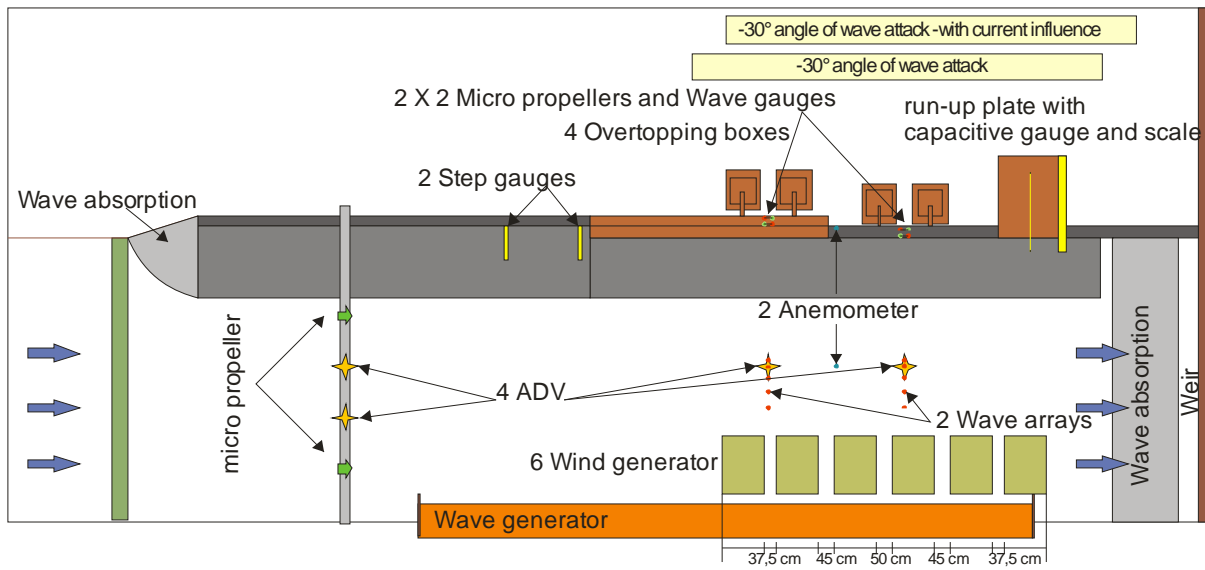


Figure A 3 Setup 2 - angles of wave attack -30° (FlowDike 1)

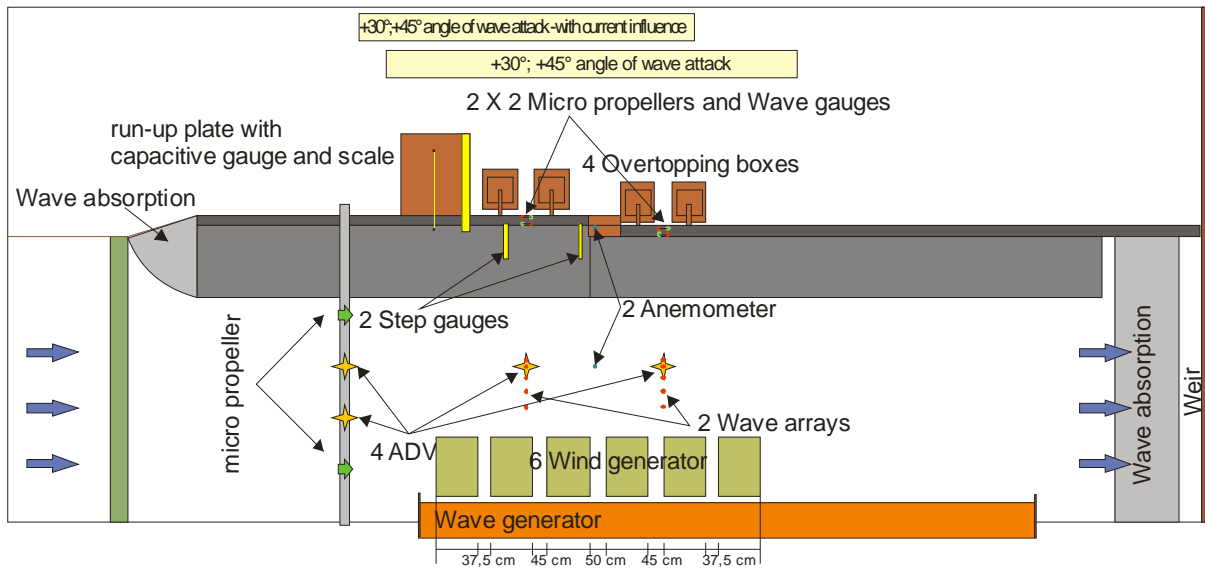


Figure A 4 Setup 3 - angles of wave attack +30° und +45° (FlowDike 1)

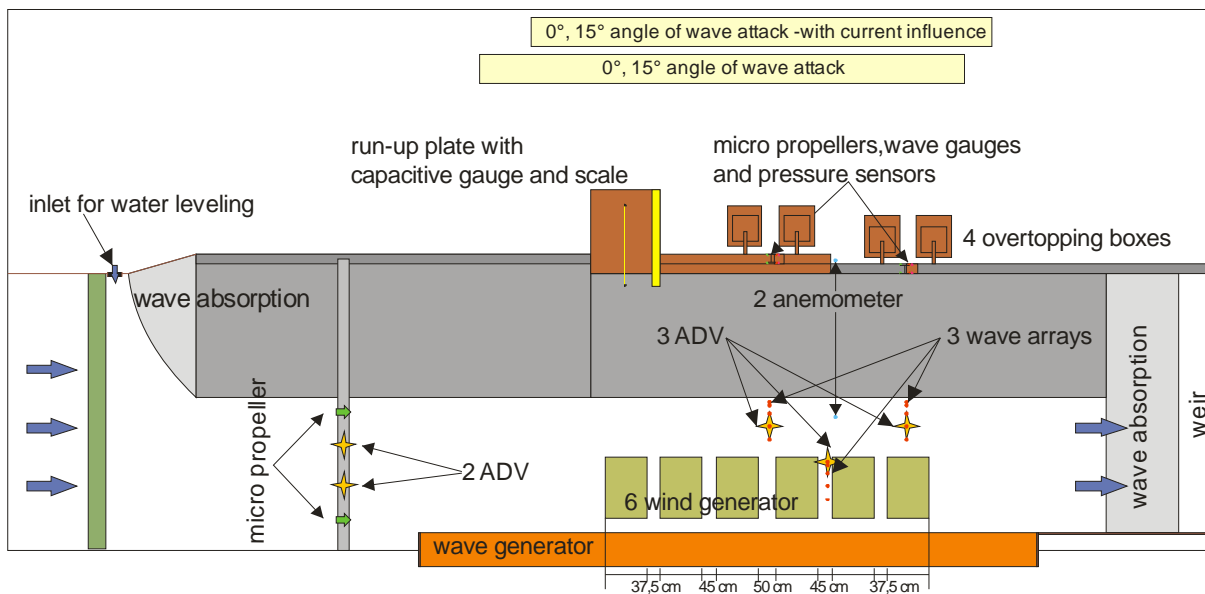


Figure A 5 Setup 4 - angles of wave attack 0°, +15° und -15° (FlowDike 2)

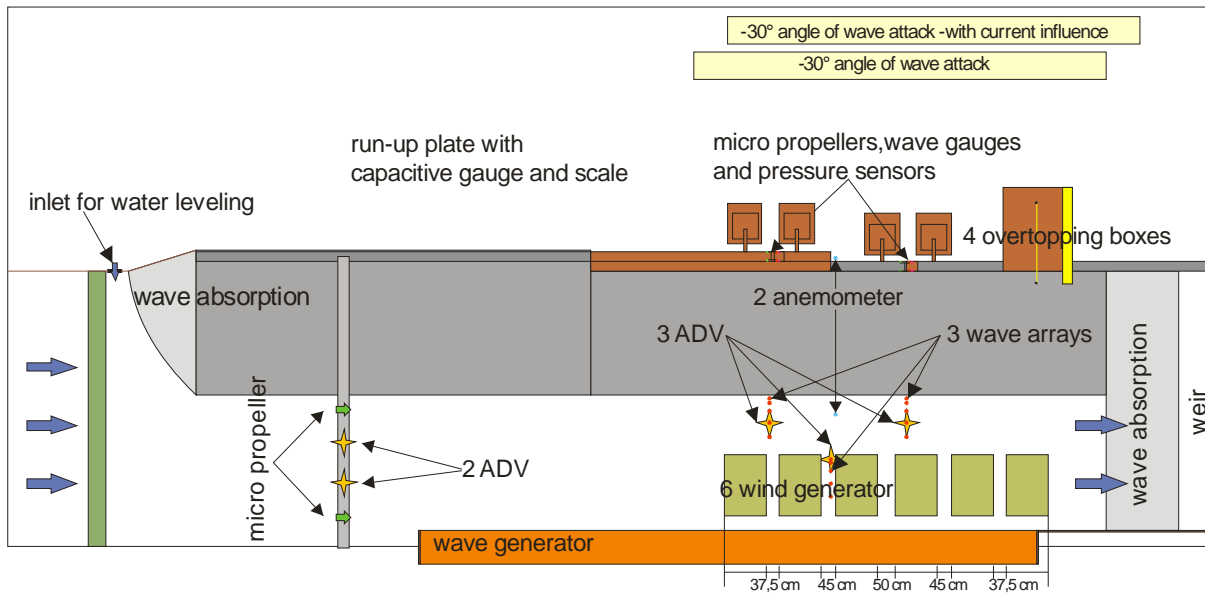


Figure A 6 Setup 5 - angles of wave attack  $-30^\circ$  (FlowDike 2)

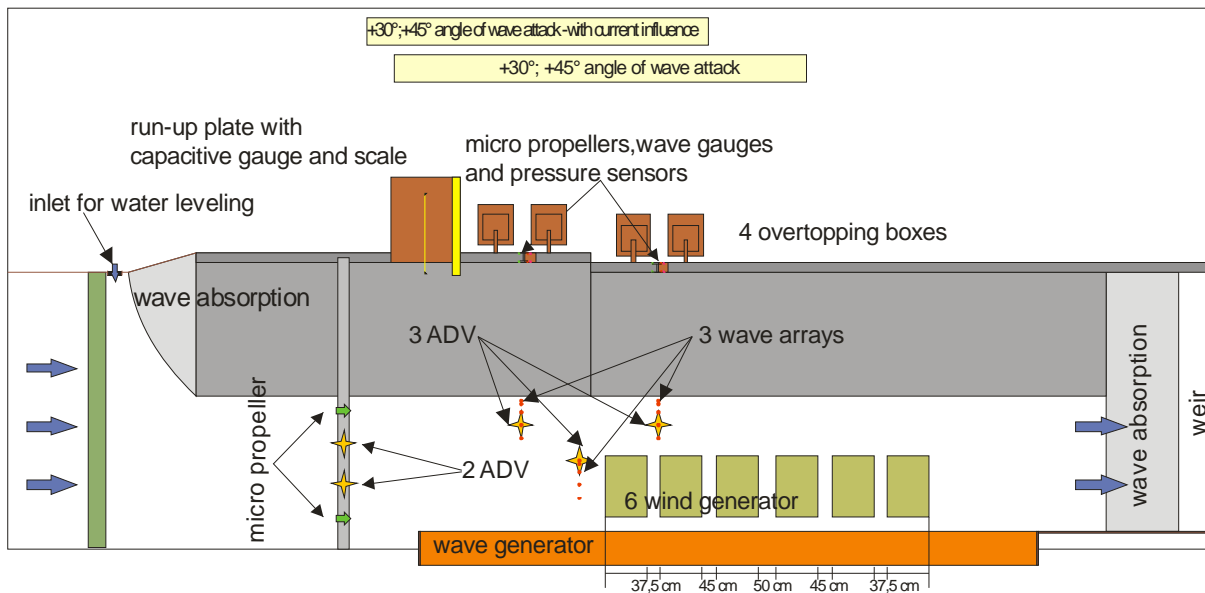


Figure A 7 Setup 6 - angles of wave attack  $+30^\circ$  und  $+45^\circ$  (FlowDike 2)

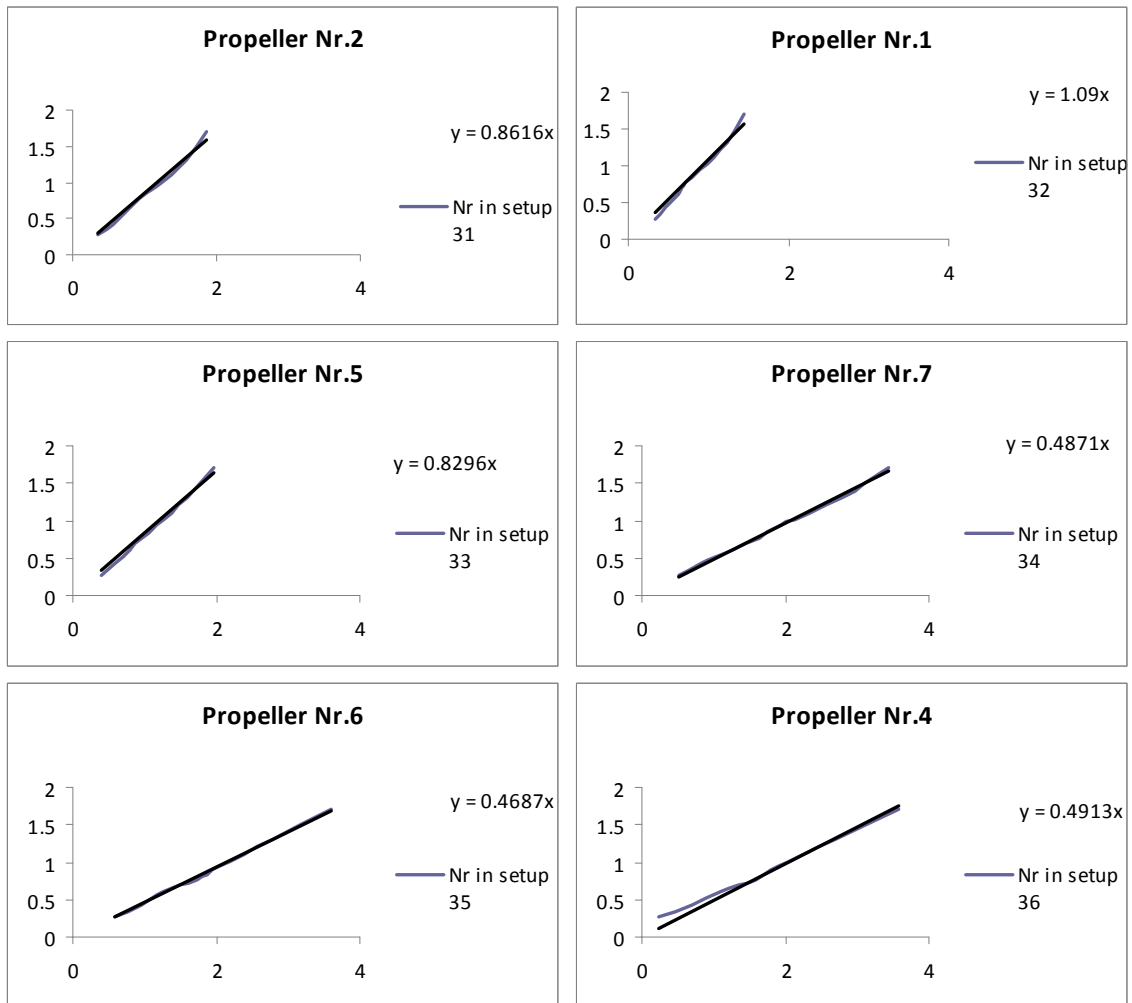


Figure A 8 Calibration curves for micropropeller from TU Braunschweig

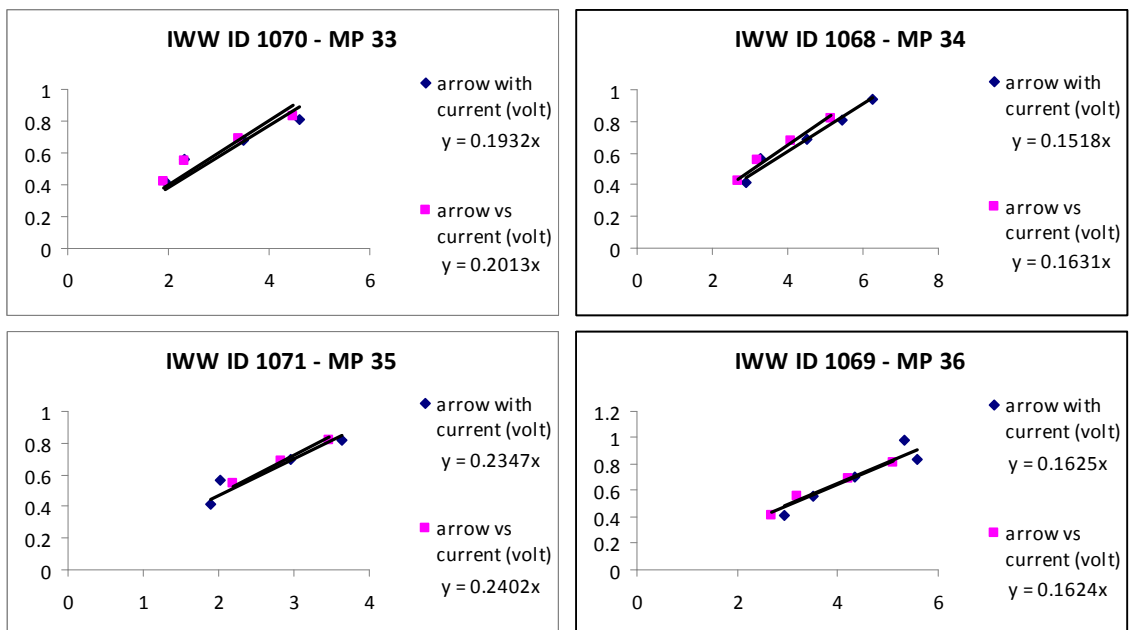


Figure A 9 Calibration curves for micropropeller of RWTH Aachen

Table A 1 Model tests and associated films (AVI-file 101 to 152)

| AVI Nr | Date     | Set-up | Test Label | File name          | Comment   | Remarks  |
|--------|----------|--------|------------|--------------------|---|--|
| 101    | 29. Jan  | 1      | RW1.1      |                    | Regular Waves   | -  |
| 102    | 29. Jan  | 1      | RW1.2      |                    | Regular Waves   | pumps switched off too late at first pumping   |
| 103    | 29. Jan  | 1      | RW1.3      |                    | Regular Waves   | -  |
| 104    | 29. Jan  | 1      | RW1.4      |                    | Regular Waves   | -  |
| 105    | 29. Jan  | 1      | RW1.5      |                    | Regular Waves   | pump (channel 46) started too late, water beside channels into collecting tank   |
| 106    | 29. Jan  | 1      | RW1.6      |                    | Regular Waves   | water beside channels into collecting tank, plug of platform 1 unplugged (current supply) for about 3 sec., possibly affected channels: microprops, stepgauges, ADV RWTH, capacitive gauge, pump (channel 48) ran dry on last pumping    |
| 107    | 30. Jan  | 1      | RW6.1      |                    | Regular Waves; error in the anemometer; replaced with 108 | temp up to 14.5, delete values during data acquisition: channels 3, 4, 33; changed range of airflow from 0-5m/s and 0-10V to 0-20m/s and 0-10V; added amplifiers for the 4 small props to reduce 10V to 5V ; repetition in test no 108   |
| 108    | 30. Jan  | 1      | RW6.2      |                    | Regular Waves; replaces 107                               | -  |
| 109    | 30. Jan  | 1      | RW6.3      |                    | Regular Waves   | -  |
| 110    | 30. Jan  | 1      | RW6.4      |                    | Regular Waves   | delete values channel 56 (step gauge 50,2m)  |
| 111    | 30. Jan  | 1      | RW6.5      |                    | Regular Waves   | container not empty before test was started  |
| 112    | 30. Jan  | 1      | RW6.6      |                    | Regular Waves   | pump 46 accidentally started, turned off immediately   |
| 113    | 30. Jan  | 1      | RW6.7      |                    | Regular Waves   | -  |
| 114    | 02. Feb. | 1      | T3.1       | s1_03_30_w1_00     | shorter Wave Period                                       | Gauges on dike and overtopping containers calibrated with water from behind the dike; distance between WG on crest: 0.6m ->0.3m, 0.7m ->0.29m  |
| 115    | 02. Feb. | 1      | T3.2       | s1_03_30_w2_00     | shorter Wave Period                                       | see test 114   |
| 116    | 02. Feb. | 1      | T3.3       | s1_03_30_w3_00     | shorter Wave Period                                       | -  |
| 117    | 02. Feb. | 1      | T3.4       | s1_03_30_w4_00     | shorter Wave Period                                       | -  |
| 118    |          |        |            |                    | replaced with 119; shorter Wave Period                    | delete values on wave gauges; splash into tank -> mounting splash board; repetition in test 119  |
| 119    | 02. Feb. | 1      | T3.5       | s1_03_30_w5_00     | replaces 118; shorter Wave Period                         | delete values on wave gauges; splash into tank -> mounting splash board; repetition in test 119  |
| 120    | 02. Feb. | 1      | T3.6       | s1_03_30_w6_00     | shorter Wave Period                                       | -  |
| 121    | 03. Feb. | 1      | T8.1       | s1_08_30_w1_49     |   |  |
| 122    | 03. Feb. | 1      | T8.2       | s1_08_30_w2_49     |   |  |
| 123    | 03. Feb. | 1      | T8.3       | s1_08_30_w3_49     | AVI truncated (last 5 minutes)                            |  |
| 124    | 03. Feb. | 1      | T19.1      | s1_19_30_w1_00_-15 |   | Hs changed to 0.07m for Wave 1   |
| 125    | 03. Feb. | 1      | T19.2      | s1_19_30_w2_00_-15 |   | Hs changed to 0.07m for Wave 2   |
| 126    | 03. Feb. | 1      | T19.3      | s1_19_30_w3_00_-15 |   |  |
| 127    | 03. Feb. | 1      | T19.4      | s1_19_30_w4_00_-15 |   |  |
| 128    | 03. Feb. | 1      | T19.5      | s1_19_30_w5_00_-15 | not recorded  | at 26:30 and 31:40 minutes, water besides the channel for loadcell 39  |
| 129    | 03. Feb. | 1      | T19.6      | s1_19_30_w6_00_-15 | not recorded  |  |
| 130    |          |        |            |                    | Test x ADV; not recorded                                  | only current to check ADV signals  |
| 131    | 04. Feb. | 1      | T16.1      | s1_16_30_w1_00_+15 | AVI truncated   | ADV + SD moved closer to gauges  |
| 132    | 04. Feb. | 1      | T16.2      | s1_16_30_w2_00_+15 |   |  |
| 133    | 04. Feb. | 1      | T16.3      | s1_16_30_w3_00_+15 |   |  |
| 134    | 04. Feb. | 1      | T16.4      | s1_16_30_w4_00_+15 |   |  |
| 135    | 04. Feb. | 1      | T16.5      | s1_16_30_w5_00_+15 |   | waves touching windmaker (?)   |
| 136    | 04. Feb. | 1      | T16.6      | s1_16_30_w6_00_+15 |   | pump 47 ran dry at about 8:30 min  |
| 137    | 04. Feb. | 1      | T8b.1      | s1_08b_30_w4_25    | restarted   |  |
| 138    | 04. Feb. | 1      | T8b.3      | s1_08b_30_w5_25    |   |  |
| 139    |          |        |            |                    | replaced with 140; error in Water Gauges; AVI deleted     | recalibration of gauges 5 - 14 to a range of 0.4m (change of calibration factor + voltage; 2.5V -> 0.1m); correction of calibration factors for gauges in overtopping tanks (-> now 0.04, before 0.0025); repetition of test in test 140 |
| 140    | 04. Feb. | 1      | T8b.5      | s1_08b_30_w6_25    | replaces 139; new position of the Videocamera (mark "2")  | repetition of test 139   |
| 141    |          |        |            |                    | Calibration of capitive gauge                             | regular waves for calibration of capacitive gauge  |
| 142    |          |        |            |                    | Calibration of capitive gauge                             | regular waves for calibration of capacitive gauge  |
| 143    |          |        |            |                    | Calibration of capitive gauge                             | regular waves for calibration of capacitive gauge  |
| 144    | 05. Feb. | 1      | T1.1       | s1_01_00_w1_00     | longer Video because replacing USB cable                  | Testseries 1 with JONSWAP not regular waves  |
| 145    | 05. Feb. | 1      | T1.2       | s1_01_00_w2_00     |   |  |
| 146    | 05. Feb. | 1      | T1.3       | s1_01_00_w3_00     |   |  |
| 147    | 05. Feb. | 1      | T1.4       | s1_01_00_w4_00     |   |  |
| 148    | 05. Feb. | 1      | T1.5       | s1_01_00_w5_00     |   |  |
| 149    | 05. Feb. | 1      | T1.6       | s1_01_00_w6_00     |   |  |
| 150    | 05. Feb. | 1      | T6b.1      | s1_06b_00_w1_25    |   |  |
| 151    | 05. Feb. | 1      | T6b.2      | s1_06b_00_w2_25    |   |  |
| 152    | 05. Feb. | 1      | T6b.3      | s1_06b_00_w3_25    |   | pumps 46,47 ran dry at about 11:55; recognized, that there is no signal from prop 34 -> solution: amp. Turned off an on again  |

Table A 2 Model tests and associated films (AVI-file 153 to 201)

| AVI Nr | Date     | Set-up | Test Label | File name           | Comment  | Remarks  |
|--------|----------|--------|------------|---------------------|--|--|
| 153    | 05. Feb. | 1      | T6.1       | s1_06_00_w4_49      |  |  |
| 154    | 05. Feb. | 1      | T6.2       | s1_06_00_w5_49      |  |  |
| 155    | 05. Feb. | 1      | T6.3       | s1_06_00_w6_49      | replaces the 155a = no data saved  |  |
| 155.5  |          |        |            |                     | no data saved; replaced with 155   |  |
| 156    | 06. Feb. | 1      | T12.1      | s1_12_00_w1_00_-15  | new cassette - first on the cassette                                     |  |
| 157    | 06. Feb. | 1      | T12.2      | s1_12_00_w2_00_-15  | only avi   |  |
| 158    | 06. Feb. | 1      | T12.3      | s1_12_00_w3_00_-15  | only avi   |  |
| 159    | 06. Feb. | 1      | T12.4      | s1_12_00_w4_00_-15  | only avi   |  |
| 160    | 06. Feb. | 1      | T12.5      | s1_12_00_w5_00_-15  | only avi   |  |
| 161    | 06. Feb. | 1      | T12.6      | s1_12_00_w6_00_-15  | only avi   |  |
| 162    | 06. Feb. | 1      | T11.1      | s1_11_15_w1_00      | second on the cassette   |  |
| 163    | 06. Feb. | 1      | T11.2      | s1_11_15_w2_00      | third on the cassette - end  |  |
| 164    | 06. Feb. | 1      | T11.3      | s1_11_15_w3_00      | new cassette - first on the cassette                                     | after this test offset factor for ADV (19-21) changed from -100 to -1; effect on all test since change from cm to m                                    |
| 165    | 06. Feb. | 1      | T11.4      | s1_11_15_w4_00      | second on the cassette   |  |
| 166    | 06. Feb. | 1      | T11.5      | s1_11_15_w5_00      | third on the cassette  | pump 47 ran dry at about 5:30 min  |
| 167    | 06. Feb. | 1      | T11.6      | s1_11_15_w6_00      | new cassette - first on the cassette                                     | pump 47 was stopped after end of waves   |
| 168    | 09. Feb. | 1      | T13.1      | s1_13_15_w1_00_-15  | only avi   |  |
| 169    | 09. Feb. | 1      | T13.2      | s1_13_15_w2_00_-15  | only avi   |  |
| 170    | 09. Feb. | 1      | T13.3      | s1_13_15_w3_00_-15  | only avi   |  |
| 171    | 09. Feb. | 1      | T13.4      | s1_13_15_w4_00_-15  | only avi   |  |
| 172    | 09. Feb. | 1      | T13.5      | s1_13_15_w5_00_-15  | only avi   |  |
| 173    | 09. Feb. | 1      | T13.6      | s1_13_15_w6_00_-15  | only avi   |  |
| 174    | 09. Feb. | 1      | T15.1      | s1_15_15_w1_00_+15  | second on the cassette   |  |
| 175    | 09. Feb. | 1      | T15.2      | s1_15_15_w2_00_+15  | third on the cassette  |  |
| 176    | 09. Feb. | 1      | T15.3      | s1_15_15_w3_00_+15  | new cassette - first on the cassette                                     |  |
| 177    | 09. Feb. | 1      | T15.4      | s1_15_15_w4_00_+15  | second on the cassette   | Wavemakerfile is recorded with 15.3 -> testno 177  |
| 178    | 09. Feb. | 1      | T15.5      | s1_15_15_w5_00_+15  | third on the cassette  |  |
| 179    | 09. Feb. | 1      | T15.6      | s1_15_15_w6_00_+15  | new cassette - first on the cassette                                     | repeat this testseries with setup3, because overtopping on 60 cm crest can not be measured (waves out of range)  |
| 180    | 11. Feb. | 2      | T2.1       | s2_02_00_w1_00_-30  | second on the cassette   | micropropeller not in wave direction, but 0 degree   |
| 181    | 11. Feb. | 2      | T2.2       | s2_02_00_w2_00_-30  | third on the cassette  | micropropeller not in wave direction, but 0 degree   |
| 182    | 11. Feb. | 2      | T2.3       | s2_02_00_w3_00_-30  | new cassette - first on the cassette                                     | direction of micropropeller changed to -30 degree  |
| 183    | 11. Feb. | 2      | T2.4       | s2_02_00_w4_00_-30  | second on the cassette   |  |
| 184    | 11. Feb. | 2      | T2.5       | s2_02_00_w5_00_-30  | third on the cassette  |  |
| 185    | 11. Feb. | 2      | T2.6       | s2_02_00_w6_00_-30  | new cassette - first on the cassette                                     |  |
| 186    | 11. Feb. | 2      | T7b.1      | s2_07b_00_w1_25_-30 | second on the cassette   |  |
| 187    | 11. Feb. | 2      | T7b.2      | s2_07b_00_w3_25_-30 | third on the cassette, long video because of test restart                |  |
| 188    | 11. Feb. | 2      | T7b.3      | s2_07b_00_w5_25_-30 | new cassette - first on the cassette                                     |  |
| 189    | 11. Feb. | 2      | T7.1       | s2_07_00_w1_49_-30  | second on the cassette   |  |
| 190    | 11. Feb. | 2      | T7.2       | s2_07_00_w3_49_-30  | third on the cassette  |  |
| 191    | 11. Feb. | 2      | T7.3       | s2_07_00_w5_49_-30  | new cassette - first on the cassette                                     |  |
| 192    | 12. Feb. | 2      | T20.1      | s2_20_15_w1_00_-30  | second on the cassette   |  |
| 193    | 12. Feb. | 2      | T20.2      | s2_20_15_w2_00_-30  | third on the cassette  |  |
| 193.5  | 12. Feb. | 2      | T20.3      | s2_20_15_w3_00_-30  | 194a: wavemaker stopped during the test, replaced with 194, new cassette | breaking waves on downstream edge of the wavemaker, wavemaker stopped, new offsets can because temperature has changed, test repeated with same testno |
| 194    | 12. Feb. | 2      | T20.3      | s2_20_15_w3_00_-30  | second on the cassette   |  |
| 195    | 12. Feb. | 2      | T20.4      | s2_20_15_w4_00_-30  | third on the cassette  |  |
| 196    | 12. Feb. | 2      | T20.5      | s2_20_15_w5_00_-30  | new cassette - first on the cassette                                     |  |
| 197    | 12. Feb. | 2      | T20.6      | s2_20_15_w6_00_-30  | second on the cassette   |  |
| 198    |          |        |            |                     | rerun 146  | repeating test s1_01_00_w3_00 (microprop did not work there)   |
| 199    |          |        |            |                     | rerun 147  |  |
| 200    |          |        |            |                     | rerun 148  | overflow of overtopping tank during first time pumping, pump 43 switched on too late   |
| 201    |          |        |            |                     | rerun 149  | pump 48 pumped too long once   |

Table A 3 Model tests and associated films (AVI-file 202 to 247)

| AVI Nr | Date     | Set-up | Test Label | File name            | Comment  | Remarks   |
|--------|----------|--------|------------|----------------------|--|---|
| 202    | 12. Feb. | 2      | T4.1       | s2_04_30_w1_00_-30   | second on the cassette, (with 191)                                 |   |
| 203    | 12. Feb. | 2      | T4.2       | s2_04_30_w2_00_-30   | new cassette - first on the cassette                               |   |
| 204    | 12. Feb. | 2      | T4.3       | s2_04_30_w3_00_-30   | second on the cassette   |   |
| 205    | 12. Feb. | 2      | T4.4       | s2_04_30_w4_00_-30   | third on the cassette - end (started twice)                        |   |
| 206    | 12. Feb. | 2      | T4.5       | s2_04_30_w5_00_-30   | new cassette - first on the cassette                               |   |
| 207    | 12. Feb. | 2      | T4.6       | s2_04_30_w6_00_-30   | second on the cassette - end (2x)                                  | test was repeated, data was overwritten   |
| 208    | 13. Feb. | 2      | T9b.1      | s2_09b_30_w1_25_-30  | new cassette - first on the cassette                               |   |
| 209    | 13. Feb. | 2      | T9b.3      | s2_09b_30_w3_25_-30  | second on the cassette   |   |
| 210    | 13. Feb. | 2      | T9b.5      | s2_09b_30_w5_25_-30  | third on the cassette  |   |
| 211    | 13. Feb. | 2      | T9.1       | s2_09_30_w1_49_-30   | new cassette - first on the cassette                               |   |
| 212    | 13. Feb. | 2      | T9.3       | s2_09_30_w3_49_-30   | second on the cassette   |   |
| 213    | 13. Feb. | 2      | T9.5       | s2_09_30_w5_49_-30   | third on the cassette  |   |
| 214    |          |        |            |                      | missing DFS0   |   |
| 215    | 18. Feb. | 3      | T18.1      | s3_18_00_w1_00_+45   | new cassette - first on the cassette                               |   |
| 216    | 18. Feb. | 3      | T18.2      | s3_18_00_w2_00_+45   | second on the cassette   |   |
| 217    | 18. Feb. | 3      | T18.3      | s3_18_00_w3_00_+45   | third on the cassette  |   |
| 218    | 18. Feb. | 3      | T18.4      | s3_18_00_w4_00_+45   | new cassette - first on the cassette                               |   |
| 219    |          |        |            |                      | replaced with 220  | Wavemaker stopped after 21 min repetition in test 220   |
| 220    | 18. Feb. | 3      | T18.5      | s3_18_00_w5_00_+45   | second on the cassette   | repeating test 219  |
| 221    |          |        |            |                      | wavemaker stopped during the test, no existing data, test left out | new testseries with 40 degree angle, -> 45 did not work (breaking waves at the paddle); 40 Degree did not work as well, dataacquisition not started |
| 222    | 19. Feb. | 3      | T5.1       | s3_05_30_w1_00_+30   | new cassette - first on the cassette                               | changed ADV positions: SD12 to WG array (10-14), ADV RWTH (25-27) to WG array (5-9), ADV DHI (19-21) not in use anymore                             |
| 223    | 19. Feb. | 3      | T5.2       | s3_05_30_w2_00_+30   | second on the cassette   |   |
| 224    | 19. Feb. | 3      | T5.3       | s3_05_30_w3_00_+30   | third on the cassette  |   |
| 225    | 19. Feb. | 3      | T5.4       | s3_05_30_w4_00_+30   | new cassette - first on the cassette                               |   |
| 226    | 19. Feb. | 3      | T5.5       | s3_05_30_w5_00_+30   | second on the cassette   | pump 47 interrupted too late 12:10 min  |
| 227    | 19. Feb. | 3      | T5.6       | s3_05_30_w6_00_+30   | third on the cassette  |   |
| 228    | 20. Feb. | 3      | T14.1      | s3_14_30_w1_00_+45   | new cassette - first on the cassette                               |   |
| 229    | 20. Feb. | 3      | T14.2      | s3_14_30_w2_00_+45   | second on the cassette   |   |
| 230    | 20. Feb. | 3      | T14.3      | s3_14_30_w3_00_+45   | third on the cassette  |   |
| 231    | 20. Feb. | 3      | T14.4      | s3_14_30_w4_00_+45   | new cassette - first on the cassette                               |   |
| 232    | 20. Feb. | 3      | T14.5      | s3_14_30_w5_00_+45   | second on the cassette   |   |
| 233    | 20. Feb. | 3      | T14.6      | s3_14_30_w6_00_+45   | third on the cassette  | without absorbtion  |
| 234    | 18. Feb. | 3      | T21.1      | s3_21_15_w1_00_+30   | new cassette - first on the cassette                               | before test: changed micropeller ports 31 and 34, it seems as if port 4 of the amplifier is not working right, also changed cables at the cabinet   |
| 235    | 18. Feb. | 3      | T21.2      | s3_21_15_w2_00_+30   | second on the cassette   |   |
| 236    | 18. Feb. | 3      | T21.3      | s3_21_15_w3_00_+30   | third on the cassette  |   |
| 237    | 18. Feb. | 3      | T21.4      | s3_21_15_w4_00_+30   | new cassette - first on the cassette                               |   |
| 238    | 18. Feb. | 3      | T21.5      | s3_21_15_w5_00_+30   | second on the cassette   |   |
| 239    | 18. Feb. | 3      | T21.6      | s3_21_15_w6_00_+30   | third on the cassette  |   |
| 240    | 19. Feb. | 3      | T17.1      | s3_17_15_w1_00_+45   | new cassette - first on the cassette                               |   |
| 241    | 19. Feb. | 3      | T17.2      | s3_17_15_w2_00_+45   | second on the cassette   |   |
| 242    | 19. Feb. | 3      | T17.3      | s3_17_15_w3_00_+45   | third on the cassette  |   |
| 243    | 19. Feb. | 3      | T17.4      | s3_17_15_w4_00_+45   | new cassette - first on the cassette                               |   |
| 244    | 19. Feb. | 3      | T17.5      | s3_17_15_w5_00_+45   | second on the cassette   |   |
| 245    | 19. Feb. | 3      | T17.6      | s3_17_15_w6_00_+45   | third on the cassette  | without absorbtion  |
| 246    | 20. Feb. | 3      | T23.3      | s3_23_00_w3_00_+30MD | only AVI, multidirectional   | multi directional waves   |
| 247    | 20. Feb. | 3      | T23.5      | s3_23_00_w5_00_+30MD | only AVI, multidirectional   | multi directional waves   |
| -      | 18. Feb. | 3      | T18.6      | s3_18_00_w6_00_+45   |  |   |



FlowDike-D

**Freibordbemessung von Ästuar-  
und Seedeichen unter  
Berücksichtigung von Wind und  
Strömung**

Zusammenstellung der aus dem Projekt  
resultierten Veröffentlichungen  
März 2010

Dipl.-Ing. Stefanie Lorke<sup>1</sup>  
Dipl.-Ing. Anja Brüning<sup>1</sup>  
Dr.-Ing. Antje Bornschein<sup>2</sup>  
Dipl.-Ing. Stefano Gilli<sup>2</sup>  
cand.-Ing. Nadine Krüger<sup>2</sup>  
Univ.-Prof. Dr.-Ing. Holger Schüttrumpf<sup>1</sup>  
Prof. Dr.-Ing. habil. Reinhard Pohl<sup>2</sup>

Aachen und Dresden, März 2010

---

<sup>1</sup> Institut für Wasserbau und Wasserwirtschaft (IWW), RWTH Aachen

<sup>2</sup> Institut für Wasserbau und Technische Hydromechanik (IWD), TU Dresden

## Veröffentlichungen

Brüning, A.; Gilli, S.; Lorke, S.; Pohl, R.; Schlüter, F.; Spano, M.; van der Meer, J.; Werk, S.; Schüttrumpf, H. (2009); FlowDike - Investigating the effect of wind and current on wave run-up and wave overtopping; 4th SCACR - International Short conference on APPLIED COASTAL RESEARCH, Barcelona

Brüning, A.; Gilli, S.; Lorke, S.; Pohl, R.; Schlüter, F.; Spano, M.; van der Meer, J.; Werk, S.; Schüttrumpf, H. (2010); FlowDike - Investigating the effect of wind and current on wave run-up and wave overtopping; Hydralab III Joint User Meeting, Hannover

Lorke, S., Brüning, A.; Bornschein, A.; Gilli, S.; Pohl, R.; Spano, M.; van der Meer, J.; Werk, S.; Schüttrumpf, H. (2010); On the effect of wind and current on wave run-up and wave overtopping; 32nd International Conference on Coastal Engineering. Schanghai (accepted for publication)

Pohl, R. (2010); Neue Aspekte der Freibordbemessung an Fluss- und Ästuardeichen; Wasserbauliche Mitteilungen des Institutes für Wasserbau und Technische Hydromechanik der Technischen Universität Dresden, Heft 40, S. 467 - 478 (nicht beigefügt)

Rahlf, H.; Schüttrumpf, H. (2010); Critical overtopping rates for Brunsbüttel lock; 32nd International Conference on Coastal Engineering. Schanghai (accepted for publication)

Schüttrumpf, H. (2009) Wellenüberlauf an Deichen - Stand der Wissenschaft und aktuelle Untersuchungen. 3. Siegener Symposium "Sicherung von Dämmen, Deichen und Stauanlagen". Tagungsband

Van der Meer, J.; Hardeman, B.; Steendam, G.J.; Schüttrumpf, H.; Verheij, H. (2010) Flow depths and velocities at crest and inner slope of a dike, in theory and with the wave overtopping simulator. 32nd International Conference on Coastal Engineering. Schanghai (accepted for publication)